National Technical University of Athens

School of Rural, Surveying and Geoinformatics Engineering

DATA-DRIVEN PEDESTRIAN SIMULATION / AN ALTERNATIVE TO THEORY-BASED PEDESTRIAN SIMULATION?

Doctoral Dissertation

George Kouskoulis

Engineer of Urban Planning and Regional Development, MSc

Advisory board:

I. Spyropoulou, Associate Professor, NTUA

C. Antoniou, Professor, TUM

G. Yannis, Professor, NTUA

Athens, March 2022

Εθνικό Μετσόβιο Πολυτεχνείο

Σχολή Αγρονόμων και Τοπογράφων Μηχανικών – Μηχανικών Γεωπληροφορικής

ΜΟΝΤΕΛΑ ΑΝΑΛΥΣΗΣ ΔΕΔΟΜΕΝΩΝ ΕΦΑΡΜΟΣΜΕΝΑ ΣΤΗΝ ΠΡΟΣΟΜΟΙΩΣΗ ΤΗΣ ΠΕΖΗΣ ΚΙΝΗΣΗΣ / ΜΙΑ ΕΝΑΛΛΑΚΤΙΚΗ ΤΩΝ ΘΕΩΡΗΤΙΚΩΝ ΜΟΝΤΕΛΩΝ ΠΡΟΣΟΜΟΙΩΣΗΣ?

Διδακτορική Διατριβή

Γιώργος Κουσκουλής

Μηχανικός Χωροτοταξίας, Πολεοδομίας και Περιφερειακής Ανάπτυξης

Συμβουλευτική Επιτροπή:

Ι. Σπυροπούλου, Αναπληρώτρια Καθηγήτρια, ΕΜΠ

Κ. Αντωνίου, Καθηγητής, TUM

Γ. Γιαννής, Καθηγητής, ΕΜΠ

Αθήνα, Μάρτιος 2022

Dedicated to the memory of my father

Acknowledgments

The elaboration of a doctoral thesis is not exactly a standalone procedure but requires the help and support from many persons (not only experts) to the writer. For this reason I would like to express my deepest appreciation and gratitude to those that provided me with all the necessary (and even more) guidance during this journey.

First of all I would like to thank my supervisor Associate Professor Ioanna Spyropoulou whose role was crucial during my thesis. She constantly encouraged me and offered advice to improve and extend my research. Her help was invaluable.

I am very grateful to Professor Constantinos Antoniou. He is the person that suggested me to explore the data analysis field, while continually stimulating me for a deeper research. He also supported me substantially in my early steps.

I wish to thank the member of my supervising committee Professor George Giannis. His comments improve the presentation of the dissertation's methodological framework and results.

Special thanks to Associate Professor Eleni Vlahogianni for her critical notes considering the employed methodologies on data-driven models.

Furthermore, I am thankful to the remaining members of my dissertation committee, namely the Assistant Professor Eleonora Papadimitriou, the Associate Professor Konstantinos Karantzalos and the Professor Socrates Basbas.

As also mentioned in the present text, one of the most important elements (probably the most important) in order to conduct an integrated research is the appropriate data. Thus, I would like to express my sincere thanks to Dr. Manos Barmpounakis for suggesting techniques to extract all the necessary data for my dissertation. I am also thankful to my cousin George who helped me during the data collection process.

Thereinafter I would like to thank Professor George Karras for his advice in photogrammetric field.

In addition I am grateful for the financial support provided from the project EMPARCO that is supported by the Action: ARISTEIA-II (Action's Beneficiary: General Secretariat for Research and Technology).

Last but not least, I would like to thank my fellow researchers at the National Technical University of Athens and in particularly Vasileia, Christine, Ioulia, Harris, Helen, Maria and Margarita for their help and support during my studies.

Abstract

The aim of the research is to examine whether data-driven pedestrian simulation models can outperform the theoretical ones and provide a robust model framework for pedestrian simulation. Initially, an extended literature review was performed to identify the existing pedestrian simulation models and the main parameters utilized in pedestrian simulation. To achieve the aim of the study, a comparative analysis of a well-known and widely applied theoretical pedestrian simulation model (i.e. the social force mode) and four data-driven techniques: the Artificial Neural Networks, the Support Vector Regression, the Gaussian Processes and the Locally Weighted Regression was conducted. A suitable methodological framework for the comparative analysis was designed. Initially, appropriate data (i.e. pedestrian trajectories) were collected from two different area types: a metro station during peak hours and a shopping mall during afternoon hours, via video recordings. Then, with the aid of an appropriate software, pedestrian trajectories were extracted. Due to the fact that the collected data include white noise, an algorithm for noise elimination was developed as a combination of existing smoothing filters. Subsequently, an appropriate pedestrian simulation model setup for the data-driven techniques was developed, as they do not cater specifically for pedestrian simulation framework. In order to conduct a fair comparison the variables of the theoretical model were employed in the data-driven models. Cross-validation was applied as the appropriate method for examining each model's performance and to cater for data overfitting, while a combination of goodness-of-fit measures the models' accuracy were estimated to assess the models in a holistic manner. The results indicate that data-driven methods have higher capability of simulating pedestrian movement as they perform better according to all of goodness-of-fit measures. Following the first level of comparison (compare models with the same parameters), additional parameters (agent's characteristics and time parameter) have been included in the data-driven models in order to examine the possibility of improving (and its magnitude) the performance of these models. Results of this analysis indicate that the employment of the selected variables can improve data-driven pedestrian simulation models performance (they performed better for almost every goodness-of-fit measure).

Keywords: Pedestrian simulation, data-driven techniques, social force model, Artificial Neural Networks, Support Vector Regression, Gaussian Processes, Locally Weighted Regression, cross-validation, goodness-of-fit measures, Unscented Kalman Filter, moving average, data noise elimination

Περίληψη

Σκοπό της παρούσας έρευνας αποτελεί η διερεύνηση της καταλληλότητας υιοθέτησης μοντέλων που βασίζονται σε μεθόδους ανάλυσης δεδομένων για την προσομοίωση της πεζής κίνησης. Για το σκοπό αυτό, σχεδιάζονται κατάλληλα μοντέλα και εξετάζεται αν δύναται να παράσχουν ένα αξιόπιστο μεθοδολογικό πλαίσιο στην προσομοίωση της πεζής κίνησης. Επιπλέον, αξιολογείται η απόδοσή τους σε σχέση με τα αντίστοιχα θεωρητικά μοντέλα προσομοίωσης της πεζής κίνησης. Στο πλαίσιο αυτό πραγματοποιείται μια συγκριτική ανάλυση ενός αρκετά γνωστού και ευρέως εφαρμοσμένου θεωρητικού μοντέλου προσομοίωσης της πεζής κίνησης (το μοντέλο social force) και τεσσάρων μεθόδων ανάλυσης δεδομένων: των Τεχνητών Νευρωνικών Δικτύων, των Μηχανών Διανυσμάτων Υποστήριξης, των Gaussian Processes και της Τοπικά Σταθμισμένης μη Παραμετρικής Παλινδρόμησης. Προγενέστερα αυτού μια εκτενής βιβλιογραφική ανασκόπηση ανέδειξε τα υφιστάμενα θεωρητικά μοντέλα προσομοίωσης της πεζής κίνησης και τις παραμέτρους τους. Ακολούθως σχεδιάστηκε ένα κατάλληλο μεθοδολογικό πλαίσιο για τη συγκριτική ανάλυση. Αρχικά συλλέχθηκαν τα δεδομένα (οι τροχιές των πεζών) από δυο διαφορετικούς τύπους περιοχών, την πλατφόρμα ενός σταθμού του μετρό κατά τις ώρες αιχμής και ενός εμπορικού κέντρου κατά τις απογευματινές ώρες, όλα μέσω βιντεοσκόπησης. Ακολούθως με τη βοήθεια ενός κατάλληλου λογισμικού εξήχθησαν οι τροχιές των πεζών. Καθώς τα συλλεχθέντα δεδομένα περιέχουν θόρυβο αναπτύχθηκε κατάλληλος αλγόριθμος για ελαχιστοποίηση του θορύβου των δεδομένων, υιοθετώντας έναν συνδυασμό υφιστάμενων φίλτρων ομαλοποίησης. Στη συνέχεια αναπτύχθηκε ένα κατάλληλο μοντέλο προσομοίωσης της πεζής κίνησης το οποίο ενσωματώθηκε στις μεθόδους ανάλυσης δεδομένων καθώς αυτές δεν διαθέτουν κάποιο πλαίσιο προσομοίωσης της πεζής κίνησης. Για την πραγματοποίηση μιας δίκαιης σύγκρισης χρησιμοποιήθηκαν στα μοντέλα ανάλυσης δεδομένων οι παράμετροι του θεωρητικού μοντέλου προσομοίωσης της πεζής κίνησης. Η μέθοδος της διασταυρωμένης επικύρωσης (cross-validation) υιοθετήθηκε ως η καταλληλότερη μέθοδος για την εξέταση της απόδοσης των μοντέλων και για τον περιορισμό του προβλήματος της υπερμοντελοποίησης (overfitting). Επιπλέον χρησιμοποιήθηκε ένας συνδυασμός δεικτών απόδοσης για να ποσοτικοποιηθεί η καλή προσαρμογή και η ακρίβεια των μοντέλων. Τα αποτελέσματα υποδεικνύουν πως οι μέθοδοι ανάλυσης δεδομένων παρουσιάζουν μεγαλύτερη δυνατότητα

προσομοίωσης της πεζής κίνησης καθώς αποδίδουν καλύτερα με βάση όλους τους προαναφερθέντες δείκτες. Μετά το πρώτο επίπεδο της συγκριτικής αξιολόγησης (όπου συγκρίνονται μοντέλα με τις ίδιες παραμέτρους), επιπλέον παράμετροι (τα χαρακτηριστικά των πεζών και η παράμετρος του χρόνου) ενσωματώθηκαν στα μοντέλα ανάλυσης δεδομένων για εξεταστεί περαιτέρω βελτίωση της απόδοσής τους. Τα αποτελέσματα αυτής της ανάλυσης υποδεικνύουν πως η υιοθέτηση των συγκεκριμένων μεταβλητών μπορεί να βελτιώσει την απόδοση των μοντέλων ανάλυσης δεδομένων που αφορούν στην προσομοίωση της πεζής κίνησης.

Λέξεις κλειδιά: Προσομοίωση της πεζής κίνησης, μέθοδοι ανάλυσης δεδομένων, social force μοντέλο, Τεχνητά Νευρωνικά Δίκτυα, Μηχανές Διανυσμάτων Υποστήριξης, Gaussian Processes, Τοπικά Σταθμισμένη μη Παραμετρική Παλινδρόμηση, cross-validation, δείκτες καλής προσαρμογής, Unscented Kalman Filter, κινητός μέσος όρος, ελαχιστοποίηση θορύβου δεδομένων

Extended abstract

The analysis of pedestrian movement has attracted the interest of the scientific community. Some of the reasons that have contributed in this, are the change of the urban environment (e.g. higher buildings and high centralization of activities in smaller spaces that results in higher densities), as well as a change of focus of transportation policies in which walking plays a crucial role.

Initially, an overview of several theoretical pedestrian simulation models was conducted. These rely on pedestrian dynamics and flow principles and are classified according to their level of analysis (microscopic, macroscopic, etc.). On the other hand the emergence of data-driven models is offering new possibilities in pedestrian simulation. Data-driven techniques have proved their simulation robustness in terms of clustering, classification and regression although their employment does not require a priori knowledge of the model parameters' relationship.

The aim of this research is to examine whether data-driven methods can provide a robust model framework for pedestrian simulation. To achieve this, several data-driven models were designed for pedestrian simulation utilizing various widely used data-driven techniques. To display their potential utility these models were compared against a theoretical pedestrian simulation model. Due to the fact that data-driven models do not include a pedestrian simulation framework, an appropriate one, based on the theoretical pedestrian simulation models principles, has been developed. Furthermore, the incorporation of these principles in the data-driven models allowed for a fair comparison between data-driven models and theoretical pedestrian simulation ones.

To achieve the objective of this research a five-step process was followed. First, the appropriate data i.e. pedestrian trajectories, were collected. Two different area types, which exhibit different walking patterns, were selected. Due to the fact that the raw data include white noise, a smoothing algorithm that eliminates data's white noise was developed as a combination of existing filters. Subsequently, five models were designed: one based on a representative pedestrian simulation model in the field of theoretical approaches and four models utilizing different data-driven techniques. For the latter, an appropriate

pedestrian simulation model setup was developed. In order to assess in a fair manner the performance of the different models, the variables of the theoretical model were employed in the data-driven models' design. Cross-validation was performed as it comprises an appropriate method for examining each model's performance, while it caters for data overfitting, a common issue with data-driven models. At the same time, a combination of goodness-of-fit (GoF) measures was utilized to estimate the models' performance in a holistic manner. Following the first level of comparison (compare models with the same parameters), additional parameters were included in the data-driven models in order to examine their potential improvement (and its magnitude) in their performance. The methodological framework of the present research follows:

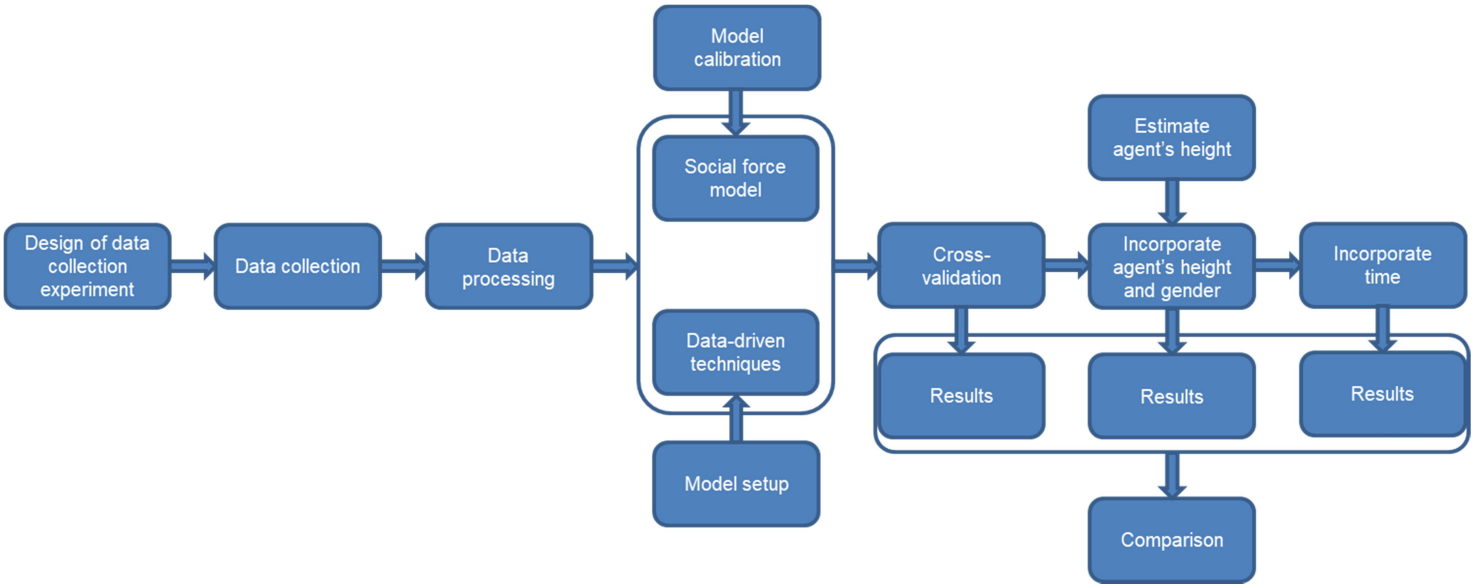

FIGURE 1: Methodological framework

Prior to this process an extended literature review was conducted. The state of the art considering pedestrian simulation models was explored. The models were categorized according to their analysis level and according to the adopted theory describing pedestrian dynamics. The models that analyze pedestrian movement are, mostly, microscopic. Thus, three main categories were identified: a) social force, b) cellular automata and c) lattice gas models. Route choice theory was also elaborated, mostly, in parallel to the aforementioned theories leading to combined models. Data-driven models were also mentioned in the literature review, as initial attempts for modeling pedestrian movement.

Another aim of the literature review was to investigate the factors that affect pedestrian movement. Certain parameters that affect pedestrian movement have been specified. They were organized in a new framework, clustered in three main categories: a) facilities' geometry, b) pedestrian flow properties, and c) pedestrian characteristics (e.g. agent's gender and height), and were further analyzed.

Within the literature review different data collection techniques were elaborated including video recording and sensors [Global Positioning System (GPS), Radio Frequency Identification (RFID), Light Detection and Ranging (LiDAR)]. In this research, data have been collected from the field through video recordings. The experimental design focused on facilities where only pedestrians are present, thus interactions with other traffic modes (e.g. vehicles, bicycles) were not considered. Two different types of areas were employed, a metro station and a shopping mall. Two digital cameras were placed at both locations at an upper level point. The first camera was focused on the terrain where pedestrians walk, and the second captured their characteristics (height, gender etc.). An appropriate software was applied for the extraction of pedestrian trajectories from video recordings, which utilizes both automatic and semi-automatic processes for pedestrian tracking. In this research a manual process was employed in order to ensure high level of accuracy in pedestrian tracking.

Accurate data is a prerequisite for developing reliable simulation models, particularly when applying data-driven theories, as they rely highly on the utilized data. Data-driven methods are applied for simulating phenomena without a priori knowledge of parameter relations/connections. Due to the fact that the extracted data include noise, a suitable algorithm for data noise reduction was developed. The proposed algorithm relies on the Kalman filter framework. In particular, the Unscented Kalman Filter (UKF) was employed for relaxing standard Kalman filter assumptions. The filtering process was conducted in three steps. The first step includes video recording segmentation, in the second step the UKF extension was adopted, and in the third step the moving average filter was incorporated to UKF. An innovation of this research is the incorporation of moving average in the UKF that provides more accurate pedestrian trajectory estimations.

In addition, a procedure for evaluating Kalman filter noise covariance matrices was suggested, which comprises another contribution of this research. Algorithm

results from real pedestrian trajectory data indicated high efficacy level in reducing data noise, thus improving their contribution in calibrating and validating pedestrian simulation models.

Two different simulation approaches were considered, a theory-derived model and four data-driven techniques. The social force model was employed as the theory-derived model, due to its ascendancy to other pedestrian simulation models (relies on the same principle, but is a continuous space model) and its wide application in pedestrian simulation and pedestrian simulation software. As for data-driven techniques, four promising methods were explored: a) the well-known Articial Neural Networks (ANN), b) the classical Support Vector Machines (SVM) [in particular as we refer to regression analysis, Support Vector Regression (SVR) is employed], c) the rising Gaussian Processes (GP), and d) the Locally Weighted Regression (Loess).

The social force model utilizes five parameters: the distances between the simulated agent and pedestrians triggering repulsive effects, pedestrians triggering attractive effects, space boundaries and to the next destination point and the velocity of pedestrians that trigger repulsive effects. In this research a fair comparison between the social force model and the data-driven techniques was attempted, thus, the parameters utilized in the social force model were also employed in the model setup for the data-driven techniques. A limitation of this procedure is that the Loess technique can only model up to three variables. Hence, for this technique the following parameters (employed from the social force model) were considered: pedestrian velocity at the current time step and the distances between the examined agent and a) the pedestrians triggering repulsive effects and b) the space boundaries.

In the model setup the distances were separated in the two axes representing the horizontal and the vertical projections of the adjacent pedestrian/obstacle. Due to the fact that data-driven models consider one value for every variable, in cases of more than one “repulsive” or “attractive” agents or/and obstacles, a selection criterion was specified. This criterion is an angular dependence factor based on the agent’s view. It considers that pedestrians who walk outside of the agent’s sight view (i.e. behind them) or close to its contour (i.e. vertically to agent) affect

the simulated pedestrian's movement at a substantially lower degree than those who are in front of them and close to their trajectory.

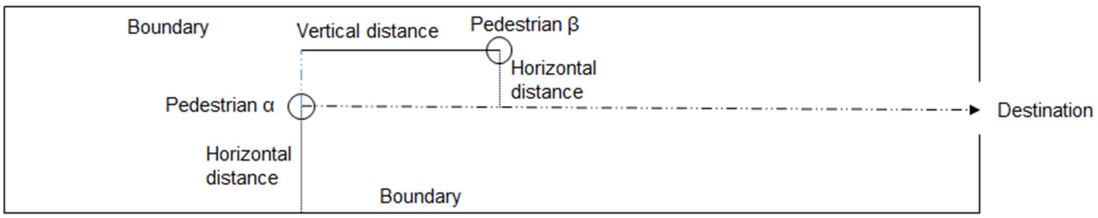

FIGURE 2: Data-driven model setup

Models' performance was examined under a cross-validation pattern and in particular a 5-fold one, in order to overcome overfitting problems that data-driven methods suffer from. The two datasets (one from the metro station platform and the other from the shopping mall) were merged together and then shuffled and divided into five equally sized datasets. Considering the design of the data-driven models, these were developed following a training process the aim of which was to estimate each model's parameters that minimize the cost function, set to be the Mean Squared Error (MSE) of the agent's velocity. As agent's velocity was presented in two axes, multi-output data-driven models were employed. In addition, as the social force model does not incorporate a training algorithm (in contrast to data-driven techniques) a genetic algorithm was utilized, for model calibration. Two alternative processes that examine the most effective parameters and then train the social force model only around them were also presented (one-at-time sensitivity analysis and global sensitivity analysis). Though, due to the fact that genetic algorithms overcome the aforementioned need of examining the most effective parameters and have proven their robustness in the field of optimization, they were employed in this research.

A set of GoF indices was used to evaluate each model's performance. Results indicate that data-driven methods have higher capability of simulating pedestrian movements, as they performed better according to all of GoF measures. The theoretical simulation model (social force) included large errors compared to the data-driven models, while the Loess method displayed the highest performance. Also, the social force model included both systematic and unsystematic biases that almost did not exist in data-driven models. Furthermore, data-driven methods accomplished the cross-validation process significantly faster compared to the

social force model. On the other hand, it should be noted that the social force model provides an integrated simulation framework where every parameter is directly related to the model output. It explains in a clear manner the way that pedestrians walk and interact with each other (high level of interpretability), while data-driven methods are considered to be, at some level, as black boxes.

In addition, a comparison among the four data-driven methods revealed that the Loess model performed better considering almost every index. ANN and GP presented similar performance levels, while SVR provided inferior predictions. It should also be mentioned that the Loess model performed better although it employed a smaller number of predictors compared to the other data-driven methods, while also accomplishing the cross-validation procedure in significantly less time. In contrast, it is clear that there are limitations, related to the opacity and the (lack of) interpretability of the data-driven models. A comparison of the GoF measures in every run of the cross-validation procedure revealed that data-driven methods tend to overfit as they learn/develop from the data.

In the last step of the present research, three additional variables were incorporated in the data-driven models in order to examine if any further enhancement of their performance can be accomplished. Additional variables have been selected based on the literature review. Initially agent's height and gender were added. Agent's height was estimated with the aid of photogrammetric tools. It should be noted that this analysis was not performed for the Loess method, as it cannot employ further parameters. Results of this analysis indicated that the employment of agent's characteristics can improve data-driven pedestrian simulation models performance (they performed better in almost every GoF measure). The additional adoption of the time parameter in the data-driven pedestrian simulation models was also tested. The models following the incorporation of the time parameter seemed to perform better, but not for all the of the GoF measures. In general, the adoption of the extra variables seemed to improve mainly the performance of the ANN model implying that this technique can "handle" more efficiently the incorporation of these variables.

The research contributions and conclusions are outlined below:

- Provide a framework for data (pedestrian trajectories) noise elimination

    - Enhance UKF performance with the incorporation of symmetric moving average
    - Estimate UKF noise covariances when unknown
- Provide a framework for setting up a pedestrian model for data-driven simulations
- Apply a time efficient social force model calibration method
- Display data-driven modelling efficiency in the field of pedestrian simulation (in relation to existing theoretical models)
- Improve the performance of data-driven models including additional pedestrian simulation variables

Directions for future research were also provided. An amplification of the data-driven models can be accomplished with the incorporation of further variables. An example of this could be the employment of a density measure in order to capture not only one agent that affects mostly the simulated one, but also all the agents in close vicinity. In addition, extra data can be considered for an improved evaluation of the models. Furthermore, an interesting research objective might be the investigation of pedestrian movement, while interacting with vehicles in more complex scenarios and situations. The application of data-driven models in these scenarios should be examined. This notation is crucial as it can enhance the performance of pedestrian collision warning systems and autonomous vehicles. Moreover the parameter of time was tested in the current research for its impact in the data-driven pedestrian simulation model. Recurrent Neural Networks (RNN), a class of ANN, and in particular Long Short-Term Memory (LSTM) architecture can also be tested for their applicability in terms of pedestrian simulation. Finally, a comparison in pedestrian movements between normal and emergency situations should be further explored to identify the differences in pedestrian behavior under emergencies. This, as well as the incorporation of vehicle-pedestrian interactions will represent pedestrian movement in a more holistic manner, and thus enhance pedestrian simulation models' performance.

Εκτεταμένη περίληψη

Η ανάλυση της πεζής κίνησης έχει προσελκύσει το ενδιαφέρον της επιστημονικής κοινότητας. Κάποιοι από τους λόγους που συνέβαλαν σε αυτό αφορούν στην αλλαγή του αστικού περιβάλλοντος (π.χ. κατασκευή υψηλότερων κτιρίων και μεγαλύτερη συγκέντρωση δραστηριοτήτων σε μικρότερους χώρους που οδήγησε σε μεγαλύτερες χωρικές πυκνότητες) όπως επίσης και η αλλαγή των κεντρικών στόχων των συγκοινωνιακών στρατηγικών στους οποίους η πεζή κίνηση διαδραματίζει σημαντικό ρόλο.

Στην παρούσα έρευνα πραγματοποιήθηκε επισκόπηση των θεωρητικών μοντέλων προσομοίωσης της πεζής κίνησης η οποία παρουσιάζεται στον παρόν κείμενο. Τα εν λόγω μοντέλα βασίζονται στις δυναμικές και στους βασικούς κανόνες της ροής και κατηγοριοποιούνται σύμφωνα με το επίπεδο της ανάλυσής τους (μικροσκοπικά, μακροσκοπικά, κλπ.). Από την άλλη πλευρά, η εμφάνιση των μεθόδων ανάλυσης δεδομένων παρέχει νέες δυνατότητες στην προσομοίωσης της πεζής κίνησης. Οι συγκεκριμένες μέθοδοι έχουν αποδείξει την αποτελεσματικότητά τους σε θέματα συσταδοποίησης, κατηγοροποίησης και πρόβλεψης (παλινδρόμησης) παρόλο που δεν απαιτούν την εξ' αρχής γνώση της σχέσης μεταξύ των παραμέτρων του μοντέλου.

Σκοπό της παρούσας έρευνας αποτελεί η διερεύνηση της δυνατότητας υιοθέτησης μεθόδων ανάλυσης δεδομένων για την προσομοίωση της πεζής κίνησης. Για να επιτευχθεί αυτό χρησιμοποιήθηκαν ευρέως εφαρμοσμένες μέθοδοι ανάλυσης δεδομένων, σχεδιάστηκαν αντίστοιχα μοντέλα προσομοίωσης πεζής κίνησης, ενώ για να εκτιμηθεί η απόδοσή τους συγκρίθηκαν με ένα θεωρητικό μοντέλο προσομοίωσης πεζής κίνησης. Εξαιτίας του γεγονότος πως τα μοντέλα ανάλυσης δεδομένων δεν εμπεριέχουν κάποιο πλαίσιο προσομοίωσης πεζής κίνησης, αναπτύχθηκε ένα κατάλληλο μοντέλο βασιζόμενο στις αρχές των θεωρητικών μοντέλων προσομοίωσης. Επιπλέον η εισαγωγή των εν λόγω αρχών στα μοντέλα ανάλυσης δεδομένων έδωσε τη δυνατότητα για μια δίκαιη σύγκριση μεταξύ των συγκεκριμένων μοντέλων και του θεωρητικού.

Για την πραγματοποίηση της προαναφερθείσας σύγκρισης ακολουθήθηκε μια διαδικασία πέντε σταδίων. Αρχικά συλλέχθηκαν τα κατάλληλα δεδομένα (οι τροχιές των πεζών). Η συλλογή δεδομένων πραγματοποιήθηκε σε δύο περιοχές

που παρουσιάζουν διαφορετικά χαρακτηριστικά ώστε να εξαχθούν τα διαφορετικά μοτίβα κίνησης των πεζών. Λόγω του ότι τα αρχικώς συλλεχθέντα δεδομένα περιέχουν θόρυβο αναπτύχθηκε ένας αλγόριθμος που ελαχιστοποιεί τον θόρυβο δεδομένων και βασίζεται σε υφιστάμενα φίλτρα ομαλοποίησης. Στη συνέχεια, συγκρίθηκε η απόδοση ενός αντιπροσωπευτικού θεωρητικού μοντέλου από τον τομέα της προσομοίωσης της πεζής κίνησης και τεσσάρων μοντέλων που σχεδιάστηκαν υιοθετώντας μεθόδους ανάλυσης δεδομένων. Για λόγους διεξαγωγής μιας δίκαιης συγκριτικής ανάλυσης χρησιμοποιήθηκαν οι μεταβλητές του θεωρητικού μοντέλου στα αντίστοιχα μοντέλα των μεθόδων ανάλυσης δεδομένων. Η μέθοδος της διασταυρωμένης επικύρωσης (cross-validation) χρησιμοποιήθηκε ως η καταλληλότερη για την εξέταση της απόδοσης των μοντέλων, μέθοδος η οποία περιορίζει και τις επιπτώσεις του προβλήματος της υπερμοντελοποίησης (overfitting) από το οποίο πάσχουν οι μέθοδοι ανάλυσης δεδομένων. Επίσης χρησιμοποιήθηκε ένας συνδυασμός δεικτών απόδοσης για να ποσοτικοποιηθεί η καλή προσαρμογή και η ακρίβεια των μοντέλων. Τέλος και σε συνέχεια του πρώτου επιπέδου της συγκριτικής ανάλυσης, όπου συγκρίθηκαν τα μοντέλα με τις ίδιες μεταβλητές, επιπλέον παράμετροι προσομοίωσης της πεζής κίνησης προστέθηκαν στα μοντέλα ανάλυσης δεδομένων για να εξεταστεί τυχούσα αύξηση της απόδοσης τους. Το μεθοδολογικό πλαίσιο της παρούσας έρευνας παρατίθεται παρακάτω:

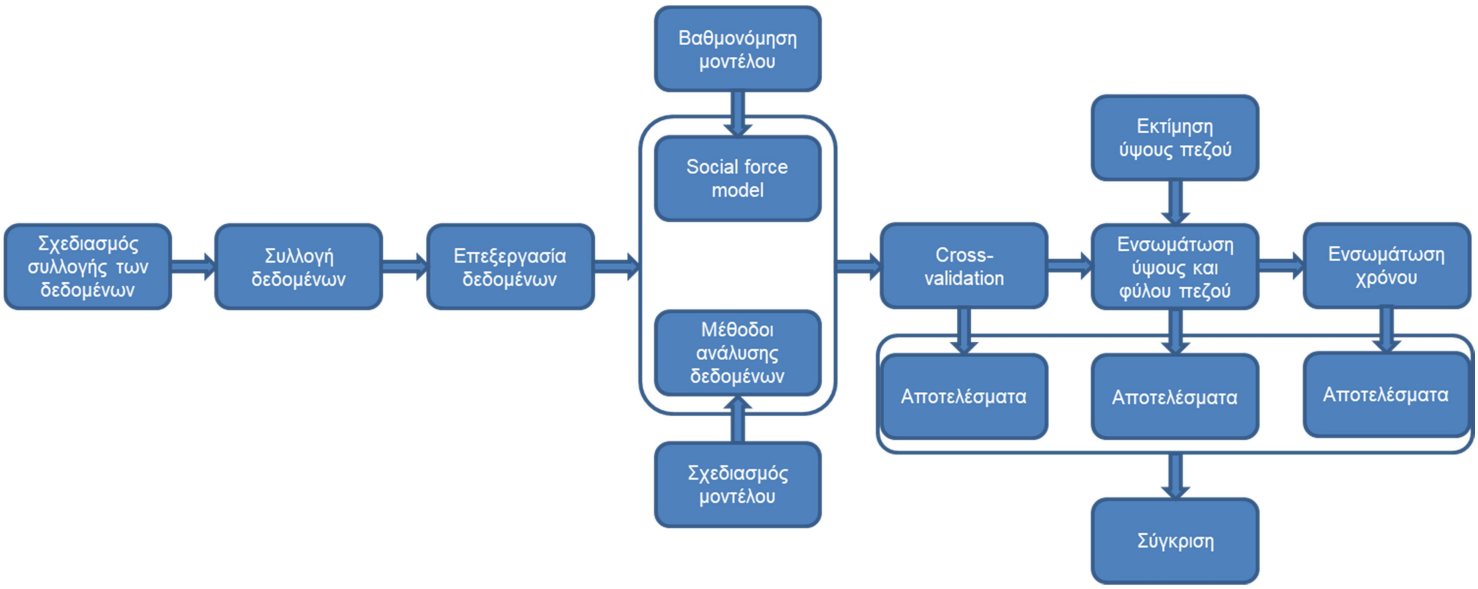

ΣΧΗΜΑ 1: Μεθοδολογικό πλαίσιο

Προγενέστερα της παραπάνω διαδικασίας διεξήχθη μια εκτενής βιβλιογραφική ανασκόπηση όπου διερευνήθηκε η επιτομή των μοντέλων προσομοίωσης της πεζής κίνησης. Τα μοντέλα κατηγοριοποιήθηκαν σύμφωνα με το επίπεδο ανάλυσής τους και σύμφωνα με τη θεωρία που περιγράφει τη δυναμική της κίνησης των πεζών. Τα μοντέλα που αναλύουν τις κινήσεις των πεζών είναι, κυρίως, μικροσκοπικά. Τρεις κύριες κατηγορίες εντοπίστηκαν: α) social force, β) κυτταρικά αυτόματα (cellular automata), και γ) lattice gas μοντέλα. Η θεωρία της επιλογής διαδρομής στην προσομοίωση της πεζής κίνησης παρουσιάστηκε, κυρίως, παράλληλα με τις παραπάνω θεωρίες οδηγώντας σε συνδυαστικά μοντέλα. Τα μοντέλα ανάλυσης δεδομένων επίσης αναφέρονται στη βιβλιογραφική ανασκόπηση, όμως σαν αρχικές προσπάθειες μοντελοποίησης της κίνησης των πεζών.

Ένας επιπλέον σκοπός της βιβλιογραφικής ανασκόπησης ήταν να διερευνήσει τους παράγοντες που επηρεάζουν την κίνηση των πεζών. Συγκεκριμένοι παράγοντες προσδιορίστηκαν, οι οποίοι κατατάχθηκαν σε τρεις κύριες κατηγορίες: α) γεωμετρία της περιοχής κίνησης, β) ιδιότητες της ροής της κίνησης των πεζών, και γ) χαρακτηριστικά των πεζών (π.χ. ύψος και φύλο πεζού), και εν συνεχεία αναλύθηκαν.

Στα πλαίσια της βιβλιογραφικής ανασκόπησης διαφορετικές τεχνικές συλλογής δεδομένων εξετάστηκαν συμπεριλαμβανομένων της βιντεοσκόπησης και των αισθητήρων (GPS, RFID, LiDAR). Στην παρούσα έρευνα τα δεδομένα συλλέχθηκαν από το πεδίο μέσω βιντεοσκόπησης. Ο σχεδιασμός του πειράματος της έρευνας πεδίου εστίασε σε εγκαταστάσεις όπου κυκλοφορούν μόνο πεζοί και ως εκ τούτου αλληλεπιδράσεις με άλλα μέσα μεταφοράς (π.χ. αυτοκίνητα, ποδήλατα) δεν περιλαμβάνονται. Δύο διαφορετικοί τύποι υποδομών ελήφθησαν υπόψη, ένας σταθμός του μετρό και ένα εμπορικό κέντρο. Δύο ψηφιακές κάμερες τοποθετήθηκαν και στις δυο περιοχές σε ένα υψηλό σημείο. Η πρώτη κάμερα εστίαζε στο έδαφος, όπου οι πεζοί περπατούν, και η δεύτερη αποτύπωνε τα χαρακτηριστικά τους (ύψος, φύλο κλπ.). Επισημαίνεται πως υπάρχουν λογισμικά τα οποία παρέχουν αυτόματες ή ημι-αυτόματες διαδικασίες εξαγωγής της τροχιάς των πεζών από δεδομένα βίντεο. Στην παρούσα έρευνα μια χειροκίνητη διαδικασία επιλέχθηκε για να διασφαλιστεί το υψηλό επίπεδο ακρίβειας των αποτελεσμάτων της.

Η ακρίβεια στα δεδομένα είναι προαπαιτούμενο για την ανάπτυξη αξιόπιστων μοντέλων προσομοίωσης, ειδικότερα όταν εφαρμόζονται θεωρίες ανάλυσης δεδομένων, καθώς αυτές βασίζονται κυρίως στα ίδια τα δεδομένα. Οι μέθοδοι ανάλυσης δεδομένων εφαρμόζονται για την προσομοίωση φαινομένων χωρίς την εκ των προτέρων γνώση της σχέσης μεταξύ των παραμέτρων. Καθώς τα εξαχθέντα δεδομένα εμπεριέχουν θόρυβο, αναπτύχθηκε ένας κατάλληλος αλγόριθμος για μείωση του θορύβου. Ο προτεινόμενος αλγόριθμος βασίζεται στο φίλτρο Κάλμαν. Ειδικότερα η παραλλαγή Unscented Kalman Filter (UKF) χρησιμοποιήθηκε για να περιοριστεί η επίδραση των υποθέσεων του βασικού φίλτρου Κάλμαν. Η διαδικασία περιορισμού του θορύβου των δεδομένων πραγματοποιήθηκε σε τρία στάδια. Στο πρώτο στάδιο ομαδοποιήθηκαν τα καρέ της καταγραφής της βιντεοσκόπησης, στο δεύτερο στάδιο υιοθετήθηκε η παραλλαγή UKF του φίλτρου Κάλμαν και στο τρίτο στάδιο το φίλτρο του κινητού μέσου όρου ενσωματώθηκε στην προαναφερθείσα παραλλαγή. Μια καινοτομία της παρούσας έρευνας είναι η ενσωμάτωση του κινητού μέσου όρου στο φίλτρο UKF κάτι που παρέχει ακριβέστερες εκτιμήσεις των τροχιών των πεζών. Συγκεκριμένα ο συμμετρικός κινητός μέσος όρος αντανακλά την τάση της κίνησης ενός πεζού καθώς ενσωματώνει τα προηγούμενα και τα επόμενα βήματα στην εκτίμηση της τροχιάς.

Επιπροσθέτως προτάθηκε μια διαδικασία για εκτίμηση των μητρώων συνδιακύμανσης σφαλμάτων της παραλλαγής του φίλτρου Κάλμαν. Τα αποτελέσματα του αλγόριθμου από πραγματικά δεδομένα τροχιών πεζών υποδεικνύουν ένα υψηλό επίπεδο απόδοσης στη μείωση του θορύβου των δεδομένων και ως εκ τούτου στη βελτίωση της συνεισφοράς τους στη βαθμονόμηση και στην επικύρωση των μοντέλων πεζής προσομοίωσης.

Δύο διαφορετικές προσεγγίσεις ελήφθησαν υπόψη: ένα θεωρητικό μοντέλο και τέσσερις μέθοδοι ανάλυσης δεδομένων. Το social force model χρησιμοποιήθηκε ως το θεωρητικό μοντέλο λόγω της υπεροχής του σε σχέση με άλλα μοντέλα προσομοίωσης της πεζής κίνησης (βασίζεται στις ίδιες βασικές αρχές προσομοίωσης με τα υπόλοιπα μοντέλα, αλλά σε αντίθεση με αυτά είναι ένα συνεχές στο χώρο μοντέλο) και λόγω της ευρύτερης αποδοχής του και της υιοθέτησής του από ευρέως διαδεδομένα λογισμικά προσομοίωσης της πεζής κίνησης. Όσον αφορά τις μεθόδους ανάλυσης δεδομένων, τέσσερις μέθοδοι διερευνήθηκαν: α) τα ευρέως διαδεδομένα Τεχνητά Νευρωνικά Δίκτυα (ΤΝΔ), β)

οι κλασσικές Μηχανές Διανυσμάτων Υποστήριξης [ειδικότερα η παραλλαγή της μεθόδου που αφορά σε ζητήματα πρόβλεψης/παλινδρόμησης (SVR)], γ) οι ανερχόμενες Gaussian Processes (GP) και δ) η Τοπικά Σταθμισμένη μη Παραμετρική Παλινδρόμηση (Loess).

Το μοντέλο social force περιέχει πέντε παραμέτρους: τις αποστάσεις μεταξύ του εξεταζόμενου πεζού και των πεζών που του ασκούν απωθητικές επιδράσεις, των πεζών που του ασκούν ελκτικές επιδράσεις, των σταθερών σημείων στο χώρο κίνησης (εμπόδια) και του επόμενου σημείου προορισμού και της ταχύτητας των πεζών που ασκούν απωθητικές επιδράσεις. Στην παρούσα έρευνα μια δίκαιη σύγκριση μεταξύ του μοντέλου social force και των τεσσάρων μεθόδων ανάλυσης δεδομένων επιχειρήθηκε. Για τον σκοπό αυτό για το σχεδιασμό του μοντέλου κίνησης των μεθόδων ανάλυσης δεδομένων υιοθετήθηκαν οι παράμετροι που χρησιμοποιούνται από το μοντέλο social force. Ένας περιορισμός σε αυτή τη διαδικασία αφορά στο γεγονός πως η μέθοδος Loess μπορεί να χρησιμοποιήσει έως τρεις μεταβλητές. Ως εκ τούτου για τη συγκεκριμένη μέθοδο οι ακόλουθες παράμετροι (οι οποίες υιοθετήθηκαν από το social force μοντέλο) ελήφθησαν υπόψη, ήτοι η ταχύτητα του πεζού στο παρόν χρονικό βήμα και οι αποστάσεις μεταξύ του εξεταζόμενου πεζού και α) των πεζών που του ασκούν απωθητικές επιδράσεις και β) των εμποδίων.

Στον προσδιορισμό του μοντέλου (που πρόκειται να ενσωματωθεί στις μεθόδους ανάλυσης δεδομένων) οι αποστάσεις διαχωρίστηκαν σε δύο άξονες αντιπροσωπεύοντας τις οριζόντιες και τις κάθετες προβολές από τους/τα πεζούς/εμπόδια. Σε περιπτώσεις όπου υπάρχουν πλέον τους ενός πεζού (που ασκεί είτε απωθητικές είτε ελκτικές επιδράσεις) ή εμποδίου και εξαιτίας του γεγονότος πως οι μέθοδοι ανάλυσης δεδομένων λαμβάνουν υπόψη μία τιμή για κάθε μεταβλητή, προσδιορίστηκε ένα κατάλληλο κριτήριο επιλογής. Το συγκεκριμένο κριτήριο βασίζεται στον παράγοντα του οπτικού πεδίου του πεζού και θεωρεί πως πεζοί που κινούνται εκτός του οπτικού του πεδίου (πίσω από αυτόν) ή κοντά στο όριό του (κάθετα σε αυτόν) επηρεάζουν την κίνηση του εξεταζόμενου πεζού σημαντικά λιγότερο από τους πεζούς που κινούνται μπροστά του και κοντά στην πορεία της κίνησής του.

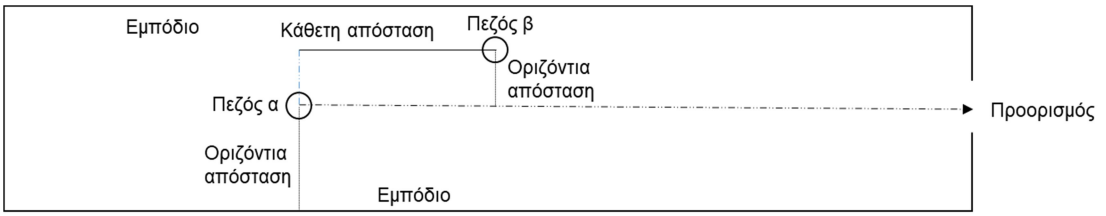

ΣΧΗΜΑ 2: Προσδιορισμός μοντέλου κίνησης για τις μεθόδους ανάλυσης δεδομένων

Η απόδοση των μοντέλων εξετάστηκε σύμφωνα με τη μέθοδο της διασταυρωμένης επικύρωσης ώστε να υπερκεραστούν τα ζητήματα μοντελοποίησης από τα οποία πάσχουν οι μέθοδοι ανάλυσης δεδομένων. Τα δύο σετ δεδομένων (ένα από την πλατφόρμα του σταθμού του μετρό και ένα από το εμπορικό κέντρο) ομαδοποιήθηκαν και στη συνέχεια αναμίχθηκαν και χωρίστηκαν σε πέντε ισομεγέθη σετ δεδομένων. Κατά τη διαδικασία εκπαίδευσης των μοντέλων ο στόχος είναι να εκτιμηθούν οι παράμετροι του κάθε μοντέλου που ελαχιστοποιούν τη συνάρτηση κόστους, ήτοι το μέσο τετραγωνικό σφάλμα της ταχύτητας του πεζού. Καθώς η ταχύτητα του πεζού διαχωρίστηκε σε δύο άξονες, χρησιμοποιήθηκαν μοντέλα ανάλυσης δεδομένων πολλαπλών αποτελεσμάτων. Επιπροσθέτως, καθώς το social force μοντέλο δεν διαθέτει έναν αλγόριθμο εκπαίδευσης (σε αντίθεση με τις μεθόδους ανάλυσης δεδομένων), χρησιμοποιήθηκε ένας γενετικός αλγόριθμος για την εκπαίδευσή του. Δυο εναλλακτικές προσεγγίσεις που εξετάζουν τις παραμέτρους με τη μεγαλύτερη επίδραση και στη συνέχεια εκπαιδεύουν το social force μοντέλο μόνο γύρω από αυτές παρουσιάστηκαν επίσης. Καθώς, όμως, οι γενετικοί αλγόριθμοι υπερτερούν της προαναφερθείσας ανάγκης για εξέταση των παραμέτρων με τη μεγαλύτερη επίδραση ενώ έχουν αποδείξει την ευρωστία τους στον τομέα της βελτιστοποίησης, υιοθετήθηκαν στην παρούσα έρευνα.

Ένα σύνολο δεικτών χρησιμοποιήθηκε για την ποσοτικοποίηση της καλής προσαρμογής και της απόδοσης των μοντέλων. Τα αποτελέσματα υποδεικνύουν πως οι μέθοδοι ανάλυσης δεδομένων έχουν καλύτερη δυνατότητα προσομοίωσης της κίνησης των πεζών καθώς αποδίδουν καλύτερα με βάση όλους τους προαναφερθέντες δείκτες. Το θεωρητικό μοντέλο (social force) εμφάνισε υψηλότερες τιμές σφαλμάτων σε σχέση με τα μοντέλα ανάλυσης δεδομένων, με το μοντέλο της Loess να εμφανίζει την υψηλότερη απόδοση. Επίσης το μοντέλο social force εμφάνισε υψηλά συστημικά και μη συστημικά

σφάλματα τα οποία σχεδόν δεν υπήρχαν στα μοντέλα ανάλυσης δεδομένων. Επιπλέον τα μοντέλα ανάλυσης δεδομένων διεξήγαν τη διαδικασία της διασταυρωμένης επικύρωσης σημαντικά ταχύτερα από το social force μοντέλο. Από την άλλη πλευρά πρέπει να επισημανθεί πως το social force μοντέλο παρέχει ένα ολοκληρωμένο πλαίσιο προσομοίωσης όπου η κάθε παράμετρος σχετίζεται με το αποτέλεσμα του μοντέλου. Το μοντέλο επεξηγεί ευκρινώς τις αλληλεπιδράσεις των πεζών και τον τρόπο με τον οποίο κινούνται (υψηλό επίπεδο ερμηνευσιμότητας) εν αντιθέσει με τις μεθόδους ανάλυσης δεδομένων που αντιμετωπίζονται, σε κάποιο βαθμό, ως «μαύρα κουτιά».

Επιπροσθέτως μια σύγκριση μεταξύ των τεσσάρων μοντέλων ανάλυσης δεδομένων κατέδειξε πως το μοντέλο της Loess αποδίδει καλύτερα σύμφωνα σχεδόν με κάθε δείκτη, τα ΤΝΔ και οι GP παρουσίασαν αντίστοιχο επίπεδο απόδοσης, ενώ οι SVR παρείχε υποδεέστερες προβλέψεις. Πρέπει επίσης να επισημανθεί πως το μοντέλο της Loess απέδιδε καλύτερα ακόμη και αν ενσωμάτωνε μικρότερο αριθμό μεταβλητών σε σχέση με τις υπόλοιπες μεθόδους ανάλυσης δεδομένων, ενώ διεξήγε τη διαδικασία της διασταυρωμένης επικύρωσης σε σημαντικά λιγότερο χρόνο. Σε αντίθεση είναι ξεκάθαρο πως υπάρχουν περιορισμοί που σχετίζονται με την αδιαφάνεια και την έλλειψη ερμηνευσιμότητας των μοντέλων ανάλυσης δεδομένων. Μία σύγκριση των δεικτών σε κάθε γύρο της διαδικασίας της διασταυρωμένης επικύρωσης αποκάλυψε πως τα μοντέλα ανάλυσης δεδομένων τείνουν να υπερμοντελοποιούν καθώς μαθαίνουν/εξελίσσονται από τα δεδομένα.

Στο τελευταίο στάδιο της παρούσας έρευνας ενσωματώθηκαν τρεις επιπλέον μεταβλητές στα μοντέλα ανάλυσης δεδομένων ώστε να εξεταστεί αν δύναται να βελτιωθεί η απόδοσή τους. Οι επιπλέον μεταβλητές επιλέχθηκαν σύμφωνα με τη βιβλιογραφική ανασκόπηση. Αρχικά προστέθηκαν το ύψος και το φύλο του πεζού. Το ύψος του πεζού εκτιμήθηκε με τη βοήθεια φωτογραμμετρικών εργαλείων. Η μέθοδος Loess δεν δύναται να εφαρμοσθεί σε αυτήν την ανάλυση καθώς αδυνατεί να συμπεριλάβει επιπλέον μεταβλητές. Τα αποτελέσματα αυτής της ανάλυσης υποδεικνύουν πως η ενσωμάτωση των χαρακτηριστικών του πεζού μπορεί να βελτιώσει την απόδοση των μοντέλων ανάλυσης δεδομένων που αφορούν στην προσομοίωση της πεζής κίνησης (αποδίδουν καλύτερα σύμφωνα σχεδόν με κάθε δείκτη). Ακόμη εξετάστηκε η πρόσθετη ενσωμάτωση της παραμέτρου του χρόνου στα μοντέλα ανάλυσης δεδομένων. Τα

αποτελέσματα αυτής της διαδικασίας μοιάζουν αρκετά με τα αποτελέσματα των μοντέλων ανάλυσης δεδομένων με τις επιπλέον μεταβλητές των χαρακτηριστικών του πεζού. Ειδικότερα τα μοντέλα μετά την ενσωμάτωση της παραμέτρου του χρόνου φαίνεται να αποδίδουν καλύτερα με βάση κάθε δείκτη. Γενικά η ενσωμάτωση επιπλέον μεταβλητών φαίνεται να βελτιώνει, κυρίως, την απόδοση του μοντέλου των ΤΝΔ υποδεικνύοντας πως η συγκεκριμένη μέθοδος δύναται να «χειριστεί» αποδοτικότερα την ενσωμάτωση επιπλέον μεταβλητών.

Τα συμπεράσματα και η συνεισφορά της έρευνας παρατίθενται παρακάτω:

- Παροχή ενός πλαισίου ελαχιστοποίησης του θορύβου των δεδομένων (τροχιές πεζών)
    - Ενίσχυση της απόδοσης του Unscented Kalman Filter με την ενσωμάτωση σε αυτό του συμμετρικού κινητού μέσου όρου
    - Εκτίμηση των μητρώων συνδιακύμανσης σφαλμάτων σε περιπτώσεις που αυτές δεν είναι γνωστές
- Ανάπτυξη μοντέλου προσομοίωσης της πεζής κίνησης για την ενσωμάτωσή του στις μεθόδους ανάλυσης δεδομένων
- Χρονικά αποδοτική βαθμονόμηση του μοντέλου social force
- Υπόδειξη της αποδοτικότητας των μοντέλων ανάλυσης δεδομένων στον τομέα της προσομοίωσης της πεζής κίνησης (σε σχέση με τα θεωρητικά μοντέλα προσομοίωσης)
- Βελτίωση της απόδοσης των μοντέλων ανάλυσης δεδομένων όταν αυτά ενσωματώνουν επιπλέον παραμέτρους της προσομοίωσης της πεζής κίνησης

Μια ενίσχυση των μοντέλων ανάλυσης δεδομένων μπορεί να επιτευχθεί με την ενσωμάτωση επιπλέον παραμέτρων. Ένα παράδειγμα θα μπορούσε να αποτελέσει η υιοθέτηση του μεγέθους της πυκνότητας των πεζών ώστε να συμπεριληφθεί στο μοντέλο όχι μόνο ο πεζός που επιδρά περισσότερο στον εξεταζόμενο πεζό αλλά όλοι οι πεζοί που βρίσκονται σε κοντινή απόστασή του. Επιπλέον, πρόσθετα δεδομένα θα μπορούσαν να συμπεριληφθούν για μια βελτιωμένη αξιολόγηση των μοντέλων. Ακόμη ένα ενδιαφέρον ερευνητικό αντικείμενο θα μπορούσε να αποτελέσει η διερεύνηση της κίνησης των πεζών όταν αυτοί αλληλεπιδρούν με οχήματα. Θα μπορούσε να εξεταστεί η εφαρμογή μοντέλων ανάλυσης δεδομένων σε αυτές τις περιπτώσεις. Αυτή η σημείωση είναι

σημαντική καθώς πιθανώς να ενίσχυε την απόδοση των αυτόνομων οχημάτων. Επιπλέον στην παρούσα έρευνα εξετάστηκε η παράμετρος του χρόνου για την επίδρασή στα μοντέλα ανάλυσης δεδομένων. Κατά συνέπεια τα Αναδρομικά Νευρωνικά Δίκτυα (κατηγορία των ΤΝΔ) και ειδικότερα η αρχιτεκτονική των δικτύων Μακράς και Βραχείας Μνήμης θα μπορούσαν να εξεταστούν σε περιπτώσεις προσομοίωσης της πεζής κίνησης. Τέλος, μια σύγκριση στην κίνηση των πεζών υπό κανονικές συνθήκες και υπό συνθήκες εκτάκτου ανάγκης θα μπορούσε να διερευνηθεί ώστε να προσδιοριστούν οι διαφοροποιήσεις στη συμπεριφορά των πεζών όταν αυτοί κινούνται σε συνθήκες έκτακτης ανάγκης. Αυτό θα βελτίωνε την απόδοση των μοντέλων προσομοίωσης της πεζής κίνησης παρέχοντας ένα πιο ολιστικό πλαίσιο, όπως επίσης και τα μοντέλα προσομοίωσης της κίνησης οχήματος – πεζού.

Contents

List of figures

List of tables

List of abbreviations

ANN:	Artificial Neural Networks
CA:	Cellular Automata
CTM:	Cell Transmission Model
DML:	Dynamic Multi-Lane
EKF:	Extended Kalman Filter
EMA:	Exponential Moving Average
GIS:	Geographic Information Systems
GoF:	Goodness-of-Fit
GP:	Gaussian Processes
GPS:	Global Positioning System
GSA:	Global Sensitivity Analysis
ICM:	Intrinsic Coregionalization Model
IRWLS:	Iterative Re-Weighted Least Square
LiDAR:	Light Detection and Ranging
LMC:	Linear Model of Coregionalization
Loess:	Locally Weighted Regression
LSTM:	Long Short – Term Memory
MLP:	Multi-Layer Perceptron
MPE:	Mean Percentage Error
MPT:	Matlab Photogrammetric Toolbox
MSE:	Mean Squared Error
MSVR:	Multioutput Support Vector Regression
OAT:	One-At-a-Time
sSMA:	symmetric Simple Moving Average
SVC:	Support Vector Clustering
SVM:	Support Vector Machines
SVR:	Support Vector Regression
RBF:	Radial Basis Function
ReLU:	Rectified Linear Unit
RFID:	Radio Frequency Identification
RMSN:	Normalized Root Mean Square Error
RMSPE:	Root Mean Square Percentage Error

RNN:	Recurrent Neural Networks
UAV:	Unmanned Aerial Vehicles
UKF:	Unscented Kalman Filter
UT:	Unscented Transformation
WMA:	Weighted Moving Average

1. INTRODUCTION

1.1. Overview

1.1.1. Theoretical models

The significant increase of urbanization which has resulted in the formation of densely populated cities i.e. the concentration of a relatively large number of people in a limited space, has significantly affected everyday living. At the same time, modern urban infrastructures, (underground railway stations, shopping malls, tall buildings) being a significant element of city design, greatly affect travel patterns (Klingsch, 2010), resulting in substantial changes in transportation network elements design. Therefore, the construction of necessary infrastructures and the management/regulation of existing ones are of great importance considering quality of life in the cities.

For this reason it is necessary to understand the movement behaviour of citizens; and with walking being a major component of all urban trips nowadays, the need to comprehend pedestrians' behaviour comprises a prerequisite for the design of a sustainable transportation system. Pedestrian movement differs substantially from vehicle movement, and is much more complex. As Burstedde et al. (2001) mentioned, pedestrians are more flexible and more intelligent than cars, and they can choose an optimum route according to the environment around them taking into account only a small number of constraining elements. Even slight bumping is acceptable and need not be absolutely avoided as in traffic flow models (Burstedde et al., 2001).

Pedestrian simulation has gained greater interest from researchers during the last two decades. Advanced models of traffic simulation, which can determine, with considerable accuracy, traveller behaviour at a macroscopic or a microscopic level (e.g. trip generation and distribution, model choice, traffic assignment and driver and pedestrian behaviour), have been developed. In many studies, pedestrian movement is compared with fluid movement (e.g. Helbing, 1992). Econometric models, which rely greatly on probabilities as well as models, which take into account psychological factors, are also used in pedestrian

simulation. Moreover, models based on scientific disciplines (physics, biology, chemistry, etc.) have also been developed. On the other hand, most of the studies on pedestrian simulation, focus on specific parameters (e.g. infrastructure architecture, pedestrian characteristics, time period in a day, etc.) failing to consider a more integrated approach. In general, a wide range of pedestrian simulation models have been developed, including the social force model, cellular automata, lattice gas and route choice models (for a review cf. Kouskoulis and Antoniou 2017). All of the aforementioned models consider the agent's desired path and surroundings; in this case being pedestrians and obstacles.

1.1.2. Data-driven models

Statistics set the ground for basic modeling. Regression analysis (linear, polynomial etc.) is a useful tool for quantifying parameters' impact. Nevertheless, regression analysis is subject to parametric limitations (e.g. data obtained from Gaussian distribution, hard to define a priori the type of the mathematical model, etc.) and is applied in cases where the researcher has specific clues for the most appropriate model.

A revolution in many scientific fields has been observed during the past decades with the emergence of data-driven analytics and machine learning theory. Following up on the continuous widespread availability of data and computational advances, data-driven modeling has been increasingly gaining researchers' interest over the last decades. Several methods and techniques [including Artificial Neural Networks (ANN) and Support Vector Machines (SVM), among others] have been developed and provide their simulation robustness in terms of clustering, classifying and regression. These techniques do not require a priori knowledge of the relationships among the model variables, but they "learn" from the data.

Data-driven theory differs from classical statistics as its methods are non-parametric. Theoretical models, on the other hand, provide a straight mathematical framework, while relating model parameters based on logical principles and rules. Hence, data-driven methods are not subject to parametric limitations (data obtained from Gaussian distribution, complexity of defining a

priori the type of the mathematical model, etc.) and, as a consequence, are widely applicable. They are based on data (data-driven), without providing a specific mathematical framework, and can deal with large and complicated data. Locally weighted regression (Loess, Cleveland 1979) is an example of a data-driven regression method, a non-parametric tool that can deal with complicated data and model circumstances. Its validity on the development of traffic simulation models has already been demonstrated (e.g. Antoniou et al., 2013; Papathanasopoulou and Antoniou, 2015).

Data-driven models require a vast amount of data in order to gain the accurate modeling information, which in turn necessitates higher computational requirements. Though these methods were initially developed several years ago, they have been spreading only recently due to growing data availability and the enhancement of computational power.

1.2. Aim

The aim of this research is to examine whether data-driven methods can provide a robust model framework for pedestrian simulation. To achieve this, their performance is compared against a “traditional” (i.e. widely used) pedestrian simulation model. The inherent difference of these two categories is that conventional models can stipulate a straight mathematical framework based on logical principles, while data-driven techniques do not comprise a clear mathematical model. While no clear drawbacks of the theoretical pedestrian simulation models have been considered, according to the literature review, the goal of this thesis is to investigate if data-driven techniques (whose presence is strong in many research fields during the last decades) can produce a more efficient pedestrian simulation modelling framework.

The present research proposes a data-driven pedestrian simulation framework and investigates its appropriateness of use alongside theoretical models (a first attempt considering one standalone data-driven method is presented in Kouskoulis et al., 2018). Pedestrian trajectories are therefore collected and simulated using both a theoretical model and data-driven techniques – namely, the social force model and four well-known data-driven methods.

Prior to the application of these methods, an appropriate data noise elimination filter is applied, i.e. a combination of Unscented Kalman filtering and the moving average method due to the fact that initially extracted data include noise.

Subsequently to the models' comparison improved models that incorporate additional pedestrian simulation parameters are tested in order to evaluate their performance compared to the initially designed data-driven pedestrian simulation models.

Thus, the objectives of this thesis are described explicitly below:

- Extend/improve an algorithm for reducing noise in pedestrian trajectories data
- Develop a framework for pedestrian simulation that can be employed in data-driven techniques
- Assess the performance of data-driven techniques (using the pedestrian simulation model) by comparing them with an established theoretical pedestrian simulation model utilizing the appropriate methodology and metrics
- In case data-driven pedestrian simulation models perform better (than the theoretical one), enhance them with additional potentially relevant, i.e. that are anticipated to affect pedestrian movement, parameters and evaluate their performance.

The first objective revolves around the proposal and validation of a Kalman–filtering–based (Kalman, 1960) procedure for noise reduction. An extension [Unscented Kalman filter (Wan and Van der Merwe, 2000)] of the filter is employed in order to relax standard algorithm assumptions. A method for estimating noise covariance matrices is presented, while an extension of the moving average is incorporated in the Kalman filter.

The second and third objectives involve the comparison between data-driven and theoretical pedestrian simulation models. In this research, the social force model is selected as the most representative theoretical model. The social force model has been widely used in pedestrian simulations and forms the basis for simulation software [e.g. VisWalk (PTV, 2015) and SimWalk (Zainuddin et al.,

2009)]. Furthermore, it relies on the same principles as the other main pedestrian simulation models.

As for machine learning techniques, four promising methods are utilized: a) the well-known ANN, b) the classical SVM [in particular as we refer to regression analysis, Support Vector Regression (SVR) is employed], c) the rising Gaussian Processes (GP), and d) the Locally Weighted Regression (Loess).

In parallel a continuous updated literature review is conducted in order to identify additional parameters that affect pedestrian movement or/and improved versions of the employed models.

It should be clarified that in this study we focus only on pedestrian movement, where pedestrians interact only with stationary obstacles and/or stationary or moving pedestrians. Pedestrian – vehicle interactions are not considered.

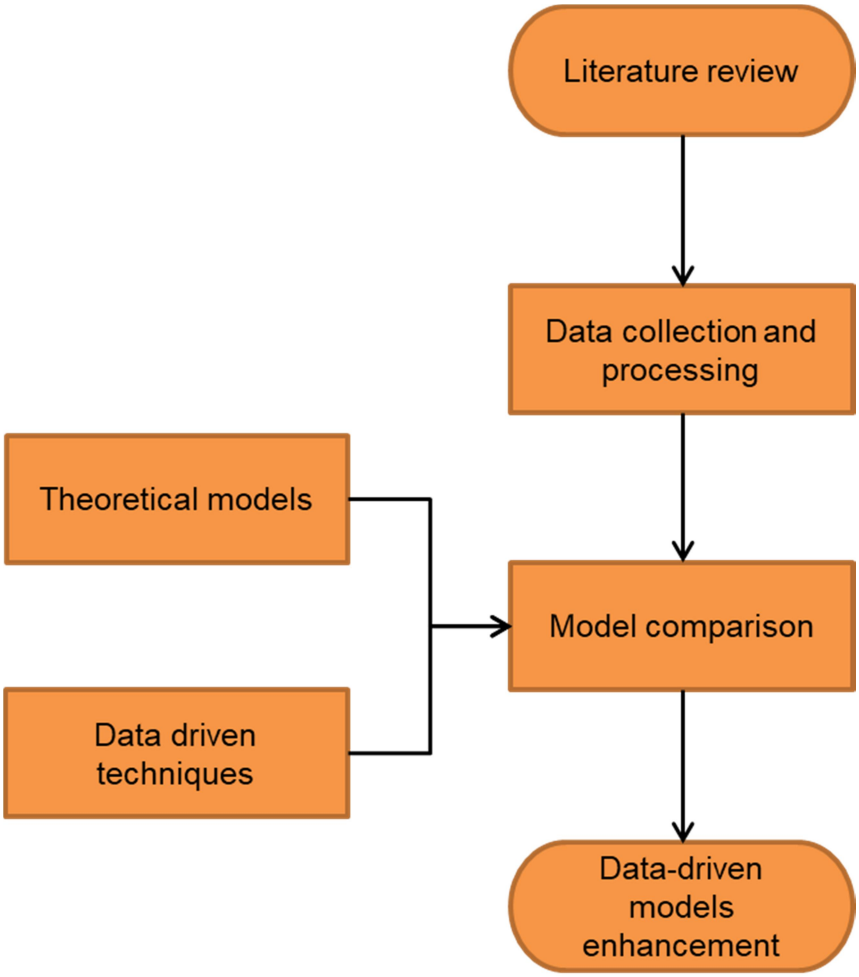

Figure 1.1: Conceptual framework

1.3. Structure

The remainder of this thesis is organized as follows. Chapter 2 comprises the literature review in which relevant studies with their results are described. In an extended review the basic theoretical approaches for pedestrian movement are presented. The parameters that affect pedestrian movement in theoretical approaches are also highlighted. In addition, data-driven methods for pedestrian simulation are also described. A specific section on emergency situations is presented due to the increased interest of the research community. Validation and data collection methods are also presented in this Chapter.

In Chapter 3, the methodological framework is illustrated. Initially the design of the data collection experiment is presented. Due to the fact that the collected data (i.e. pedestrian trajectories) include noise, the main methods for data filtering (existing smoothing filters) are described. Subsequently a presentation of the social force model is provided through its governing rules and its parameters, while also considering the most recent model updates. The main data-driven methods are demonstrated with their extensions related to the present experiments (most of these techniques result to one dimensional output, while the current experiment is a two dimensional one). Their pros and cons are also discussed. Finally the framework for the comparative analysis is outlined.

Chapter 4 describes the methodology for data collection and processing. The data collection sites are defined. The cameras' setup and the experimental design for this procedure are presented. The photogrammetric technique utilized to estimate agent's ground coordinates is also described. An extension of this technique leads to the estimation of pedestrian's height, a parameter that will be used next in the analysis. A specialised software that performs automated tracking from moving objects (in general), utilized in this research, is also described. Last, the algorithm that has been developed based on existing smoothing filters and leads to data noise elimination is provided.

Chapter 5 illustrates the comparative analysis results. The performance of the theoretical pedestrian simulation model and the data-driven approaches is compared. Prior to this the description of the machine learning model setup, appropriate for pedestrian simulation, is elaborated. Suitable transformations of

the model parameters are conducted where required. Cross-validation process is used to avoid data-driven models' overfitting, while a genetic algorithm is employed for calibrating the theoretical pedestrian simulation model's parameters. Complementary two different types of sensitivity analysis which reveal the model parameters with the highest impact are presented. Due to the fact that genetic algorithms overcome the need of examining the most effective parameters, the sensitivity analysis methods are cited in the current thesis for the sake of an integrated approach. The results of the simulations are also presented in this Chapter. An extended data-driven model that includes additional pedestrian movement parameters is also designed and evaluated.

Chapter 6 presents the results of the comparative analysis described in the previous chapter. The findings of this research are discussed and their contributions are clarified, while also limitations of the study (related to the data-driven theory) are provided. Ultimately, directions for future research are outlined.

1.4. Acknowledgment

Part of this research was supported by the Action: ARISTEIA-II (Action's Beneficiary: General Secretariat for Research and Technology), co-financed by the European Union (European Social Fund – ESF) and Greek national funds.

2. BACKGROUND ON PEDESTRIAN MODELING

2.1. Overview

In this section the literature review that is relevant to pedestrian simulation is presented. The results of the relevant studies are discussed and the parameters employed in the different pedestrian simulation models are classified in meaningful distinct categories. The section is based on the review of Kouskoulis and Antoniou (2017).

Pedestrian simulation has become a crucial element in integrated transport analysis, mainly in the past three decades, as transport engineers have realized its significance considering traffic management (Akin and Sisiopiku, 2007; Helbing et al., 2005) and public transportation network design (Daamen et al., 2002). Furthermore, reliable pedestrian simulation models comprise a prerequisite for the implementation of specific intelligent transportation systems and autonomous vehicles (Matthews et al., 2017). Therefore the necessity for exploring pedestrian walking behaviour and forecasting pedestrian movement has brought a lot of attention to pedestrian simulation.

The principle for every simulation method is model development. In general, simulation models are classified according to their level of analysis in microscopic, for individual pedestrian behavior, and macroscopic, for aggregated dynamics. Mesoscopic models have been also developed though at a lesser degree. Pedestrian simulation models can also be classified according to the pedestrian walking theory that is applied to represent their dynamics. Examples of microscopic models considering the adopted walking theory include social force models, cellular automata, and so on, and are presented in section 2.2.

Fundamental diagrams are, also, of major importance in traffic simulation and as a consequence in pedestrian simulation. Through these diagrams the relation between density and velocity (or other fundamental magnitudes) is visualized and a better overview to the planner is provided. An analysis of these diagrams is presented in section 2.3.

In the recent years, a relatively low – yet increasing – number of approaches that deal with pedestrian simulation problems employing data-driven methods have been presented. Still these models are at a rather early stage of development and have not been widely applied yet. Some of those models also adopt principles from the existing microscopic models. These are presented in section 2.4.

As it is widely known, a model is not reliable unless its results are validated. Validation techniques have attracted the interest of the scientific community because they are essential in model development. Data collection tools, such as sensors, cameras and so on, are utilized to provide to the researchers the appropriate data in order to verify their theory. In terms of pedestrian simulation models the appropriate data involve, mainly, pedestrian trajectories. The existing tools and methods for collecting pedestrian trajectory data are demonstrated in section 2.7.

Pedestrian simulation under emergency conditions, has gained researchers' interest, mainly during the last decade. Although the design of pedestrian simulation models for emergency situations is significant, only a small number of studies focus on pedestrian evacuation (Vermuyten et al., 2016). Still this number has increased in the recent years. Urban and metropolitan areas exhibit an increase in population and as a consequence the frequency of emergencies has also increased. Floods, tsunamis, volcanic eruptions and fires are examples of such emergencies. The importance the representation of pedestrian movement under emergencies is acknowledged and the adopted approaches are presented in section 2.6.

2.2. Theoretical approaches

Pedestrian behavior considering walking follows specific rules. Several researchers have focused on simulating pedestrian movement based on various sets of logical rules. These efforts resulted in the development of analytical approaches. In the same manner as in traffic simulation, pedestrian models are divided in two major categories according to the level of analysis:

- Microscopic (e.g. Gipps and Marksjo, 1985; Helbing and Molnár, 1995; Teknomo, 2006) focusing on individual pedestrian dynamics and characteristics; and

- Macroscopic (Hughes, 2000), which consider aggregate characteristics of pedestrian flows (e.g. mean velocity, mean density) and are used at a substantially lesser degree.

Macroscopic approaches may fail to capture accurately specific phenomena in pedestrian simulation (Løvås, 1994). As a result microscopic models are mainly developed for pedestrian simulation. At the same time microscopic simulation has a high computational cost, which has been reduced with the enhancement of hardware and software capacities (Teknomo, 2006). Nikolić et al. (2013) mentioned mesoscopic models, an intermediate level between microscopic and macroscopic, which has not been widely applied in pedestrian simulation. A typical example is that of Tordeux et al. (2018a) where pedestrian movement is described at an aggregated level while, at the same time, individual pedestrians are considered. Another example is that of cell transmission models (CTM) where obstacles are discretized into grids. This type of models can describe both general and detailed characteristics of pedestrian flows (Li and Guo, 2020). In addition, Duives et al. (2013) referred to hybrid models as a combination of microscopic and macroscopic models. Not significantly different from mesoscopic models, hybrid models consider human interactions at a microscopic level while using macroscopic background for reducing the models' computation time.

Pedestrian simulation models are also classified pertaining to the theory which describes the way that pedestrians walk. Three major categories can be identified considering microscopic models (Figure 2.1):

- Social force;

- Cellular automata; and

- Lattice gas.

Complementary to the above categories route choice theory is a method that is mainly utilized in combination with other models (for example the behavioral

theory model arises from a combination of the social force model and the route choice theory), rather than as a stand-alone model.

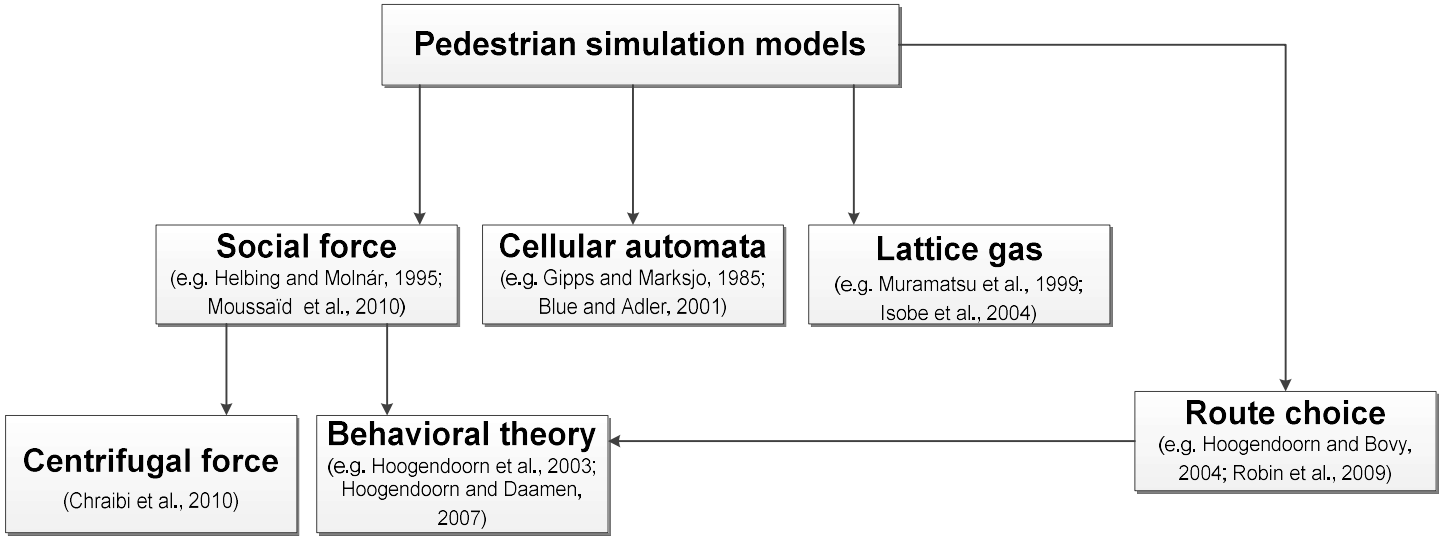

Figure 2.1: Categorization of pedestrian simulation models (microscopic)

Other types of pedestrian model categories have also been found in the literature. Duives et al. (2013) presents a more detailed classification in pedestrian modeling as:

- Cellular automata;
- Social force;
- Activity choice;
- Velocity based;
- Continuum;
- Hybrid;
- Behavioral; and
- Network models.

Guo et al. (2010) added semi-continuous models, while Ma and Song (2013) focused on distinguishing continuous and discrete pedestrian simulation models. Das et al. (2014) categorized microscopic (pedestrian simulation) models as:

- Cellular automata;
- Forced based;
- Queuing; and
- Agent-based.

Last, Vermuyten et al. (2016) classified pedestrian simulation models as:

- Continuum;
- Network based;
- Cellular automata;
- Agent based;
- Social force; and
- Game theoretic.

Many of the aforementioned categories are not clearly separated from the others. For example agent-based models comprise a rather general category that does not provide any specific rules (i.e. as a stand-alone model) in terms of the theory according to which an agent walks, but can overlap with other models (e.g. social force as mentioned in Xing et al., 2017). The four most commonly used categories of theoretical pedestrian models are presented in the following sections.

2.2.1. Social force

The principle of social force models, or in general force based models, arises from the assumption that pedestrian dynamics are determined from the repulsive and attractive forces that are acted on the moving pedestrian (Figure 2.2). In one

of the earliest approaches, when the need introducing microscopic models in pedestrian simulation was suggested, mostly, due to the inability of macroscopic models to capture the variations in pedestrians' movements, Gipps and Marksjo (1985) simulated pedestrian movement using cellular automata and applied social forces in order to determine pedestrians' direction. A gain function was calculated for every adjacent cell and pedestrians moved to the cell with the highest gain. An advantage of this method is that it refers to the perceived - by the pedestrian - distance and not to the actual distance.

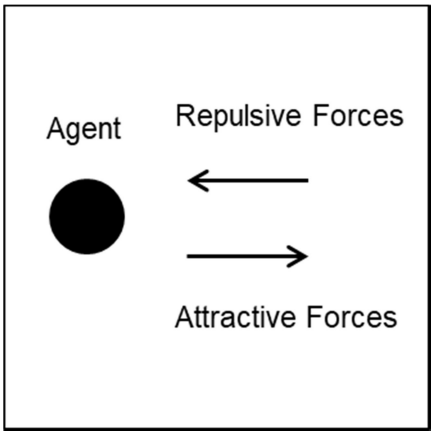

Figure 2.2: Social force model approach

Subsequently, Helbing and Molnár (1995) set the principles for the application of social force models in pedestrian simulation. Based on Langevin equations (stochastic equations) they examined pedestrian movement taking into account the environment's influence. The model considers three elements:

a) the aim of reaching a certain destination;

b) the influence of other pedestrians, borders, or both; and

c) the attractive effects of other persons or objects.

The first element is related to the agent's desired direction. This is determined considering the pedestrian's objective, which is to reach their destination. It is also related to the deviation of the pedestrian's actual velocity compared to their desired velocity (τ – relaxation factor). The second element concerns the repulsive effects that are provoked by the pedestrian's surroundings. The repulsive forces decrease exponentially as the distance from the obstacle(s)

increases. The third element is the opposite of the second and can be caused by objects (e.g. advertisements) or persons that attract pedestrian's attention and disrupt them while moving towards their destination. Helbing and Molnár (1995) study also suggests that in a narrow door, where only one stream can pass through, pedestrians of the opposite stream will have to wait.

The basic function describing the dynamics of social force models is (Helbing and Molnár, 1995):

$$\vec{F_\alpha}(t) = \vec{F_\alpha^0}(\vec{u_\alpha}, u_\alpha^0 \vec{e_\alpha}) + \sum_\beta \vec{F_{\alpha\beta}}(\vec{e_\alpha}, \vec{r_\alpha} - \vec{r_\beta}) + \sum_B \vec{F_{\alpha B}}(\vec{e_\alpha}, \vec{r_\alpha} - \vec{r_B^\alpha}) + \sum_i \vec{F_{\alpha i}}(\vec{e_\alpha}, \vec{r_\alpha} - \vec{r_i}, t)$$

where

$\vec{F_\alpha}(t)$ = pedestrian's total motivation;

$\vec{F_\alpha^0}$ = pedestrian's desire;

$\vec{F_{\alpha\beta}}$ and $\vec{F_{\alpha B}}$ = repulsive forces from other pedestrians and from borders (e.g. walls, obstacles), respectively; and

$\vec{F_{\alpha i}}$ = attractive forces.

A grouping factor in social force models was introduced by Moussaïd et al. (2010). They mentioned that pedestrians move not only individually, but also in groups due to their social lives. In particular they found out that the proportion of pedestrian groups in the pedestrian population follows a Poisson distribution. They imported a group force in the equation of the social force model and transformed the model as (Moussaïd et al., 2010):

$$\frac{d\vec{u_\alpha}}{dt} = \vec{F_\alpha^0} + \vec{F_\alpha^{wall}} + \sum_\beta \vec{F_{\alpha\beta}}(\vec{e_\alpha}, \vec{r_\alpha} - \vec{r_\beta}) + \vec{F_\alpha^{group}}$$

$\vec{F_\alpha^{wall}}$ = the repulsive effects of boundaries;

$\vec{F_\alpha^{group}}$ = the response of pedestrian α to other group members.

The above groups only apply to up to 4 agents. In cases of more pedestrians the groups are split up.

Chraibi et al. (2010) introduced the collision detection technique to limit overlapping between pedestrians, while a heuristic function that defines pedestrian direction in cases of trying to avoid obstacles was mentioned by Moussaïd et al. (2011).

An extensive presentation of the social force model is provided in section 3.3 in order to be explicitly described for the scope of the models' comparison. In that section an improved modified version of the social force model, developed by Helbing and Johansson (2010), is also presented.

2.2.2. Cellular automata

Although cellular automata (CA) are most commonly used in microscopic approaches (e.g. Gipps and Marksjo 1985; Burstedde et al., 2001; Blue and Adler, 2001; Weifeng et al., 2003; Flötteröd and Lämmel, 2015), they have also been adopted in a mesoscopic context (Papadimitriou et al., 2014).

Gipps and Markjso (1985) set the groundwork for CA in the field of pedestrian simulation. Since, the first adoption of CA for simulation in the transport field, CA was revised in 1992 by Nagel and Schreckenberg who introduced the CA for vehicular traffic. Their model proved to be quite effective and increased its popularity in the transport field. The CA theory is based on space discretization (rather than considering space as a continuous element as in the social force model). The explored area is separated in cells of specific dimensions, in which pedestrians move (Figure 2.3).

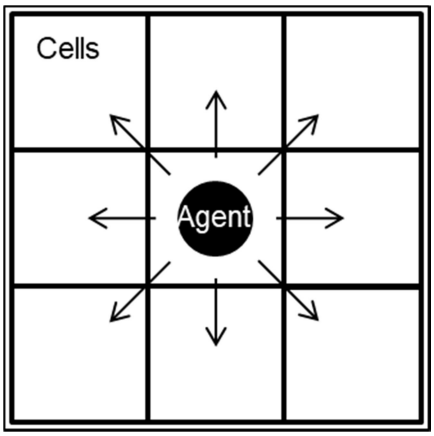

Figure 2.3: Cellular automata approach (based on Burstedde et al., 2001)

In most studies, the cell dimensions are 0.4m X 0.4m (Burstedde et al., 2001; Isobe et al., 2004; Ma and Song, 2013; Li et al., 2019; Lu et al., 2015; Weifeng et al., 2003), while in Gipps and Markjso (1985) they are 0.5m X 0.5m. In addition, Löhner and Haug (2014), though not related to the cellular automata theory, estimated agent's length and width (in crowd situations) to be 0.3m and 0.5m respectively. Furthermore, Kretz et al. (2011) determined the lower range of human body diameters between 0.15m and 0.20m. Guo et al. (2012) specified cell dimensions as 0.2m X 0.2m to be able to represent also objects' dimensions. Hexagonal cells have also been found in recent studies (e.g. Torres-Ruiz et al., 2017).

According to the CA adaptation for pedestrian simulation, obstacles, walls, and people occupy cells of the space. Each cell can be occupied at most by one agent. In the initial simulation step, the space is divided in occupied and unoccupied cells. At every simulation step, the condition movement of the agent is updated and the agent can either move to one of the neighbouring cells or remain at the same cell. A new layout of occupied and unoccupied cells is then created. The same process is repeated for each simulation step. Both von Neumann neighborhoods (four cells neighborhood type) and Moore neighborhoods (nine cells neighborhood type) have been studied. Cellular automata models can also simulate pedestrian group movement (Vizzari et al., 2013).

CA's advantage is the simplicity of their rules (Lu et al., 2015), while their disadvantage becomes evident in large simulation scenarios where increased memory requirements are noted (Gloor et al., 2004).

CA theory was also employed in evacuation modeling by examining pedestrian coupling and its impact on evacuation time (Müller and Schadschneider, 2016). Burstedde et al. (2001) extended cellular automata in evacuation plans by introducing the floor field, which is a second grid of cells underlying the main grid that acts as a substitute for pedestrian intelligence. This floor field demonstrates the interactions between pedestrians.

Combinations of CA and social force models are also found in the literature (Table 2.1). In such models (the combinations of CA and social force) the space segmentation element is adopted from the CA theory and the forces among pedestrians and other obstacles from the social force theory.

2.2.3. Lattice gas

Unlike the aforementioned models, lattice gas models have not been widely applied in pedestrian simulation (e.g. Muramatsu et al., 1999; Muramatsu and Nagatani, 2000; Isobe et al., 2004). They rely on the concept that pedestrians move according to the flow's strength, also referred to as drift strength. Drift strength is the primary parameter for the probability function that defines the direction of the pedestrian in the next simulation step. Pedestrians prefer to follow other pedestrians than create their own paths. Lattice gas models evince that pedestrians tend to follow their leader as they move (Isobe et al., 2004).

Muramatsu et al. (1999) applied one of the primary approaches for lattice gas models in pedestrian simulation. They separated walkers in right walkers (move to the right) and left walkers (move to the left). Their model relies on the probability of walkers to choose their next site in the next time step, which depends on the drift strength. They concluded that:

- the mean velocity increases with increasing drift;

- the mean velocity, the occupancy and the jamming transition do not depend on the ratio of the right walkers to all walkers.

This study did not include the option for pedestrian's back step. Subsequently, Muramatsu and Nagatani (2000) introduced two different types of pedestrian simulation models, one for two-way pedestrian flow and one for four-way pedestrian flow. In the first model, walkers can only move up or right, and in the second in all possible directions. The simulation of the first model (two-way) was conducted under the assumption that the density of the right walkers is equal to the density of the up walkers. Simulation experiments revealed that by increasing drift strength, critical density (the value of density when the jamming transition begins to occur) decreases while mean velocity increases. In the simulation of the second model (four-way) the density is equal for each type of walker (the walker type is defined by the direction they move). The mean velocity above the transition point is almost zero in the four-way experiment and slightly higher in the two-way. Critical density and mean velocity "react" in the same manner in both models (two-way and four-way), but the patterns are different.

Isobe et al. (2004) also utilized a lattice gas model for simulating pedestrian movement. They presented a bi-directional pedestrian flow simulation inside a channel with the assumption that the number of pedestrians is equal in each direction. The walls of the channel acted as boundaries for the pedestrians and applied repulsive forces on them. They found that the probabilities of the movement direction of an agent (transition probabilities – p_t) depend on the drift strength.

Lattice gas models have been applied in pedestrian simulation, but not as extensively as social force and cellular automata models. A thorough review of pedestrian models resulted in only 5 studies where lattice gas models were applied for pedestrian simulation. Considering the fact that all of them were edited by the same or related researchers, the real applicability of lattice gas models seems to be rather limited.

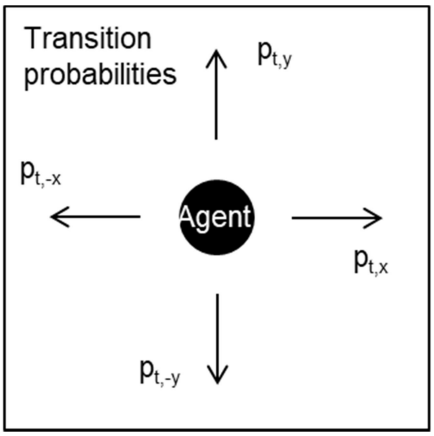

Figure 2.4: Lattice gas approach (based on Isobe et al., 2004)

2.2.4. Route choice

Naturally, route choice theory is also relevant in modeling pedestrian behavior, while it resembles its applications in vehicle traffic. Route choice probability is computed according to maximum likelihood theory.

Nested logit models have been used for maximizing the utility that an agent gains from moving from a place to another (Robin et al., 2009). The utility function consists of the following factors:

a) the tendency of an agent to keep their direction;

b) the aim of reaching their destination;

c) their acceleration in free flow conditions;

d) the tendency of following their leader;

e) the aim to avoid collisions.

In the same data sample, different categories of logit models (e.g. cross-nested and mixed nested) provide similar coefficient values (Antonini et al., 2006). An extensive literature review of pedestrian route choice models is presented in Papadimitriou et al. (2009).

Hoogendoorn and Bovy (2004) modified route choice models (behavioral theory) by inserting infinite alternative choices in pedestrian's route. Behavioral theory force models comprise actually a sub-category of social force models that combine social force and route choice models (Hoogendoorn and Bovy, 2003; Hoogendoorn and Daamen, 2007). Guo et al. (2010) introduced logit models in social force models and applied differential equations to compute movement probability. At this point it is mentioned that another sub-category of social force models are centrifugal force models, which take into consideration pedestrian velocity while adopting collision detection techniques in order to avoid conflicts and overlaps among pedestrians. Centrifugal force models are also practical for evacuating buildings (Chraibi et al., 2010).

Li et al. (2019) combined choice behavior models with cellular automata in order to simulate pedestrian movements at a ticket gate machine at a rail transit station. They set three pedestrian choice strategies including pedestrians' preferences for i) minimizing their distance, ii) selecting the queue with the minimum number of pedestrians and iii) eliminating their estimated time. Poisson distribution was applied to model pedestrians entering the station interval.

It is worth mentioning that under high-density conditions all of the aforementioned models are incapable of accurately reproducing the existing phenomena (Duives et al., 2013). Cellular automata and social force models appear more suitable for pedestrian crowd simulation.

A recent study on the field of route choice models has been conducted by Wu et al. (2021). The researchers made their experiments in a subway station. Considering the factor of local view (i.e. the fact that pedestrian's field of vision can be blocked by obstacles) they concluded that the exit's choice is related to the agent's space familiarity, while temporary directions before determining the final exit are possible and local view factor can make pedestrians to re-select their final exits.

Table 2.1: Overview of pedestrian simulation models

Source	Model level	Model category	Fundamental diagram	Experiment validation
Antonini et al. (2006)	Microscopic	Route choice theory	×	×
Blue and Adler (2001)	Microscopic	Cellular automata	✓	✓
Burstedde et al. (2001)	Microscopic	Cellular automata	×	×
Chaibi et al. (2010)	Microscopic	Social force (centrifugal force)	✓	✓
Flötteröd and Lämmel (2015)	Microscopic	Cellular automata	✓	✓
Gipps and Marksjo (1985)	Microscopic	Combined of cellular automata and social force models	×	×
Gloor et al. (2004)	Microscopic	Combined of cellular automata and social force models	×	×
Guo et al. (2010)	Microscopic	Social force (behavioural theory)	✓	✓
Helbing and Molnár (1995)	Microscopic	Social force	×	×
Helbing et al. (2007)	Microscopic	Social force	✓	✓
Hoogendoorn and Bovy (2003)	Microscopic	Social force (behavioural theory)	✓	✓
Hoogendoorn and Bovy (2004)	Microscopic	Route choice theory	×	×
Hoogendoorn and Daamen (2007)	Microscopic	Social force (behavioural theory)	×	✓
Hughes (2000)	Macroscopic	Route choice theory	×	×
Isobe et al. (2004)	Microscopic	Lattice gas	✓	×
Kneidl and Borrmann (2011)	Microscopic	Combination of cellular automata and social forces	×	×
Kretz et al. (2011)	Microscopic	Social force	×	×
Li et al. (2019)	Microscopic	Combination of cellular automata and choice behavior analysis	×	×
Li and Guo (2020)	Mesoscopic	Cell transmission model	✓	✓
Løvås (1994)	Microscopic	Route choice theory	✓	×
Lu et al. (2015)	Microscopic	Combination of cellular automata and social force	×	✓ (from one intersection)
Moussaïd et al. (2010)	Microscopic	Social force	×	✓
Moussaïd et al. (2011)	Microscopic	Social force	×	✓
Muramatsu et al. (1999)	Microscopic	Lattice gas	✓	×
Muramatsu and Nagatani (2000)	Microscopic	Lattice gas	✓	×
Nagatani (2001)	Microscopic	Lattice gas	✓	×
Nagatani (2002)	Microscopic	Lattice gas	✓	×
Okazaki and Matsushita (1993)	Microscopic	Force based	×	×
Robin et al. (2009)	Microscopic	Route choice	×	✓
Song et al. (2013)	Microscopic	Social force	×	×
Teknomo (2006)	Microscopic	Social force	✓	✓
Tordeux et al. (2018a)	Mesoscopic	Hexagon lattice	✓	✓
Torres-Ruiz et al. (2017)	Microscopic	Cellular automata	✓	✓
Weifeng et al. (2003)	Microscopic	Cellular automata	✓	×
Wu et al. (2021)	Microscopic	Route choice theory	×	✓
Zanlungo et al. (2014a)	Microscopic	Social force	×	✓
Zhao et al. (2012)	Microscopic	Social force	×	×

2.3. Fundamental diagram

Fundamental diagrams are an essential element for traffic simulation. Relying on the relations between basic traffic magnitudes, they evince the validity of the proposed models. Similarly in pedestrian simulation they are considered to be an important tool, particularly in terms of model calibration (e.g. Tordeux et al., 2018a), as considered in the previous table (2.1).

One of the earliest studies on pedestrian fundamental diagrams was that of Weidmann's (1993). The proposed fundamental diagram correlates pedestrian density and pedestrian velocity by illustrating that velocity is inversely related to density. The diagram has also been verified in later studies, for example in Seyfried et al. (2005) where four regimes have been identified (Figure 2.3).

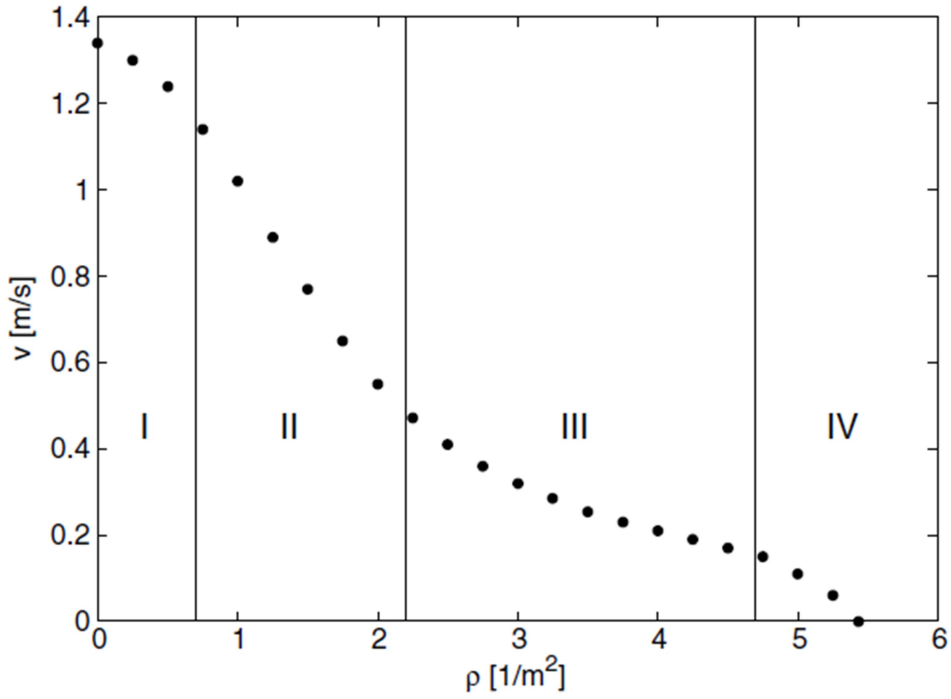

Figure 2.5: Fundamental diagram for pedestrians (Seyfried et al., 2005)

It is worth mentioning that the measuring unit of density (p) in pedestrian flows refers to square meters ($1/m^2$) and is related to the area, rather than the length that pedestrians occupy. This is not the case for traffic flow where density is expressed in vehicles per unit of length e.g. lane-kilometers (veh/km/lane). The cause of this difference is that vehicles are organized in specific lanes and they typically follow each other, thus the vertical dimension is not so relevant. It only

becomes relevant when modelling heterogeneous traffic where power-two-wheelers are present. Is such cases, event approaches are introduced to include the vertical dimension. As pedestrians do not necessarily walk in specific lanes (expect in specific cases that are analysed below), but in an un-directional i.e. a scattered (to some degree) manner in space, it is crucial to examine the area that the pedestrian occupies. Thus, both length and width need to be considered.

Maximum density value in Figure 2.5, is reached when velocity almost zeroes and is 5.4 pedestrians/m^2. Helbing et al. (2007) noted from their experiments that density can slightly exceed 9 pedestrians/m^2. In addition, Løvås (1994) mentions that maximum pedestrian flow varies between different populations, situations and walkways.

Hughes (2000) analysed the way that pedestrian velocity decreases when density increases (without providing a fundamental diagram) by developing a macroscopic pedestrian simulation model. This study implied that velocity depends only on density without considering surface heterogeneity, in contrast to Løvås (1994). Additionally, Hughes's approach does not consider different types of pedestrians. The application of his approach in a case study revealed that the psychological state of pedestrians can completely change the flow pattern. Hughes (2000) simulated pedestrian velocity using differential equations and postulated three hypotheses:

- Pedestrian velocity depends on surrounding pedestrian density and pedestrians' behavioral characteristics;
- Pedestrians move towards their destination; and
- Pedestrians minimize their travel time, but relax this in order to avoid high densities.

Blue and Adler (2001) recognized the fact that pedestrian velocity depends on the location of other pedestrians in the neighboring area (see section 2.4). They utilized cellular automata for pedestrian simulation using microscopic models and examined the way that pedestrians act as they move. They set possibilities regarding whether or not pedestrians will change lane. They classified bidirectional flow in to a) separated flow, b) interspersed flow and c) dynamic

multi-lane (DML) flow, and they concluded that the velocity/density curve (pattern) differs between unidirectional to bidirectional flow.

Isobe's et al. (2004) study also demonstrated the relationship between velocity and density in one-way and on two-way pedestrian traffic flow. In the first case the relationship was found to be linear and in the second logarithmic (with R^2 equal to 0.82 and 0.90 respectively).

A specific type of density, local density (the density at a certain space and time), has also been studied (e.g. Helbing et al., 2007; Lu et al., 2015). Helbing et al. (2007) made the first attempt of assigning local density and local velocity. They determined the level of the difference between local and average values and suggested that local density can reach twice the value of average density. In very high densities, the movement of each pedestrian was determined, mainly from the crowd movement.

Daamen et al. (2015) pointed out the significance of variation in pedestrian density (similarly to Helbing et al., 2007). Particularly, they concluded that density variations are proportionate to pedestrian flow and inversely proportionate to pedestrian velocity.

Furthermore, pedestrian velocity under normal conditions has also been examined. Weifeng et al. (2003) estimated it about 1.0m/s, Lu et al. (2015) about 1.2m/s, while Antonini et al. (2006) refer to an average pedestrian's speed in their datasets of about 1.6m/s. On the other hand, Brščic et al. (2014) characterized as moving pedestrians those who have an average velocity of more than 0.5m/s.

Last, Tordeux et al. (2018a) employed, besides the velocity–density fundamental diagram, the flow–density diagram in order to test the applicability of their model. Both in uni-directional and multi-directional experiments fundamental diagrams were used as a tool for examining model validity.

2.4. Data-driven models on pedestrian simulation

During the past years an increasing adoption of data-driven techniques in the field of pedestrian simulation has been observed. These techniques are

described in a separate subsection: the terminology and a detailed description of data-driven theory are presented in detail in section 3.4.

Data-driven modeling is not an unfamiliar approach to pedestrian simulation and has been applied only recently, though not as extensively. One of the early attempts was that of Tay and Laugier (2008) who performed a motion pattern analysis with the aid of Gaussian Processes (GP). The researchers utilized GP for modeling paths into a typical path with the mean function equal to the mean of the GPs, without considering surroundings. They employed the Expectation Maximization algorithm as a useful tool for model training.

Ma et al. (2016) employed Neural Networks (ANN) and pointed out their paramount advantages (nonlinearity and adaptability) in an attempt of predicting agents' movement by collecting data in a crosswalk on a street in Hong Kong. The model parameters were initially categorized in five groups, regarding pedestrian's current velocity, interactive agents' relative positions and velocities, obstacles' relative positions, relative positions of the desired targets and pedestrian characteristics (i.e. physiology and emotions). Due to homogenous pedestrian flow hypothesis, the fifth group of parameters was ruled out. Additionally, as the simulation involved a crosswalk, no obstacles were considered except for the boundaries. Subsequently, a single hidden layer Multi-Layer Perceptron (MLP) was trained on real data, recorded from a camera, and proved its efficiency.

Alahi et al. (2016) predicted pedestrian next step position in a time series framework with the aid of Long Short-Term Memory (LSTM) networks, a type of ANN (particularly Recurrent Neural Networks). Their model is a mix of social force and LSTM considering the locations of the neighboring pedestrians. They applied LSTM in every examined pedestrian, while a "social" hidden state pooled the multiple LSTMs in one model. Alahi et al. (2016) compared their model with the social force demonstrating the superiority of data-driven modeling in their datasets.

Ridel et al. (2019) went one step further in the LSTM technique (applied for pedestrian simulation) by taking under consideration pedestrian-vehicle interactions. The researchers used as inputs in their model pedestrian positions, head orientation and ego-vehicle locations while they predicted pedestrian future

positions in the next 2 seconds. They developed their model with the aid of PyTorch (an open-source machine learning library for Python programming language) using Adam as the optimization algorithm and the mean squared error (MSE) as the loss function. Their study limitations arise from the fact that although they consider pedestrian-vehicle interactions, pedestrian-pedestrian and pedestrian-obstacles (e.g. buildings) interactions were not included in their approach.

Martinez-Gil et al. (2017) employed reinforcement learning theory to simulate pedestrian behaviors in groups. In terms of control theory, the reinforcement learning model consists of two stages. First, pedestrians independently learn, by interaction with the environment, their behavior and then each learned behavior is replicated in pedestrian groups.

Tordeux et al. (2018b) applied ANN in pedestrian simulation to predict agent's velocity. They indicated ANN's efficiency, while comparing them with a fundamental-diagram based model. In terms of cross-validation process, half of the data were used as the training set while the other as the testing set. Mean squared error was the error function in the back-propagation algorithm. The model that performed better was a single hidden layer network with three nodes.

Duives et al. (2019) also used Recurrent Neural Networks in pedestrian simulation. With the aid of cell sequences (agent's previous steps ordered by time), utilizing GPS data, they trained and tested their model during a festival in the Netherlands.

Prior to pedestrian simulation, ANN have been utilized extensively in transportation research [e.g. Antoniou et al., 2013, Karlaftis and Vlahogianni, 2011, Papathanasopoulou and Antoniou, (2015, 2017)]. For example, Antoniou et al. (2013) employed ANN, among other data-driven methods, for predicting traffic states, while Papathanasopoulou and Antoniou (2015, 2017) adopted ANN as an alternative traffic simulation technique with significant results. On the other hand, Karlaftis and Vlahogianni (2011) pointed out ANN's limited descriptive ability, when applying them in transportation modeling. In cases of primary parameters' relationships, ANN could be avoided. Compared to statistical methods, ANN may be advantageous when dealing with complicated data, but they do not produce a

relationship between inputs and outputs. Karlaftis and Vlahogianni (2011) mention that a “fair” comparison between them is not always feasible.

2.5. Parameters specification

The most commonly used models that simulate pedestrian movements are described in section 2.2. The process of developing the simulation models includes the determination of the factors that affect pedestrian movement. Models are then calibrated and validated.

It should be noted that each study in section 2.2 holds different assumptions. For example, considering movement directions, a few studies take into consideration only one directional movement (e.g. Nagatani, 2002), while others do not include the possibility of back stepping (e.g. Weifeng et al., 2003).

The parameters that affect pedestrian movement as determined in the relevant studies and have been incorporated in pedestrian simulation models can be classified in the following distinct categories (presented in Figure 2.4):

- Facilities geometry
- Pedestrian flow properties
- Pedestrian characteristics

Facilities geometry

Løvås (1994) concluded that pedestrian velocity is not affected considerably by the direction of traffic, but is a function of personal and conditional factors. At the same time he noted that walking through a door versus a corridor of the same width restricts pedestrian flow. He also noticed that the queue phenomenon (pedestrians are standing in queues) can occur next to doors.

The relative dimensions of a corridor i.e. width of the narrow part/width of the wide part affect critical density (Nagatani, 2001). The width of the corridor in which pedestrians walk is not very crucial as long as it does not impede the free flow of the pedestrians (Seyfried et al., 2005). At the same time, density at the

exit point affects the relation between the mean flow rate and the entrance density (Nagatani, 2001).

Depending on the type of infrastructure e.g. stairs, ramps, bottlenecks or halls and the number of assumed directions of the streams (uni-directional/bi-directional), the fundamental velocity - density relationship may differ (Seyfried et al., 2005). In particular, in four-way systems, the mean velocity above the transition point is almost zero, whereas in two-way systems, it has a low non-zero value (Muramatsu and Nagatani, 2000). In addition, Hoogendoorn and Bovy (2004) referred to the spatial distribution of the alternative route choices (route choice models) that affects pedestrian movement.

Pedestrian flow properties

The density of the moving area, similarly to traffic simulation, is the most crucial factor considering pedestrian movement (Gipps and Marksjo, 1985; Helbing and Molnár, 1995; and Isobe et al., 2004). Density increases proportionally to the density at the entry point (Nagatani, 2001). For a specific value of the critical entry density, which depends on the dimension of the corridor (see Facilities geometry), the conditions become saturated. In bi-directional movement, when pedestrians walking in opposite direction come close, they tend to diverge from their initial trajectory in order to increase their lateral distance. This phenomenon occurs for density values lower than a threshold value, after which pedestrians are restricted by the presence of other pedestrians, and this phenomenon stops occurring (Isobe et al., 2004).

Nagatani (2002) showed that the higher the density of a corridor's exit, the higher the possibility of merging two pedestrian flows, in the same direction, downstream of a meeting point inside the corridor. His simulations were conducted without the possibility of back stepping and under unidirectional movement.

Hoogendoorn and Bovy (2004), in the application of route choice models, defined crucial factors for pedestrian simulation. Expected travel time, interactions between pedestrians and obstacles, maintaining a certain speed, interactions

between pedestrians and environmental stimuli were categorized as running costs, while the cost of the delay in the destination as the terminal cost (though maintaining certain speed and cost of delay factors are categorized as “pedestrian characteristics”). Pedestrian velocity depends on the time of day; higher velocities are observed in peak hours (even in high densities), and lower velocities are observed in later hours (Brščic et al., 2014). Also, pedestrian velocity depends on the location of other pedestrians in the area (Blue and Adler, 2001). Anisotropy (whether a pedestrian is influenced only by people that are in front of them) and pedestrian reaction time are crucial factors (Hoogendoorn and Daamen, 2007). Pedestrians with higher free flow speed anticipate other agents in greater distances.

Weifeng et al. (2003) broke the deadlock of back stepping adopting the von Neumann neighborhood, which involves four adjacent cells. The simulation results suggested that in low density pedestrians move freely, while in crowded situations the system is self-organized in lanes. These results are in line with the findings of Brščic et al. (2014). Lane segregation policy has high influence in the average delay and in the average velocity compared to the mix lane policy (Teknomo, 2006). Pedestrians generally tend to move on the same side of the corridor/tunnel/road in a bidirectional movement (Blue and Adler, 2001). As the total density increases, the existing lanes merge in two lanes: the right lane contains “up walkers” and the left the “down walkers”. In the jammed state (higher density) only some of the pedestrians can move. Also due to the back stepping, the system will not reach easily a jammed state (as pedestrians can easily adjust their positions). Finally, a factor determining whether pedestrians prefer to walk on the right-hand side of the road or on the left-hand (depending on each country) was introduced.

Conflict delay is another crucial factor of pedestrian simulation (Flötteröd and Lämmel, 2015). It declares the delay between two pedestrians from the opposite directions when they interact with each other. In their model, the ratio of density in each direction was 50/50. Pedestrians’ conflicts could lead to velocity reduction (by up to one-third) in a bidirectional flow (Lu et al., 2015). As also mentioned above, pedestrians want to minimize their travel time (Hughes, 2000).

In social groups, pedestrians walk side by side to improve their communication, but they change the shape of the walking line (that is, perpendicular to the direction movement) into a U-shape as the population of the group increases or/and the density increases (Moussaïd et al., 2010). The U-shape does not change in bidirectional flows. According to Zanlungo et al. (2014a), as the size of a pedestrian group increases, the velocity decreases and pedestrians are forced to move from the surrounding environment towards the centre of the group.

Pedestrian characteristics

Hoogendoorn and Daamen (2007) calibrated five parameters (agent's free speed, agent's acceleration time, interaction constant, interaction distance and agent's reaction time – though interaction constant and interaction distance are categorized as "Pedestrian flow properties") that affect pedestrian's movement. Drift strength is another essential factor, encountered on lattice gas models (Muramatsu et al., 1999; Muramatsu and Nagatani, 2000; and Isobe et al., 2004). Muramatsu et al. (1999) deduced that mean velocity increases with increasing drift, and the jamming transition is independent of the ratio of the walkers moving to the right side of all the walkers. The jamming transition point depends on the system size for small systems (Muramatsu and Nagatani, 2000). Drift strength also affects mean arrival time and route choice (Isobe et al., 2004). A similar factor to drift strength is crowd pressure (Kretz, 2011).

The existence of elderly people in the pedestrian flow influences pedestrian velocity (Isobe et al., 2004). Specifically, average velocity decreases logarithmically as the proportion of the elderly pedestrians increases (Teknomo, 2006). Additionally, agent height affects velocity, almost linearly between 1.45 and 1.8 m (Brščic et al., 2014). While taller people walk faster, their movement is inhibited as the number of short persons increases. Agent dimensions are related to the headway and to their step size (Kretz, 2011). Generally, personal characteristics comprise a crucial factor determining pedestrian movement (Nikolić et al., 2013).

The agents' intentions relevant to whether they desire to reach their destination as soon as possible, irrespective of the length of the route that they follow

(quickest path factor) is another important factor (Kretz et al., 2011). Emergencies are an example. It is obvious that the quickest path is not always the shortest. Furthermore, the agent's psychological state, as already mentioned, is considered as a crucial factor in pedestrian simulation (Hughes, 2000).

Finally, Hamed (2001) listed a number of factors that influence waiting time in a crossing and the number of attempts until some pedestrian passes including, amongst others, agent's age and gender.

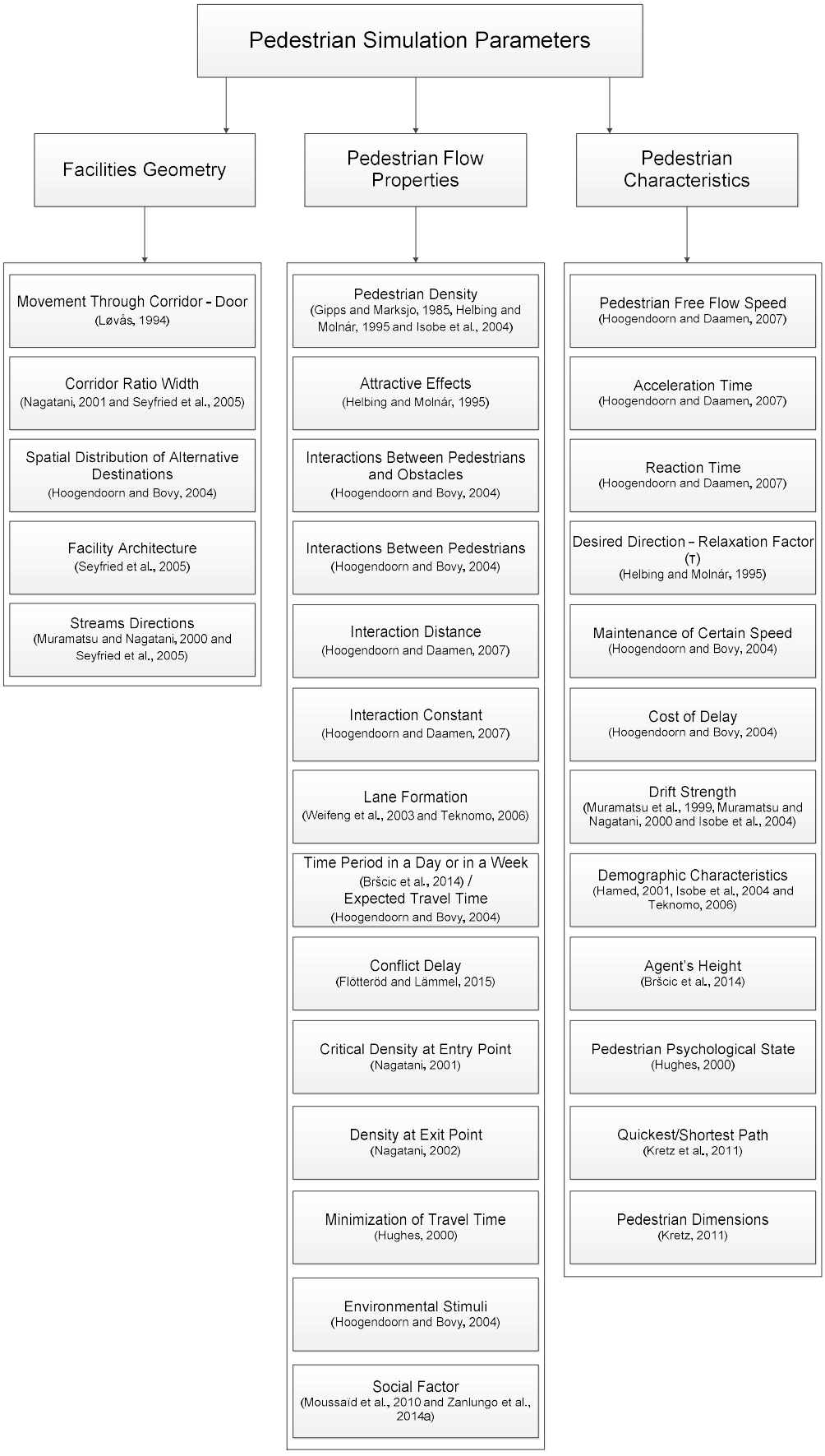

Figure 2.6: Pedestrian simulation parameters

2.6. Modeling emergencies

Due to the increased interest of the research community on pedestrian simulation modeling under emergencies, mainly during the last decade, results from some of the most representative studies, are presented.

In this thesis, emergencies are defined as situations during which, in a short period of time, sudden disruptions occur and drastic actions must be carried out to prevent serious incidents. Emergencies are classified according to their cause, in natural disasters (earthquakes, floods, etc.) and in man-made events (fires, terrorist actions, etc.).

A key difference between pedestrian simulation in normal conditions and under emergencies is the stress associated with emergencies (Yun et al., 2012). Kneidl and Borrmann (2011) categorized pedestrians in evacuation plans into three types:

- Those who know the location and can find an alternative route,
- Those who have no detailed knowledge of the area, and
- Those who are totally unaware of the area.

In evacuation methods, dynamic plans are the most effective, followed by static plans and then by evacuation methods without a plan (Yun et al., 2012). Koo et al. (2013) pointed out the contribution of hybrid strategies in evacuation plans in which only people in wheelchairs use elevators and the rest use the stairs. In addition, they concluded that evacuation in phases requires less time than a simultaneous strategy. Evacuation time (average and maximum) is the primary indicator for the assessment of the evaluation plan (Vermuyten et al., 2016).

Training for emergency situations affects evacuation plans. Chen et al. (2012) highlighted the significance of information systems and virtual reality. Studying human psychology in disaster preparedness, Paton (2003) introduced critical awareness as the way or level that people perceive danger. Motivation and danger awareness are the primary factors for triggering people to act preventively.

Simulation models are employed in evacuation plans. Cellular automata (Guo et al., 2012; Liao et al., 2014), social force (Okazaki and Matsushita, 1993; Helbing et al., 2000; Parisi and Dorso, 2005) and lattice gas models (Helbing et al., 2003) are the main categories, while route choice theory is employed complementary to them. Parisi and Dorso (2005) stated that cellular automata models lack in calculating interaction forces (between agents or between agents and objects). Route choice models are of great importance because route selection is crucial in evacuation plans. In these models, the probability for an agent to select their evacuation route plays a crucial role in evacuation effectiveness. Pedestrians choose routes that minimize distance (Guo et al., 2012), although the shortest route sometimes is not the quickest (Kretz et al., 2011).

A modulated force model was presented by Helbing et al. (2000) that takes into account two extra forces: one that raises body compression and another that focuses on tangential movement. The researchers considered parameters from pedestrian movement under normal conditions (repulsive forces, attractive forces, desired velocity, and relaxation factor) and pointed out that in emergencies their values are much higher. Desired velocity, in particular, could reach values to 10 times higher. Parisi and Dorso (2005), who also pointed out that desired velocity in emergencies can reach much higher values (up to 8 m/s), concluded, surprisingly, that the minimum evacuation time occurs under intermediate desired velocity values. They found that evacuation time increases in low and high desired velocity values because of clogging (in high-level values).

Under panic conditions, when desired velocities are high, congestion problems occur in door exits and in corridor widenings. Exit door width is inversely proportional to the probability of congestion at the exit (Parisi and Dorso, 2005). Evacuation time is reduced exponentially by an increase in the width of the exit door.

Okazaki and Matsushita (1993) described a social force model for pedestrian movements under building evacuation. The model is based on the process of negative and positive poles, where positive poles are pedestrians and their obstacles and negative poles are the destinations. Thus, pedestrians, because of the magnetic fields, are repelled from the obstacles or the other pedestrians and are attracted by their destination (possibly the nearest exit). A function for

physical interactions was used for overcrowded situations in which pedestrians are forced to walk in a specific direction without exercising their own will (Moussaïd et al., 2011).

The level of visibility in an emergency is an important factor in evacuation plans (Guo et al., 2012; Liao et al., 2014, Cao et al., 2018). Guo et al. (2012) used cellular automata and route choice models for specifying pedestrian behavior under good and zero visibility. Under low visibility conditions, space familiarity (also mentioned by Liao et al., 2014) for each of the evacuees was considered. Cao et al. (2018) experiments in a supermarket under good and limited visibility pointed out five main findings (a) pedestrians attempt to find the closest exit in order to minimize the movement distance in both conditions, (b) follow other neighbors, (c) help other people under low visibility conditions (that does not occur often under normal conditions), (d) try to find dependents and walk along obstacles, and (e) their speed under low visibility conditions is significantly lower than under normal conditions. Song et al. (2013) classified crowd behaviour in panic situations (in that case, the evacuation of a metro rail station because of a bioterrorism act) according to people who will (a) select the closest exit, (b) be in total panic, and (c) follow the flow of the crowd around them. The percentage in each group was 90%, 5%, and 5%, respectively. For persons who are familiar with the room, the way of finding the nearest exit (if there is more than one) may not be difficult. Additionally, pedestrians prefer moving by touching an object (wall, obstacle etc.) or another agent. Under good visibility conditions, Guo et al. (2012) indicated three parameters that affect pedestrians' route choice behavior: (a) route distance to the exit, (b) congestion on the frontal route, and (c) frontal route capacity. They deduced that pedestrian velocity under zero visibility is half of velocity under good visibility conditions. However, their simulations were conducted without taking into account psychological factors.

Liao et al. (2014) mentioned the route choice parameter introduced by Guo et al. (2012), and added building structure, agent psychology and information availability without extensively studying them. They examined three exit layout types: (a) parallel, (b) convex, and (c) concave. They concluded that the parallel layout is the least effective in evacuation plans.

A specific study on evacuation of tall buildings has been conducted by Aleksandrov et al. (2018). These building types may have a refuge floor i.e. a floor that pedestrians can have a short break as they walk with the stairs. The researchers conclude (relying on questionnaires) that pedestrians are more willing to follow instructions from staff than from sings. Also they point out that people density on the stairs, refuge floors positions, knowledge that lifts can be used for evacuation, agent's characteristics (e.g. body mass index) are critical parameters for evacuation plans.

Persons with disabilities have also been considered in evacuation plans (Manley and Kim, 2012). In this study, people were categorized in six types: (a) people without impairment, (b) motorized wheelchair users, (c) nonmotorized wheelchair users, (d) visually impaired, (e) hearing impaired, and (f) stamina impaired. The third (c) and the sixth (f) types were considered as the most vulnerable ones. Simulation results highlighted the need of assessing the type of disability that will further enhance evacuation plans.

Joo et al. (2013) studied human behavior in emergency situations and mentioned two hypotheses: (a) humans decide as a consequence of their perceived information and (b) humans set a goal to achieve with their actions. The paper does not examine human interaction and communication. Three models are referred to represent human behaviors in complex and realistic environments: Soar, Act-R, and Belief-Desire-Intention. The models follow three different approaches: (a) an economics-based approach, (b) a psychology-based approach, and (c) a synthetic engineering-based approach.

In emergency and crowd conditions, local magnitudes are more representative of pedestrian dynamics. Helbing et al. (2007) made the first attempt of considering local magnitudes, while Daamen et al. (2015) pointed out the significance of variation in pedestrian density. They concluded that density variations are proportionate to pedestrian flow and inversely proportionate to pedestrian velocity, also in emergency conditions.

Geographic Information Systems (GIS) comprise an important tool in evacuation plans (Pidd et al., 1996 and Huang and Pan, 2007). Pidd et al. (1996) developed a configurable evacuation management and planning system to be used in man-made disasters. They considered GIS as an efficient technology that can

examine static aspects of evacuation plans, such as determining evacuation zone and evacuation routes, but they noted that it cannot consider dynamic ones. Huang and Pan (2007) presented a more integrated way to simulate models appropriate for evacuation under panic conditions. They incorporated GIS with a traffic simulation engine and an optimization engine. GIS provided the primary user interface, processed network data, derived the shortest-time path and visualized the results, while a traffic simulation engine simulated incidents in the network, gathered link travel times at regular intervals and transmitted time dependent information to GIS. Finally, an optimization engine derived an optimal dispatching strategy by minimizing the total travel time of all response units.

Virtual geographic environments (a GIS specification) are useful in crowd evacuation (Song et al., 2013). The conceptual framework of virtual geographic environments has three components (Gong et al., 2009): (a) representation in a virtual geographic large-scale landscape, (b) a smaller-scale environment, and (c) a layer of collaborative participation of the users.

Furthermore, control of pedestrian behavior is a crucial factor in evacuation plans. Siques (2002) presented the effectiveness of control devices in human behavior. The author examined scenarios in grade crossings and found that active warning devices, such as pedestrian automatic gates or pedestrian flashing lights, are more powerful in preventing pedestrian grade crossing as a train approaches, than simple visual signs. Zhao et al. (2012) pointed out that the factor of pedestrian flow stability is crucial for flow control, because small perturbations in unstable flows can cause serious effects. The proportion of pedestrians that follow the traffic guidance is important for the “stabilization” of the streams (as the proportion grows the flow becomes more stable).

Recently data-driven models were employed on pedestrian movement under evacuation. Wang et al. (2019) utilized machine learning techniques, including SVM and ANN, for classifying pedestrian movement patterns under emergencies. They came up with the findings that the distance to the target exit is an important factor and that surrounding evacuees affect the examined one. In a comparison of the performance among the utilized machine learning methods, ANN was proven to be superior.

Xu et al. (2021) used ANN and particular Deep Neural Networks combined with Reinforcement Learning theory in multi-exit navigation for pedestrian evacuation. The evacuees were trying to leave the room (the examined place) as soon as possible avoiding obstacles or other pedestrians. The experiment assumes fully environmental awareness. Also in this study Neural Networks proved their outperformance.

2.7. Data collection

As noted in Table 2.1, only a few studies validate their models. The cause is the lack of real data, and the limited access to them.

Validation methods and techniques are crucial in order to prove that theory models are sensible and applicable to reality, while displaying a satisfactory representation of actual movement. Cross-validation techniques have been applied extensively and provide an effective validation technique (Robin et al., 2009; Flötteröd and Lämmel, 2015; Nikolić et al., 2016). Robin et al. (2009) performed a cross validation method by splitting the data in five subsets, utilizing one each time for validation and the rest four subsets for calibration. Flötteröd and Lämmel (2015) cross validated their results by estimating and validating among unidirectional and bidirectional flow data and vice versa. Nikolić et al. (2016) used 80% of their data (randomly selected) to estimate model parameters and the remaining 20% for validating the estimated model using Kolmogorov-Smirnov goodness-of-fit test.

Data collection is crucial for validation. The most commonly utilized data sources generally are those employing video recordings and sensors.

The basic issue of video recording techniques is structuring methods to track pedestrians accurately. In video recordings, principles of photogrammetry are utilized as it comprises a significant tool for separating agents from their background. One approach for assessing the agent's position and tracking their route is tracking the head of an agent one approach (Teknomo et al., 2000; Johansson et al., 2007). The shortcoming of this method is that the height of the agent cannot be specified. Hoogendoorn et al. (2003) and Ma and Song (2013)

placed colored caps on the agents' heads to solve the problem of accurately assessing the positions of the agents. Using a color function, they tracked pedestrians in a cluster, frame-by-frame, by the color of their hat. In a respective framework Federici et al. (2014) relied on video footage in order to track pedestrians. Teknomo et al. (2001) presented an automated method for tracking pedestrians as they are moving. The researchers used an algorithm to isolate pedestrians from their background, assessed pedestrians' contour (by their neighboring cells), connected them in each frame (tracking pedestrians), and computed pedestrians' flow characteristics. The disadvantage of this method is the confusion in high density situations due to the occlusion phenomenon (two or more persons who are too close to each other are treated as one) resulting in the mismatching of pedestrian positions after each frame.

Another issue with video techniques is the conversion of the image coordinates to real-world coordinates. Teknomo et al. (2000) used a rectangular grid to extract pedestrians' coordinates with a high level of accuracy and then converted the image coordinates to real-world coordinates. Hoogendoorn et al. (2003) and Brščic et al. (2013) used reference points.

In the sequel of video recordings, Unmanned Aerial Vehicles (UAV), better known as drones, have been employed recently in the field of trajectory tracking. Sutheerakul et al. (2017) placed a video camera in both stationary and moving UAVs to collect data on pedestrian flow characteristics (in particular they recorded pedestrian trajectories) from a shopping street in Thailand. They pointed out skills' requirements for handling the drone, batteries short-term capability and requiring flight permission from the aviation or other relative bodies as drawbacks of this method. On the other hand, the absence of the limitation for recording particular areas is mentioned as an advantage from Barmpounakis et al. (2016a) in an attempt of extracting both vehicle and pedestrian trajectories separately.

Antoniou et al. (2011) categorized the technologies for traffic data capturing as (a) point sensors, (b) point to point, and (c) areawide. Kourogi et al. (2006) utilized a combination of a Global Positioning System (GPS) sensor and a Radio Frequency Identification (RFID) tag system for tracking pedestrians in outdoors and indoors environments respectively. A Kalman Filter algorithm was employed

for enhancing GPS position estimation. Reades et al. (2007) used mobile phone antennas for assigning pedestrian flows and their distributions during the day and the week. The inability of some devices to capture the signal of all the cell phones in the area (because of out-of-range frequencies) is a shortcoming of this method. Brščic et al. (2013) employed a multi-sensor system that was set in the ceiling of the study area. Still sensor-based methods could lead to accuracy issues (they cannot capture accurately pedestrian trajectory) that affect the efficiency of microscopic simulation. Infrared sensors (Nikolić et al., 2016) and sensors that rely on the change in environmental temperature (Kerridge et al., 2007) have also been used. Lesani et al. (2020) used LiDAR (Light Detection and Ranging) sensors, a technique that relies on radiation. LiDAR sensors measure the distance from the moving objects every 20 ms. However, experiment results revealed that not all the pedestrians that participated in the experiment were tracked (e.g. pedestrians that carry an umbrella might cover other agents). An overview of data collection tools employed in pedestrian simulation studies is presented in Table 2.2.

Table 2.2: Data collection tools in pedestrian simulation studies

Data collection				
Paper		**Means of Data Collection**	**Tracking Type**	**Data Type**
Barmpounakis et al. (2016a)		Video recording (UAV)	Semi-automated	Vehicle and pedestrian trajectories
Brščic et al. (2013)		Sensors (multiple-sensor system)	Automated	Pedestrian trajectories
Federici et al. (2014)		Video recording	Automated	Pedestrian trajectories
Flötteröd and Lämmel (2015)		Video recording	Manual	Pedestrian trajectories
Guo et al. (2010)		Video recording	Manual and automated	Pedestrian trajectories
Helbing et al. (2007)		Video recording	Automated	Pedestrian positions and velocities
Hoogendoorn et al. (2003)		Video recording	Automated	Pedestrian trajectories
Hoogendoorn and Daamen (2007)		Video recording	Automated	Pedestrian trajectories
Johansson et al. (2007)		Video recording	Automated	Pedestrian trajectories
Kerridge et al. (2007)		Sensors (thermal)	Automated	Pedestrian trajectories
Kourogi et al. (2006)		Sensors (GPS and RFID)	Automated	Pedestrian trajectories
Lesani et al. (2020)		Sensors (LiDAR)	Automated	Pedestrian trajectories
Lu et al. (2015)		Video recording	Automated	Pedestrian trajectories
Ma and Song (2013)		Video recording	Automated	Pedestrian trajectories
Moussaïd et al. (2010)		Video recording	Manual	Pedestrian trajectories
Moussaïd et al. (2011)		Video recording	Automated	Pedestrian trajectories
Nikolic et al. (2016)	Lausanne experiment	Sensors (infrared)	Automated	Pedestrian trajectories
	Delft experiment	Video recording	Automated	Pedestrian trajectories
Reades et al. (2007)		Sensors (mobile phones)	Automated	Pedestrian flows
Robin et al. (2009)		Video recording	Manual	Pedestrian trajectories
Sutheerakul et al. (2017)		Video recording (UAV)	Automated	Pedestrian trajectories
Teknomo et al. (2000)		Video recording	Automated	Pedestrian trajectories
Teknomo et al. (2001)		Video recording	Automated	Pedestrian trajectories
Teknomo (2006)		Video recording	Automated	Pedestrian trajectories
Zanlungo et al. (2014a)		Sensors and video recording	Automated	Pedestrian trajectories

2.8. Resume

In this chapter a literature review of the existing pedestrian simulation models is presented, including data-driven approaches. Both microscopic and macroscopic models are described. The former have gained greater researchers' interest and are classified into three main categories: a) social force, b) cellular automata and c) lattice gas. Data-driven models, on the other hand, comprise a rather recent method in pedestrian modelling attracting researchers' interest.

The aim of this research is to examine whether data-driven methods can provide a robust model framework for pedestrian simulation. To achieve this, pedestrian models utilizing specific data-driven techniques are employed to simulate pedestrians and their performance is compared against traditional pedestrian simulation models. The social force model is employed in order to compare the models' accuracy with the data-driven techniques, as it comprises the most representative and widely used theoretical pedestrian simulation model. In particular, the social force model:

- relies on the same principle as the other two model types, i.e. pedestrian's next step is based on the positions of the adjacent pedestrians/objects, while at the same time is a continuous space model and

- is widely used and adopted in widely applied simulation software, such as VisWalk (PTV, 2015) and SimWalk (Zainuddin et al., 2009)

Considering data-driven techniques, four promising methods are employed: a) the well-known Artificial Neural Networks (ANN), b) the classical Support Vector Machines (SVM) [in particular as we refer to regression analysis, Support Vector Regression (SVR) is employed], c) the rising Gaussian Processes (GP) and d) the Locally Weighted Regression (Loess). All four methods have been adopted in traffic simulations (e.g. Papathanasopoulou and Antoniou, 2017).

To assess the performance of the aforementioned model types real data in the form of pedestrian trajectories are required. In section 2.6, the existing methods for extracting pedestrian trajectories are described. Two main sources are found: video recordings and sensors. As it can been seen in Table 2.2 most of the existing studies employed video recordings for extracting pedestrian kinematics

and characteristics, while a small number of used sensors. In line with this, video camera is the tool employed for collecting and extracting pedestrian trajectories (in order to further use these trajectories for the model comparison) in this research. An extensive description for the data collection of the experiment is provided in section 4.

3. METHODOLOGICAL FRAMEWORK

3.1. Overview

The present research is an attempt to design data-driven pedestrian simulation models and to assess them through a comparison with well-established theoretical models. It should be stated that only pedestrian movement is considered i.e. environments where pedestrians do not interact with vehicles are explored. Furthermore, this study involves pedestrian movement under normal conditions.

The methodological framework consists of specific steps and is illustrated in Figure 3.1. Initially the data collection experiment is designed. In the present research, two different area types, where pedestrians walk, are used for data collection, with the different areas expected to exhibit different walking patterns. Data processing is performed with the aid of photogrammetric tools used for the transformation of pixel coordinates to real world coordinates.

Further data processing is required, as data include noise, and a suitable algorithm is employed for reducing it. The smoothing algorithm in this research is a combination of two robust smoothing filters.

Following data noise reduction, pedestrian simulation models are developed based on the processed data. In particular, a representative model in the field of theoretical approaches and four data-driven techniques are utilized. As data-driven techniques are not inherently a pedestrian simulation model, an appropriate model setup is required. Also, in order to accomplish a fair comparison between the theoretical pedestrian simulation model and the data-driven methods the same variables that are used in the former are included in the latter.

Due to the fact that data-driven techniques suffer from overfitting, i.e. they can simulate efficiently the given data, but may fail to generalize their results on other datasets, a comparative method that captures the generalization impact is utilized both in the theoretical and in the data-driven models in a fourth step (cross-

validation method). Several goodness-of-fit measures (GoF) are estimated to demonstrate the accuracy of each simulation method.

Following the first level of comparison (compare models with the same parameters), additional parameters that affect pedestrian movements are incorporated in the data-driven pedestrian simulation models in order to examine the resulting performance. Initially, agent's height and gender are considered, while the parameter of time is also included. The estimation of agent's height was achieved with the employment of photogrammetric tools.

The methodological framework considering the design of the data collection experiment, the smoothing filters, the pedestrian simulation model and the data-driven techniques are presented in this section (3), while the data collection procedure and the methodology of noise elimination are discussed in the following section. In section 5 the comparative analysis of the theoretical pedestrian simulation model and the data-driven techniques are extensively elaborated, as well as the incorporation of the additional variables in the data-driven models and their contribution in the models' performance.

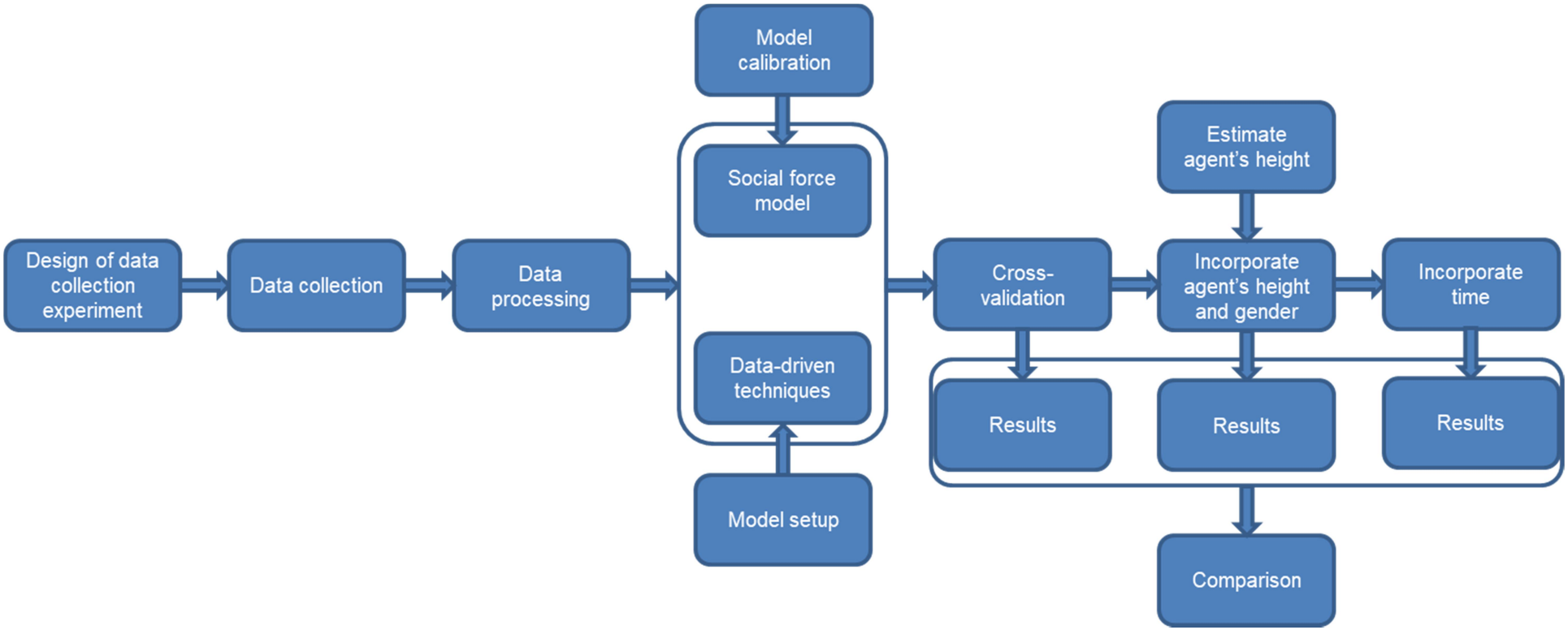

Figure 3.1: Methodological framework

3.2. Design of data collection

Prior to the overview of the data collection design (as this process is presented explicitly in section 4) the need for this must be defined. Several pedestrian trajectory databases are already available with one of the University of Edinburgh being the most widely utilized (Majecka, 2009). All of these databases include pedestrian trajectories mainly in the 2D plane, while other variables, such as pedestrian's velocity etc, can also be extracted from them. However, the present research necessitates the use of additional parameters, besides pedestrian's velocity, considering agent's characteristics (e.g. height, gender). Due to this fact it was decided to design an experiment to collect the necessary data with the principles that are described below.

In order to extract pedestrian's height a 3D video recording plane is necessary for the knowledge of all of their characteristics (including their height). Cameras were not placed close to pedestrians (at least 5m. from the ground) in order to avoid recording agents' personal characteristics (e.g. faces), while zoom level was the lowest.

Furthermore, the data collection experiment was not a controlled experiment, and as such pedestrians should not have been be aware of being recorded. The reason for this is that their natural behavior under normal circumstances was required to be captured. Thus, other types of data collection tools (e.g. sensors that are placed in their body) were excluded. At this point it should be stated that all the required permissions from the authorities that manage the recorded areas were taken.

This experiment attempts to examine pedestrian movements in a holistic manner. As a consequence pedestrians who walk in various conditions are considered, i.e. pedestrians that are relaxed and move in a non-rush manner and others for whom time is a very import parameter and is depicted in the way they walk. For this reason two different types of areas were selected. A metro station during peak hours where most of the performed trips involve commuting trips with low flexibility (involving pedestrians in a rush) and a shopping mall during afternoon hours where pedestrians enjoy their walk, stare shop windows and shop.

As the data collection output, the position of each agent in each of the recorded frames should be collected. A simple but extremely time consuming method is to note the pixel coordinates for every agent in each of the recorded frames manually. However, there is software that can track moving objects (in general) from video recordings in an automated (or at least semi-automated) mode reducing substantially the time and the manual effort of this process. A drawback of the software utilization is the fact that the outputs (i.e. the pixel coordinates of every pedestrian) may include false positions.

In addition to the above, further processing is required involving the appropriate transformation (based on photogrammetry) for converting pixel coordinates to real world coordinates to compute the trajectory of each agent. Another necessary transformation, which is relevant to the location of the camera (and photogrammetry), is also applied for extracting agents' height. An extended description of the applied methodology in the field of data collection is provided in section 4.

The data that are collected might include noise, particularly in cases where the recorded rate (the number of video frames in every second) is high or the camera is placed away from the floor where pedestrians move. In the present experiment both of these conditions exist (the recording rate is high and the camera is placed away from the moving area). In the next section the filters that can be applied to reduce noise are presented.

3.3. Smoothing Filters

The pedestrian trajectories that were extracted include noise that needs to be eliminated, prior to data analysis. Several algorithms have been developed for reducing data noise, with the most commonly used being the Kalman filter, splines and moving average.

3.3.1. Kalman Filter

Kalman filter is a method for removing noise in time series data. It is based on two principles: i) transition equations: utilizing an equation for predicting the variable in following time steps, and ii) measurement equations: correcting the measured value in this step (Kalman, 1960). Kalman filter is a time–based algorithm very popular in control theory, which evaluates the predicted value given the measured value of each time interval.

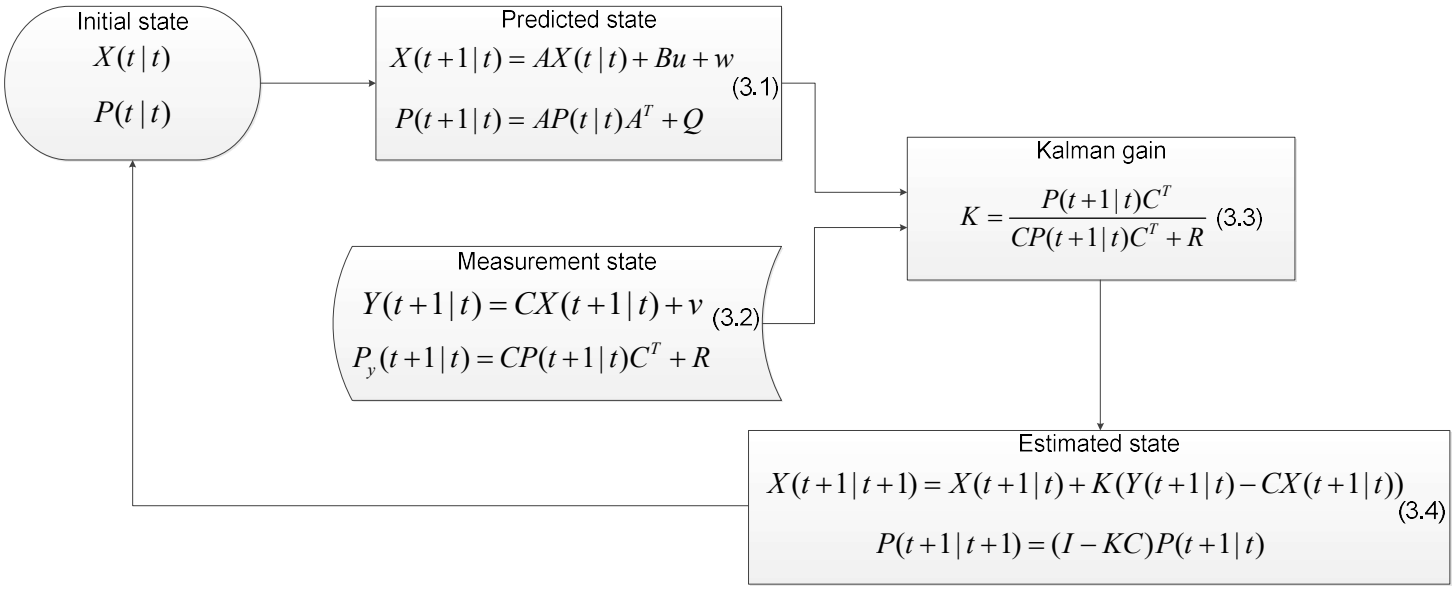

Figure 3.2: Kalman Filter method

Figure 3.2 illustrates the basic Kalman filter form, where X(t|t) stands for the vector state at the interval t, P(t|t) the covariance matrix, X(t+1|t) and P(t+1|t) the predicted values for the vector state and the covariance matrix respectively, A the state transition matrix, B the control input matrix, C the measurement matrix, u the control vector, w prediction noise with covariance matrix Q, v measurement noise with covariance matrix R and K the Kalman gain with ranging among $0 < K < 1$. As K approaches 0 the algorithm tends to rely more on the predicted value ($w \rightarrow 0$) and as K approaches 1 the algorithm tends to rely on the measurement value ($v \rightarrow 0$).

The Bu factor in Figure 3.2 (equation (3.1)) can be subtracted in case of no movement control, transforming the equation to

$$X(t+1|t) = AX(t|t) + w \quad \textbf{(3.1a)}$$

States that comprise more than one variables (e.g. position and velocity of a tracked object) are also possible to be estimated with Kalman Filter, utilizing the appropriate matrices. In cases of two-dimensional movement (as we are dealing with in our data) X state is transformed to

$$X = \begin{bmatrix} x \\ y \\ \dot{x} \\ \dot{y} \end{bmatrix} \quad \textbf{(3.5)}$$

where x and y stand for the coordinates in X and Y axes, while $\dot{x}$ and $\dot{y}$ are the velocities in these axes.

Additionally, the covariance matrix P is transformed to

$$P = \begin{bmatrix} \sigma_x^2 & \sigma_x\sigma_y & \sigma_x\sigma_{\dot{x}} & \sigma_x\sigma_{\dot{y}} \\ \sigma_y\sigma_x & \sigma_y^2 & \sigma_y\sigma_{\dot{x}} & \sigma_y\sigma_{\dot{y}} \\ \sigma_{\dot{x}}\sigma_x & \sigma_{\dot{x}}\sigma_y & \sigma_{\dot{x}}^2 & \sigma_{\dot{x}}\sigma_y \\ \sigma_{\dot{y}}\sigma_x & \sigma_{\dot{y}}\sigma_y & \sigma_{\dot{y}}\sigma_{\dot{x}} & \sigma_{\dot{y}}^2 \end{bmatrix} \quad \textbf{(3.6)}$$

where $\sigma_{...}^2$ stands for the standard deviation of each variable (in case of one variable state, the covariance matrix equals to the variance).

Standard Kalman Filter methods adopt system linearity and Gaussian noise distribution hypotheses that can be overcome by the Extended Kalman Filter (EKF) and the Unscented Kalman Filter (UKF) respectively. EKF could be utilized in non–linear systems. Based on Taylor series, EKF joints the gradient of the system equation (Gelb, 1974). In higher order, Taylor series system equation is replicated more accurately. However, due to computational performance, first order Taylor series were mainly employed. Iterated EKF modifies EKF via state vector estimation.

UKF obviates the need for noise's Gaussian assumption. Unscented Transformation (UT) remodels sample distribution to the best Gaussian approximation (Wan and Van der Merwe, 2000). Sigma points are the principal element for the transformation. They are chosen based on the distribution

dimensionality. The first sigma point is the mean. Sigma points' weights are also essential. The factor that assigns the distance of each sigma point from the mean must be stated following substantial consideration. In addition, restructuring points' dimensionality is possible from higher to lower level. A concise discussion of EKF and UKF in the context of model calibration is available in Antoniou et al. (2007).

The main requirement in Kalman Filter applications is an a priori knowledge of noise covariance matrices. Bavdekar et al. (2011) attempted to overcome the aforementioned restriction in the field of chemistry. Particularly they employed two approaches. The first relied on maximum likelihood objective function optimization and the second in the expectation maximization of EKF. They assumed that noise covariance matrices are normally distributed. The algorithms performed better when they dealt with datasets with "true" states in order to conform with the outputs. In cases where no "true" datasets existed, initial parameter guesses were essential for the comparison and error extraction.

Kalman filter requires a primary phase for eliminating estimations' variations (it does not immediately narrow down to the true values). Hence, the data on the primary phase could be considered as "off–line" and used for model calibration. Kalman filter efficiency is improved significantly during the primary phase. Antoniou (2004) adopts a "warm–up" phase, where initial ad hoc noise covariance matrices (prediction and measurement) are assumed, and the actual covariance matrices for the model application are then extracted iteratively from the output of this "warm–up" phase. For more details on Kalman Filter variants applied in Dynamic Traffic Assignment see Antoniou (2004).

3.3.2. Splines

Splines (Craven and Wahba, 1979) are a numeric method for line smoothness, and are based on polynomial functions. Polynomial degree defines spline's accuracy level. Quadratic splines comprise of two–degree polynomial, cubic splines of three–degree, and so on.

Assume a line that consists of n points; n-1 splines are required for joining them. For k polynomial degree, (k+1)*(n-1) equations are postulated for structuring the spline. In case of a quadratic spline (2^{nd} degree polynomial) equations are presented as follows:

for n points coordinated as x_i, y_i, i=1,2,…,n

$$\begin{aligned} y_{i-1} &= a_i x_{i-1}^2 + b_i x_{i-1} + c_i \\ y_i &= a_i x_i^2 + b_i x_i + c_i \\ \frac{d}{dx}(a_{i-1} x_{i+1}^2 + b_{i-1} x_{i+1} + c_{i-1}) &= \frac{d}{dx}(a_i x_{i+1}^2 + b_i x_{i+1} + c_i) \end{aligned} \quad \textbf{(3.7)}$$

Equations (3.7) illustrate that each spline merges two consecutive points, while the slopes of two conterminous splines in their merge point are equal. For higher order splines (cubic, etc.) additional differential equations (e.g second order differential in cubic splines) with increased parameters are needed.

Types of splines (B-splines) rely on control points in order to smoothen the basic line. The number of control points defines the level of smoothness.

3.3.3. Moving average

Moving average is another method for smoothing trajectories. Its principle relies on averaging data points from the previous measurements in order to predict the current one. Moving average methods comprise of more than one type. The preceding statements describe the simple moving average type. The weighted moving average results from the extension of the simple moving average with the incorporation of weight coefficients to the previous measurements in order to prioritize current data points. Exponential moving average (EMA) is also a moving average extension that emphasizes, by default, on current data points, in contrast to weighted moving average where weights are set up by the researcher. The contribution of the previous data points decreases exponentially, as described in equation 3.8.

$$x_t = aD_{t-1} + a(1-a)D_{t-2} + a(1-a)^2 D_{t-3} + a(1-a)^3 D_{t-4} + \ldots + a(1-a)^{n-1} D_{t-n} \Rightarrow$$
$$x_t = a(D_{t-1} + (1-a)D_{t-2} + (1-a)^2 D_{t-3} + (1-a)^3 D_{t-4} + \ldots + (1-a)^{n-1} D_{t-n}) \Rightarrow \quad (3.8)$$
$$x_t = a\sum_{i=1}^{n} D_{t-1}(1-a)^{i-1}$$

where x_t stands for the estimated value at time t, a is a smoothing parameter representing the weighting level, ranging between 0 and 1 and D_{t-1} is the actual measurement at time t-1.

In addition, the running average technique is a similar approach to the moving average. Instead of employing the average of the previous data points, it utilizes the median. Hence the importance of outliers in the examined dataset is limited (Hen et al., 2004).

3.4. Social Force Model

3.4.1. Overview (base model)

Social force model is presented analytically to outline the concept of the model, describe its parameters and clarify the comparison with the data-driven techniques. Data-driven predictors are selected based on the social force model's parameters.

The social force model was first developed and calibrated by Helbing and Molnár (1995) for pedestrian movement capturing well known pedestrian movement phenomena (through computer simulations). They defined three velocity types of pedestrian α : i) desired velocity $\vec{u}_\alpha^0$ as the velocity that pedestrian will walk, if they were not disturbed from surroundings, ii) preferred velocity $\overrightarrow{w_\alpha}$ that its alterations are assessed by the social forces and is constrained to the maximum acceptable speed and iii) actual velocity $\overrightarrow{u_\alpha}$. The main idea of the model is that velocity time deviations are originated by the social forces according to equation 3.9.

$$\frac{d\overrightarrow{w_\alpha}}{dt} = \overrightarrow{F_\alpha}(t) \quad \textbf{(3.9)}$$

where $\vec{F_\alpha}(t)$ stands for the total forces that are acted upon pedestrian α at time t. Helbing and Molnár (1995) added fluctuations to equation (3.9) in order to include model uncertainty. Social forces $\vec{F_\alpha}(t)$ are classified to:

- Attractive forces from destination $\vec{F}_\alpha^0$
- Repulsive forces
    - From other pedestrians β ($\vec{F_{\alpha\beta}}$)
    - From boundaries B ($\vec{F_{\alpha B}}$) and
- Attractive forces from other agents or objects i ($\vec{F_{\alpha i}}$)

Destination area forces the agent to reach their destination (attractive force). In cases of no disturbances pedestrians tend to keep their desired direction ($\vec{e_\alpha}$) with their desired speed (u_α^0). A relaxation factor (τ_α) that measures the time duration an agent needs for re-adapting its route to the desired one (when deviations from their desired route occur) is introduced. The attractive force to destination is specified in equation (3.10).

$$\vec{F}_\alpha^0 = \frac{1}{\tau_\alpha}(u_\alpha^0 \vec{e_\alpha} - \vec{u_\alpha}) \qquad \textbf{(3.10)}$$

Contrary to attractive forces, repulsive forces, generated from agents and boundaries (pedestrians avoid proximity to boundaries), are acted upon the moving pedestrian. Among other parameters, distances between the examined agent and other pedestrians ($\vec{r_{\alpha\beta}}$) or boundaries ($\vec{r_{\alpha B}}$) are crucial. Equations (3.11) and (3.12) illustrate repulsive forces from pedestrians and obstacles respectively.

$$\vec{f_{\alpha\beta}} = -\nabla_{\vec{r}_{\alpha\beta}} V_{\alpha\beta}[b(\vec{r_{\alpha\beta}})] \qquad \textbf{(3.11)}$$

$$\vec{F_{aB}} = -\nabla_{\vec{r}_{aB}} U_{\alpha B}(\|\vec{r_{aB}}\|) \qquad \textbf{(3.12)}$$

where b stands for the minor of V ellipse monotonic function, given by equation (3.13). The distance from the closest to the pedestrian obstacle point is taken into account in equation (3.13).

$$b = \frac{\sqrt{(\left\|\overrightarrow{r_{\alpha\beta}}\right\| + \left\|\overrightarrow{r_{\alpha\beta}} - u_\beta \Delta t \overrightarrow{e_\beta}\right\|)^2 - (u_\beta \Delta t)^2}}{2} \quad \textbf{(3.13)}$$

where $\upsilon_\beta \Delta t$ stands for the pedestrian's β step width.

Helbing and Molnár (1995) assessed repulsive force's functions in their experiment as:

$$V_{\alpha\beta}(b) = V_{\alpha\beta}^0 e^{-b/\sigma} \quad \textbf{(3.14)}$$

$$U_{\alpha B}(\left\|\overrightarrow{r_{\alpha B}}\right\|) = U_{\alpha B}^0 e^{-\left\|\overrightarrow{r_{\alpha B}}\right\|/R} \quad \textbf{(3.15)}$$

Nearby agents and objects might also apply attractive forces ($\overrightarrow{F_{\alpha i}}$) to the moving pedestrian. The specific force type distracts walking agents from their final destination. The difference from repulsive forces is that the parameter of time is introduced in attractive forces, due to the decreasing interest by the time.

$$\overrightarrow{f_{\alpha i}} = -\nabla_{\overrightarrow{r_{\alpha i}}} W_{\alpha i}(\left\|\overrightarrow{r_{\alpha i}}\right\|, t) \quad \textbf{(3.16)}$$

Humans do not have 360^o angle of vision and events that occur out of their sight view affect them less. As a consequence, weights that consider moving pedestrian's view angle are introduced in the estimation of repulsive and attractive forces, converting them to:

$$\overrightarrow{F_{\alpha\beta}} = w\overrightarrow{f_{\alpha\beta}} \quad \textbf{(3.17)}$$

$$\overrightarrow{F_{\alpha i}} = w\overrightarrow{f_{\alpha i}} \quad \textbf{(3.18)}$$

Ultimately, the force that affects pedestrian movement ($\overrightarrow{F_\alpha}(t)$) is estimated as the sum of the aforementioned forces.

$$\overrightarrow{F_\alpha} = \vec{F}_\alpha^{0} + (\overrightarrow{F_{\alpha\beta}} + \overrightarrow{F_{\alpha B}}) + \overrightarrow{F_{\alpha i}} \quad \textbf{(3.19)}$$

Maximal acceptable speed u_α^{max} is also introduced to social force model for preventing simulation of extreme and unrealistic pedestrian velocities.

3.4.2. Social Force Model Modifications

An improved modified version, which was developed by Helbing and Johansson (2010) and was also described in Helbing (2012), differentiated the social force model pedestrian's repulsive forces equation (3.20) by importing interaction strength (A) and interaction range (B) parameters.

$$V_{\alpha\beta}(b) = ABe^{-b/B} \quad \textbf{(3.20)}$$

Furthermore, in this version the pedestrian's velocity ($\overrightarrow{u_\alpha}$) was also included in estimation of the repulsive force. Semi-minor ellipse monotonic axis b equation is transformed to:

$$b = \frac{\sqrt{(\left\|\overrightarrow{r_{\alpha\beta}}\right\| + \left\|\overrightarrow{r_{\alpha\beta}} - (\overrightarrow{u_\beta} - \overrightarrow{u_\alpha})\Delta t\right\|)^2 - \left\|(\overrightarrow{u_\beta} - \overrightarrow{u_\alpha})\Delta t\right\|^2}}{2} \quad \textbf{(3.21)}$$

leading to the below repulsive force equation

$$\overrightarrow{f_{\alpha\beta}} = Ae^{-b/B} \frac{\left\|\overrightarrow{r_{\alpha\beta}}\right\| + \left\|\overrightarrow{r_{\alpha\beta}} - (\overrightarrow{u_\beta} - \overrightarrow{u_\alpha})\Delta t\right\|}{2b} \frac{1}{2}\left(\frac{\overrightarrow{r_{\alpha\beta}}}{\left\|\overrightarrow{r_{\alpha\beta}}\right\|} + \frac{\overrightarrow{r_{\alpha\beta}} - (\overrightarrow{u_\beta} - \overrightarrow{u_\alpha})\Delta t}{\left\|\overrightarrow{r_{\alpha\beta}} - (\overrightarrow{u_\beta} - \overrightarrow{u_\alpha})\Delta t\right\|} \right) \quad \textbf{(3.22)}$$

An improved specification of agent's angular sight view was also introduced. The angular-dependent prefactor $w(\varphi_{\alpha\beta})$ of $\varphi_{\alpha\beta}$ angle is determined as follows:

$$w(\varphi_{\alpha\beta}(t)) = \lambda_\alpha + (1 - \lambda_\alpha)\frac{1 + \cos(\varphi_{\alpha\beta})}{2} \quad \textbf{(3.23)}$$

where λ_α represents the strength of interactions from behind, ranging among 0 and 1 and $\cos(\varphi_{\alpha\beta})$ is computed as:

$$\cos(\varphi_{\alpha\beta}) = \frac{\vec{u_\alpha}}{\left\|\vec{u_\alpha}\right\|} \frac{-\vec{r_{\alpha\beta}}}{\left\|\vec{r_{\alpha\beta}}\right\|} \quad \textbf{(3.24)}$$

Moussaïd et al. (2009) presented an alternative social force approach in order to simulate interaction laws among pedestrians. Their model differs from the initial of Helbing and Molnár (1995) considering the term of repulsive forces (among agents). However, it did not provide explicitly improved simulation results compared to those of Helbing and Johansson (2010).

3.4.3. Social Force Model Parameters

The parameters that determine the model structure are:

- Moving pedestrian
  - Desired speed (u_α^0)
  - Relaxation time (τ_α)
  - Maximum acceptable speed (u_α^{max})
  - Strength of interactions from behind (λ_α)
- Repulsive force
  - From pedestrian
    - interaction strength (A)
    - interaction range (B)
  - From obstacle
    - function constant ($U_{\alpha B}^0$)
    - exponential parameter (R)
- Attractive force
  - function constant ($W_{\alpha i}^0$)
  - exponential parameter (L)

Helbing and Molnár (1995) specified social force parameters in their experiment, as presented in Table 3.1.

Table 3.1: Social force parameters (Helbing and Molnár, 1995)

Social force parameters		
Parameter	**Value**	**Units**
Desired speed	N~(1.34, 0.26)	m/s
Maximum acceptable speed	1.3 * desired speed	m/s
Relaxation time	0.5	s
Angle view	200	degrees
Outside of view influence	0.5	-
Coterminous pedestrian step time	2	s
Repulsive force from pedestrian function constant	2.1	m2/s2
Repulsive force from pedestrian exponential parameter	0.3	m
Repulsive force from obstacle function constant	10	m2/s2
Repulsive force from obstacle exponential parameter	0.2	m

Figure 3.3 provides an overview of the calibrated social force model parameters as recorded in the relevant studies. Helbing and Molnár (1995) were the first to attempt to estimate social force model parameters. Besides that, postliminary papers deal with this issue. Specifically, Zeng et al. (2014) calibrated pedestrians' desired speed, relaxation time, maximum acceptable speed and the repulsive forces' parameters in crossing scenarios, where pedestrian conflicts with vehicles occurred. They, however, did not use the most recent at the time version of the

social force model. Johansson et al. (2007) and Zanlungo et al. (2011) calibrated repulsive forces' parameters in indoor environments. Song et al. (2006) specified desired speed range in a mixed social force model (including cellular automata) in order to simulate arching, clogging and "faster is slower" phenomena. Moussaïd et al. (2009) calibrated social force parameters using video trajectories from corridors, while Voloshin et al. (2015) utilized real-world data from a metro station entrance. Voloshin et al. (2015) presented a method for calibrating the constant and exponential parameters both for repulsive forces among pedestrians, and between pedestrians and objects by employing a genetic algorithm, without providing information on parameters' optimal values and/or ranges. At the same time, attractive force parameters have not been widely examined, and thus their ranges are unknown.

The ranges noted by the different researchers will form the basis for the social force model calibration in this research. The noted range of maximal desirable speed is wider to that of acceptable speed, as Song et al. (2006) who provided the widest range of desired speed, did not provide the respective values for maximal acceptable speed. As a consequence, in the social force model training process (see Section 5.2) a range of maximal acceptable speed coefficient between 1 and 2 is employed. In addition, Johansson et al. (2007) and Helbing and Johansson (2010) provide an extremely wide range for interaction range (B) parameter that is restricted in the social force model training process (Section 5.2). Furthermore, considering the aforementioned training process, Zeng et al. (2014) relaxation time parameter range is reduced based on its mean (2.2s) and standard deviation (0.5s).

Apart from social force models, calibration techniques have been also used in other pedestrian simulation model types. For example, Teknomo (2006) developed a microscopic pedestrian model, similar to social force, and calibrated and validated its parameters focusing on minimizing the difference between simulated and tracked attributes. Guo et al. (2010) developed a discrete choice model for pedestrian simulation and calibrated it using data from experiments with the aid of a heuristic method. Daamen and Hoogendoorn (2012) employed maximum likelihood estimation for calibrating their model by using data from laboratory experiments. They assumed errors (agent acceleration difference

between simulated and obtained from data) follow zero mean normal distributions.


Desired speed
Helbing and Molnar (1995)
Moussaid et al. (2009)
Song et al. (2006)
Zeng et al. (2014)
0
1
2
3
4
5
(m/s)

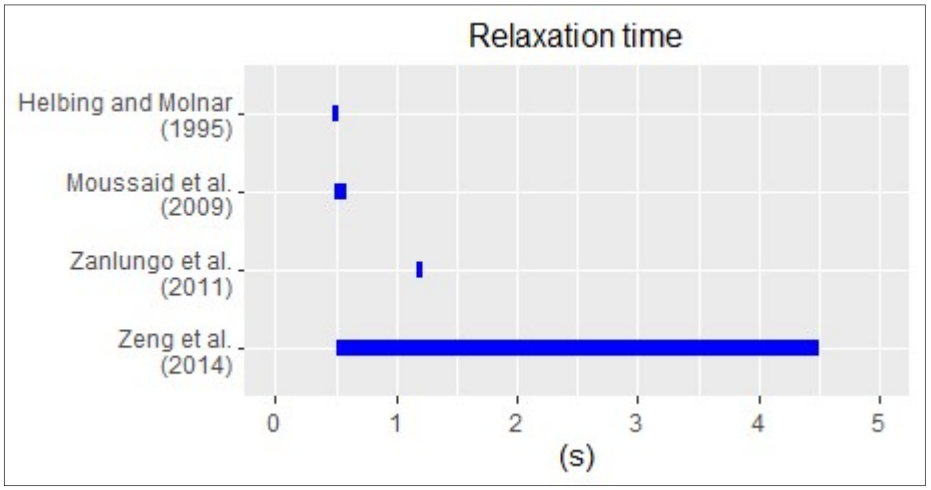
Relaxation time
Helbing and Molnar (1995)
Moussaid et al. (2009)
Zanlungo et al. (2011)
Zeng et al. (2014)
0
1
2
3
4
5
(s)

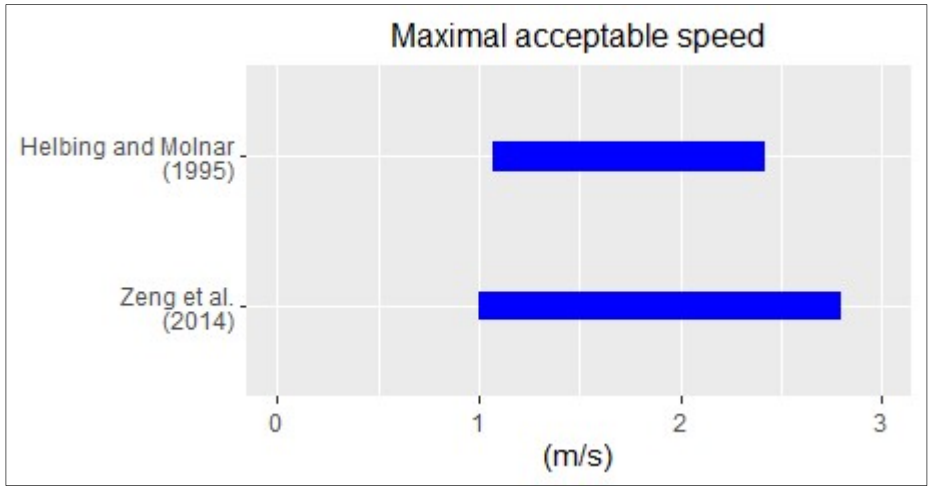
Maximal acceptable speed
Helbing and Molnar (1995)
Zeng et al. (2014)
0
1
2
3
(m/s)

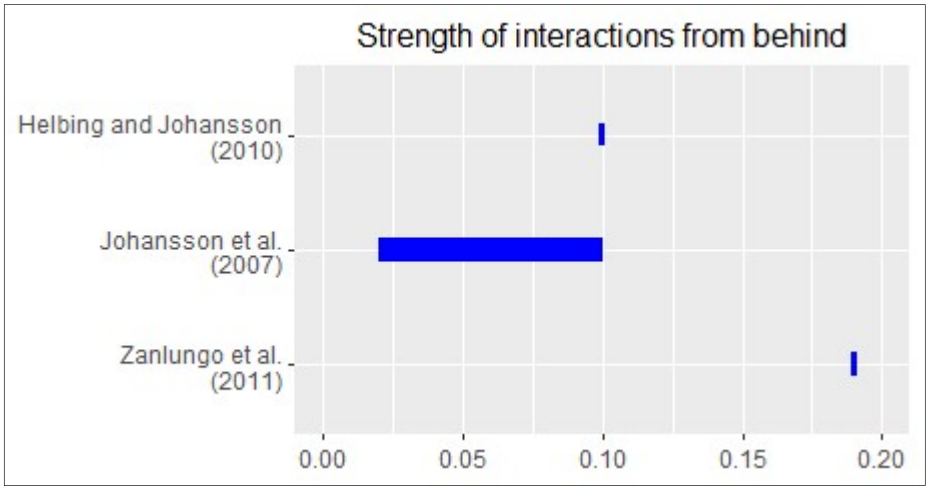
Strength of interactions from behind
Helbing and Johansson (2010)
Johansson et al. (2007)
Zanlungo et al. (2011)
0.00
0.05
0.10
0.15
0.20

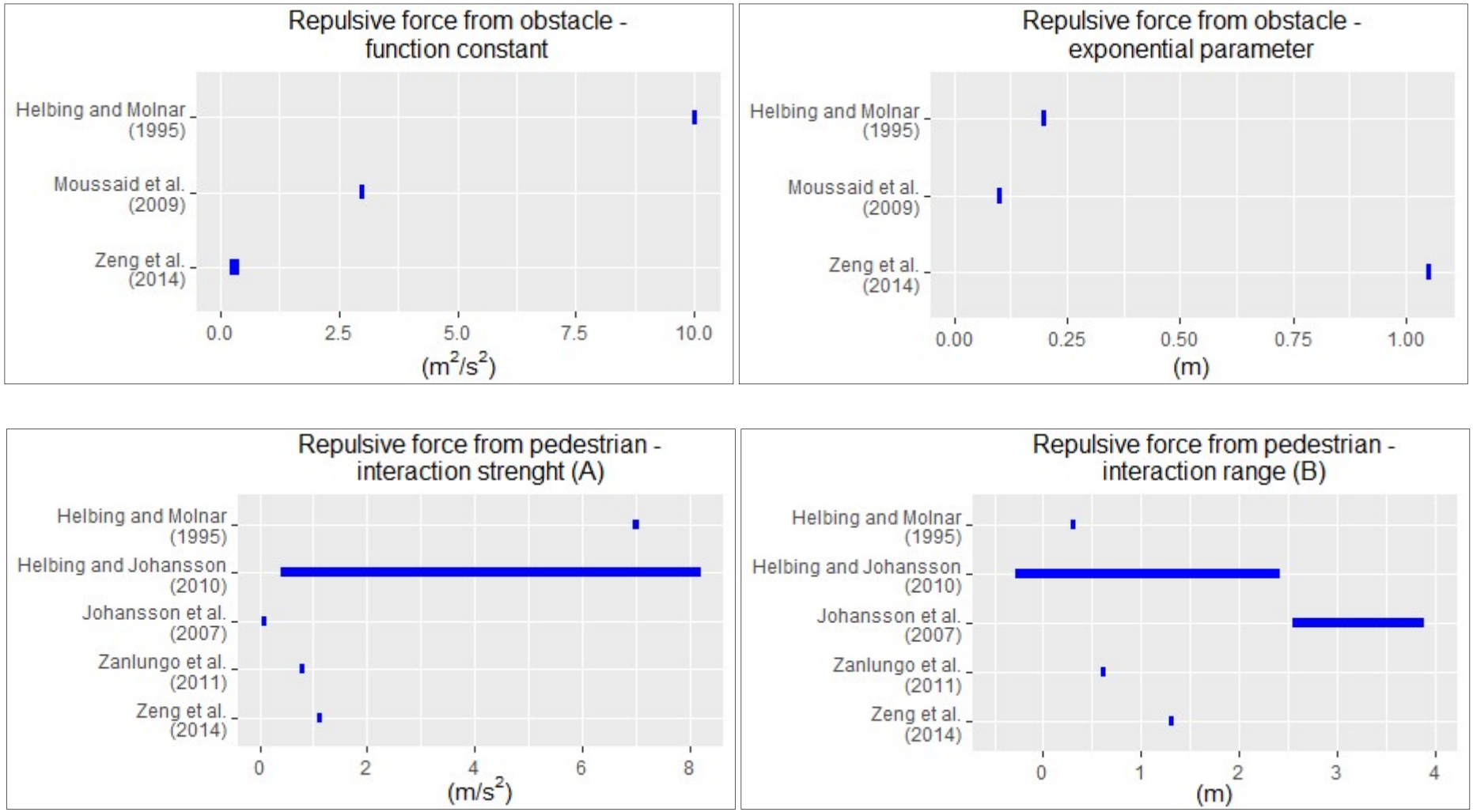

Figure 3.3: Social force model parameters range

3.5. Data-Driven Modelling

3.5.1. Overview

Data-driven models employ non-parametric methods. Algorithms are used in order to extract, in a definite manner, information from data and develop automatically a model based entirely on them (data). Classification, clustering, regression and prediction comprise data mining principles. They overcome parametric tools as they do not rely on specific assumptions and do not require a priori determination of the relationship among the variables. On the other hand, they do not provide an unambiguous relationship between variables. In the next sections the data-driven techniques that are employed in this research are described. A brief description of the comparison framework between the different models is provided in section 3.6, while an extensive description of the models' comparison procedure is provided in section 5.1.

3.5.2. Neural Networks

Artificial Neural Networks (ANN) comprise one of the most popular data-driven methods. They can be implemented in classification, clustering and regression problems. They are used both in supervised and unsupervised learning. ANN attempt to mimic the operation of biological neural networks. The information is transferred from the neurons (nodes) of the first layer to those in the next layer with the aid of the synaptic weights and the activation function until the final layer (output layer), where predicted values are estimated. The goal of the ANN training procedure is to estimate the values of the weights that minimize a cost function, i.e. an error function between predicted (output layer) and measured values.

One of the first ANN models was presented by McCullogh and Pitts (1943). In their approach one hidden layer with one neuron was employed. The neuron takes the inputs from the first layer and according to the step function fires or not. Synaptic weights and thresholds are the critical parameters for this. As McCullogh-Pitts model did not perform sufficiently well in nonlinear problems,

networks with more neurons and hidden layers were later developed, such as the Multi-Layer Perceptron (MLP). A typical MLP is presented in Fig. 3.4.

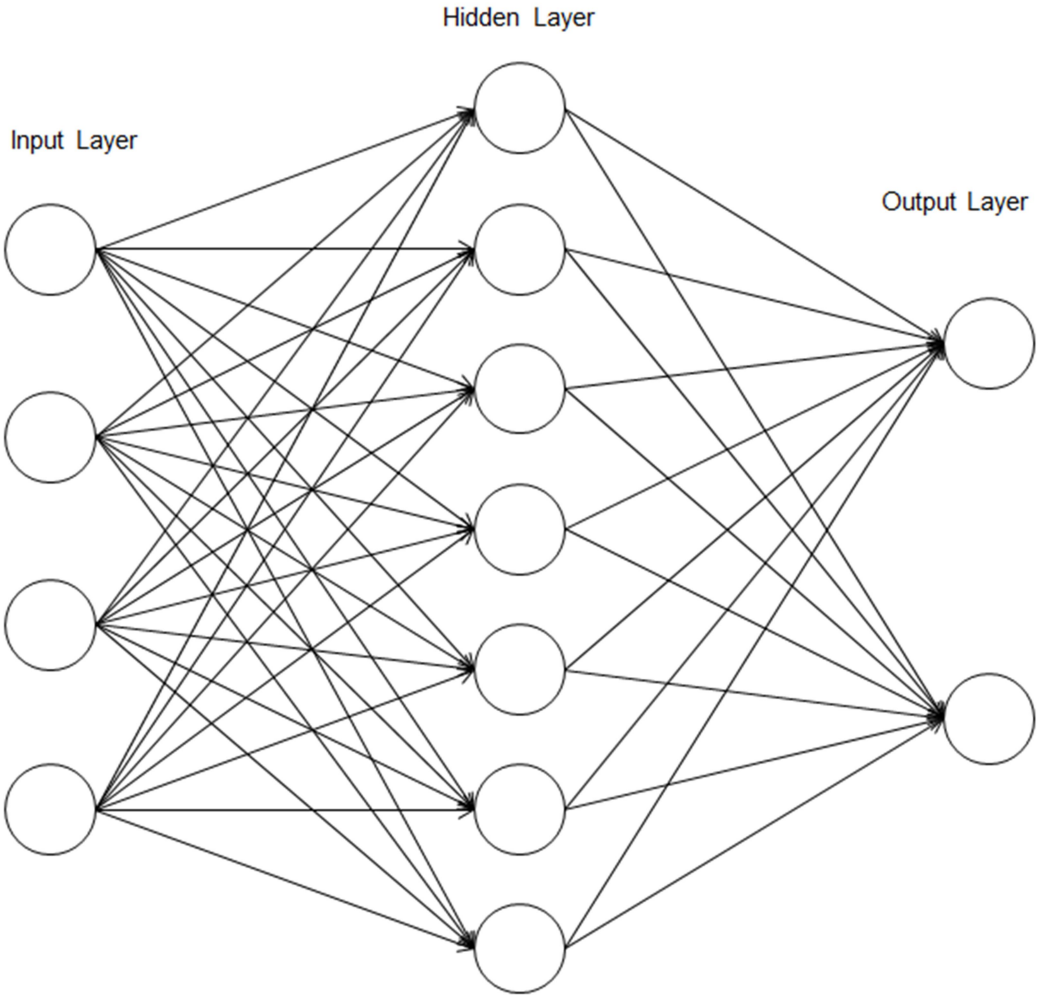

Figure 3.4: Multi-Layer Perceptron

Every node in each layer is connected to all the nodes of the next layer. Data are imported in the model in the first layer, named as input layer. Then the nodes in the hidden layer are affected by the input layer nodes according to equation (3.25).

$$u = \sum_{i=0}^{n} w_i x_i \qquad \textbf{(3.25)}$$

where w_i stands for the synaptic weights from the node i of the input layer and x_i for the input value of the node i. In case of i=0 w_0 equals to the threshold value and x_0 equals to -1. Subsequently, according to an activation function the neuron

of the hidden layer produces a specific value. This procedure is repeated to all the nodes of the hidden layer. Next, the neurons in the output layers are activated. In this case the input values are the values that have been produced in the nodes of the hidden layer. An error measure (e.g. mean square error) among the predicted and the measured (in terms of supervised learning) values is used. The goal of the ANN training procedure is to estimate the values of the weights that minimize a cost function, i.e. an error function between predicted and measured values.

A few training algorithms have been proposed with the Back-Propagation being the most widespread. It was proposed by Paul Werbos (1974) for application in ANN while a higher recognition in the ANN training process was gained by Rumelhart et al. (1986). This is a supervised learning algorithm. In this method, the algorithm “corrects” the synaptic weights in a gradient descent procedure.

Initially the inputs of the first data are passed in the ANN model with pre-defined synaptic weights values and predicted values in the output layer are computed. The algorithm alters the weights backwards (from the output layer to the input) according to the delta rule and attempting to reduce the cost function. It then computes the contribution to error (δ_i) of the output layer nodes and in the hidden layers (equation 3.26).

$$\delta_i = \begin{cases} e_i f'(u), \forall i \in \text{output layer} \\ f'(u)\sum_{j=1}^{k} \delta_j w_{ij}, \forall i \in \text{hidden layer} \end{cases} \quad \textbf{(3.26)}$$

where e_i stands for the error in the i neuron, $f'(u)$ for the derivative of the activation function, j is the neuron in the net of next layer (i.e. in one case on one hidden layer j neuron stands for the neuron of the output layer) and w_{ij} for the synaptic weight from node to neuron i to neuron j.

Weights alteration is accomplished according to equation (3.27)

$$\Delta w_{ij} = \eta \delta_j y_i \quad \textbf{(3.27)}$$

where η is the learning rate and y_i the output of neuron i.

Following the computation of the new weights, the second data are passed in the model and the same procedure is repeated. When all of the synaptic weights until the first layer are re-estimated an epoch is completed. The training procedure continues until a termination criterion is fulfilled. Termination criteria might be a) a maximum number of epochs, b) the error being lower than a priori specified threshold, c) the error remaining the same for two continuing epochs.

A careful specification of η is crucial as very low values can lead to vanishing gradient problems where the weights are updated very slowly and the algorithm needs time to converge or on the other hand to exploding gradient problems where high values of learning deter the algorithm to converge. The inclusion of momentum can restrict this problem. Thus equation (3.27) can be updated to (3.28).

$$\Delta w_{ij}(n) = \eta \delta_j(n) y_i(n) + a \Delta w_{ij}(n-1) \qquad \textbf{(3.28)}$$

where n stands for the epoch and a for the momentum variable.

In all of the above described methods the weight initialization might play a crucial role in the training of the model.

Algorithm 3.1 : Back-Propagation

Initialize synaptic weights w_{ij}

For epoch n=1:N {

Pass inputs in the model

Compute outputs in the output layer

Compute δ_i for all the neurons

Compute Δw_{ij} for all the neurons

Update synaptic weights $w_{ij}(n+1) = w_{ij}(n) + \Delta w_{ij}(n)$

}

The number of layers, the number of nodes in each layer, the activation function (can be different among the nodes), the training algorithm (back-propagation is the most common), the optimization algorithm (gradient descent procedure), its learning rate and its termination criterion, are hyperparameters that need to be specified prior to the training process. It should be mentioned that a model with more nodes in the hidden layer has greater ability to capture interactions between parameters.

The application of ANN technique in the present research is presented in section 5 (see section 5.2.3).

3.5.3. Gaussian Processes

Gaussian Processes (GP) comprise an additional method in the field of machine learning techniques, mainly used in terms of supervised learning (regression, classification). They are described below according to Rasmussen and Williams (2006). As indicated by their name they rely on Gaussian (normal) distributions and are a collection of random variables, which follow a multivariate Gaussian distribution. A GP is specified by its mean m(x) and its covariance function $K(x, x')$ (equations 3.29 – 3.31). In case of a multivariate Gaussian distribution with two or more variables, they can be partitioned to Gaussians with means and covariance matrices (marginalization property).

$$f(x) \sim GP(m(x), K(x, x')) \quad \textbf{(3.29)}$$

$$m(x) = E[f(x)] \quad \textbf{(3.30)}$$

$$K(x, x') = E\left[(f(x) - m(x))(f(x') - m(x'))^T \right] \quad \textbf{(3.31)}$$

As in most cases the mean is considered to be zero, the interest is around the covariance function. For this reason, a kernel function is necessary in order to estimate the covariance. The most commonly used kernel is the Radial Basis Function (RBF) or the Gaussian kernel (equation 3.32), while periodic and linear kernels have also been applied (Rasmussen and Williams, 2006). RBF is a stationary kernel where the covariance of two points depends on their relative

and not on their absolute (contrary to non-stationary kernels) position. In terms of mathematical calculations and in order to perform Choleksy decomposition (for estimating covariance matrix square root), the kernel matrix needs to be symmetric and positive definite.

During the training process, the GP provide the model framework relating all the data in multivariate Gaussian distributions with a predefined kernel function. As for the RBF kernel, its function consists, among others, of two parameters, the length (l) and the height (σ) of the kernel, called hyperparameters.

Furthermore, assuming of an i.i.d. noise with zero mean and σ_y^2 variance (similarly to parametric regression), the covariance matrix is updated in order to incorporate noise as in equation (3.33). Last, GP returns a predictive value adding its uncertainty (probabilistic prediction with confidence intervals).

$$k(x,x') = \sigma^2 e^{-\frac{1}{2l^2}(x-x')^2} \quad \textbf{(3.32)}$$

$$K(x,x') = k(x,x') + l\sigma_y^2 \quad \textbf{(3.33)}$$

GP perform well in a small amount of data, while they have significantly high computational requirements in models with many variables (high dimensional kernel matrices) and large datasets. Reduced-rank approximations to the covariance matrix are one way for moderating the problem.

In comparison to other data-driven techniques, Rasmussen and Williams (2006) note that SVM perform slightly better than GP in terms of classification problems. In addition, they present an alternative to the cross-validation method which is based on Bayesian statistics for estimating GP kernel function hyperparameters. The general idea of this method is that the posterior distribution $p(w \mid y, X, \theta, H_i)$ over the parameters w is related to the prior distribution $p(w \mid J, H_i)$ given the hyperparameters θ and the set of possible model structures H_i, the likelihood $p(y \mid X, w, H_i)$ and the marginal likelihood $p(y \mid X, \theta, H_i)$ of all the outputs y for all the possible datasets (equation 3.34). A prior distribution can be converted to a posterior after incorporating some data.

$$p(w \mid y, X, \theta, H_i) = \frac{p(y \mid X, w, H_i)p(w \mid \theta, H_i)}{p(y \mid X, \theta, H_i)} \quad \textbf{(3.34)}$$

Still, this Bayesian framework depends on several mathematical formulations (integrals) that may not be governable. In addition, the results are very sensitive to the prior distribution.

At this point it must be clarified that GP training optimization differs from training optimization in other machine learning methods (e.g. ANN). During the training in a GP the goal is to estimate model hyperparameters (see above) with the employment of the appropriate algorithm. On the other hand, hyperparameters in an ANN are set initially (prior to the training process) and remain constant during the whole training procedure. The goal of an ANN train is to estimate model parameters, e.g. synaptic weights. Still, in both methods initial values are important for model training.

A widespread optimization algorithm for GP training process is the Limited-memory BFGS (L- BFGS) that is based on the Broyden–Fletcher–Goldfarb–Shanno (BFGS), which was independently developed in 1970 by Broyden (1970), Fletcher (1970), Goldfarb (1970) and Shanno (1970). L- BFGS is presented by Byrd et al. (1995) as a gradient descent method in the field of quasi-Newton theory. The algorithm is relaxed of second derivatives calculation and can be applied when the Hessian matrix computation is not practical.

In the present research a multi-output regression has to be performed as the pedestrian's velocity is presented in two axes. However GP initial setup lacks the multi-output model availability. A solution might be to apply separated GP models for every output (i.e. the velocity in each axis), though the correlation among the outputs, which is a crucial information, will be discarded.

Alvarez et al. (2012) presented multi-output kernel functions for GP modeling. The method is suitable also in cases with different input spaces for every output (heterotopic models). Contrary to single–output models, multi–output models associate variables to different processes ($\{f_d\}_{d=1}^{D}$, where D is the number of outputs). Alvarez et al. (2012) developed a linear model of coregionalization (LMC), where outputs are expressed as linear combinations of independent random functions and each f_d is expressed with the aid of latent functions $u_q(x)$, of

zero mean and covariance $\mathrm{cov}\left[u_q(x), u_{q'}(x')\right]$ (equation 3.35), and scalar coefficients ($a_{d,q}$ equation 3.36). Grouping the number of latent functions that share the same covariance, they ended up with equation (3.36). R stands for the number of latent functions that share the same covariance in the group and the number Q of groups.

$$\mathrm{cov}\left[u_q(x), u_{q'}(x')\right] = k_q(x, x'), \quad \text{if } q = q' \tag{3.35}$$

$$f_d(x) = \sum_{q=1}^{Q} \sum_{i=1}^{R_q} a_{d,q}^{i} u_q^{i}(x) \tag{3.36}$$

The cross-covariance between any two functions $f_d(x)$ and $f_{d'}(x')$ is illustrated in below (equation (3.37)).

$$\mathrm{cov}\left[f_d(x), f_{d'}(x')\right] = \sum_{q=1}^{Q} \sum_{q'=1}^{Q} \sum_{i=1}^{R_q} \sum_{i'=1}^{R_q} a_{d,q}^{i} a_{d',q'}^{i'} \mathrm{cov}\left[u_q^{i}(x), u_{q'}^{i'}(x')\right] \tag{3.37}$$

Expressing equation (3.37) as a kernel function and due to the independence of latent functions, researchers came up with equation (3.38).

$$\left(K(x, x')\right)_{d,d'} = \sum_{q=1}^{Q} \sum_{i=1}^{R_q} a_{d,q}^{i} a_{d',q}^{i} k_q(x, x') = \sum_{q=1}^{Q} b_{d,d'}^{q} k_q(x, x') \tag{3.38}$$

with $b_{d,d'}^{q} = \sum_{i=1}^{R_q} a_{d,q}^{i} a_{d',q}^{i}$.

Ultimately the kernel function can be expressed in terms of a symmetric and positive semi-definite D x D matrix (B_q) that encodes correlations among the outputs (equation 3.39).

$$K(x, x') = \sum_{q=1}^{Q} B_q k_q(x, x') \tag{3.39}$$

In this paper researchers have also presented a simplified and much more restrictive method than LMC called the intrinsic coregionalization model (ICM).

The application of GP technique in the present research is presented in section 5 (see section 5.2.3).

3.5.4. Support Vector Regression (SVR)

Support vector regression (SVR) is a regression machine learning method relying on Support Vector Machines (SVM). SVM is a widespread method mainly applied in classification problems and rarely in clustering (Support Vector Clustering - SVC). They are used for separating data between two classes, though multiclass classification libraries have also been presented (e.g. Chang and Lin, 2011).

SVM estimate the best hyperplane that separates the data between the two classes. Suppose that we have a set of data points (x) that belongs either to C_0 or to C_1 class. The classification problem is defined by the equation (3.40).

$$w^T x + w_0 \begin{cases} < 0, x \in C_0 \\ > 0, x \in C_1 \end{cases} \quad \textbf{(3.40)}$$

A margin between the two classes is also set (Fig 3.5). The margin is defined by the two support vectors that in practice are the “edges” of the two classes and is equal to the inverse of their distance ($\frac{2}{\|w\|}$).

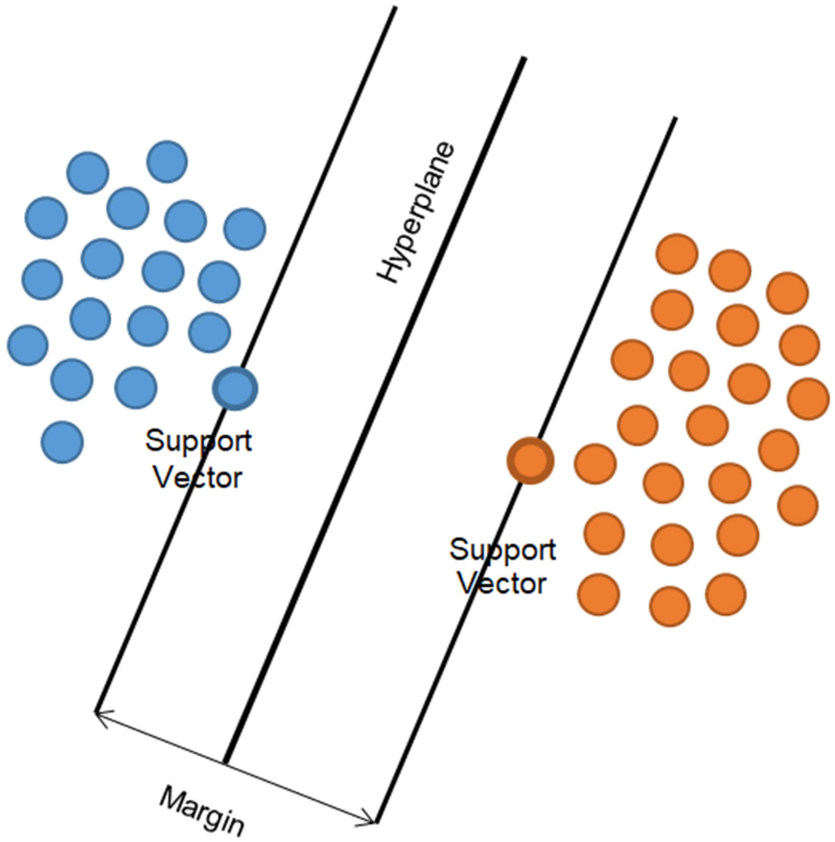

Figure 3.5: Support Vector Machine

In cases where the margin is close to zero the possibility of a false classification is high due to the fact that the two classes are not clearly separated. As a consequence SVM relies only on the support vectors ignoring all the other data points. This reduces significantly the complexity of the model and their computational requirements, but on the other hand makes it very sensitive to support vectors as a small modification of them (modification only on the support vectors and not on the rest of the dataset) change the separating hyperplane. The goal of an SVM is to estimate the coefficients w^T and w_0 of the hyperplane equation (3.41).

$$w^T x + w_0 = 0 \qquad \textbf{(3.41)}$$

In particular to find w^T and w_0 that maximize the margin and thus minimize $\|w\|$ such that all data points (x_i, y_i).

$$y_i\left(w^T x_i + w_0\right) \geq 1 \qquad \textbf{(3.42)}$$

Data outputs (y_i) equal to -1 or 1 whether the data point i belongs either to C_0 or to C_1 class. Actually the model minimizes $\frac{1}{2}\|w\|^2$ as the derivative of $\|w\|$ is also a constant value (the constant $\frac{1}{2}$ is added for simplicity reasons). As a result this is a quadratic programming optimization problem. Lagrange multipliers α_i are very useful for this type of problems. The loss function is transformed to

$$L_P\left(w, w_0, \alpha_i\right) = \frac{1}{2}\|w\|^2 - \sum_{i=1}^{N} \alpha_i \left[y_i \left(w^T x_i + w_0 \right) - 1 \right] \quad \textbf{(3.43)}$$

L function needs to be minimized w.r.t. to w and w_0 and maximized w.r.t. α_i. According to Karush-Kuhn-Tucker conditions at the optimization point we get:

$$\frac{\partial L}{\partial w_0} = 0 \quad \textbf{(3.44)}$$

$$\frac{\partial L}{\partial w} = 0 \quad \textbf{(3.45)}$$

$$\alpha_i \left[y_i \left(w^T x_i + w_0 \right) - 1 \right] = 0 \quad \textbf{(3.46)}$$

Equations (3.44) and (3.46) are then transformed to equations (3.47) and (3.48) respectively.

$$\sum_{i=1}^{N} \alpha_i y_i = 0 \quad \textbf{(3.47)}$$

$$w = \sum_{i=1}^{N} \alpha_i y_i x_i \quad \textbf{(3.48)}$$

By substituting equations (3.47) and (3.48) to equation (3.46) the optimization problem is converted to the dual problem [maximize equation (3.49)].

$$L_D\left(w, w_0, \alpha_i\right) = \sum_{i=1}^{N} \alpha_i - \frac{1}{2} \sum_{i=1}^{N} \sum_{j=1}^{N} \alpha_i \alpha_j y_i y_j x_i^T x_j \quad \textbf{(3.49)}$$

subject to

$$\sum_{i=1}^{N} y_i \alpha_i = 0 \qquad \textbf{(3.50)}$$

$$\alpha_i \geq 0 \qquad \textbf{(3.51)}$$

In cases of non-separable data slack variables ξ_i are introduced in the model. Thus equation (3.42) is transformed to

$$y_i \left(w^T x_i + w_0 \right) \geq 1 - \xi_i \qquad \textbf{(3.52)}$$

while $$\xi_i \geq 0 \qquad \textbf{(3.53)}$$

and equation (3.43) to

$$L_P \left(w, w_0, \alpha_i, \xi_i \right) = \frac{1}{2} \|w\|^2 + C \sum_{i=1}^{N} \xi_i - \sum_{i=1}^{N} \alpha_i \left[y_i \left(w^T x_i + w_0 \right) - 1 + \xi_i \right] - \sum_{i=1}^{N} \mu_i \xi_i \qquad \textbf{(3.54)}$$

where μ_i stands for the Lagrange multipliers of slack variables ξ_i and C a penalty parameter. By increasing C more weight is placed on the slack variables while setting C equal to 0 makes slack variables unimportant. In line to Karush-Kuhn-Tucker conditions

$$\frac{\partial L}{\partial \xi_i} = 0 \qquad \textbf{(3.55)}$$

leads to

$$C - \alpha_i - \mu_i = 0 \qquad \textbf{(3.56)}$$

or

$$\alpha_i = C - \mu_i \qquad \textbf{(3.57)}$$

with $$\alpha_i, \mu_i \geq 0 \qquad \textbf{(3.58)}$$

As a consequence the equation of the dual problem is

$$L_D \left(w, w_0, \alpha_i \right) = \sum_{i=1}^{N} \alpha_i - \frac{1}{2} \sum_{i=1}^{N} \sum_{j=1}^{N} \alpha_i \alpha_j y_i y_j x_i^T x_j \qquad \textbf{(3.59)}$$

subject to

$$\sum_{i=1}^{N} y_i \alpha_i = 0 \qquad \textbf{(3.60)}$$

$$0 \le \alpha_i \le C \qquad \textbf{(3.61)}$$

The aforementioned analysis is referred to as linear classification problems. In nonlinear classification the problem is converted nearly to linear with the aid of kernel functions (mentioned also in GP regression). In particular a nonlinear transformation function Φ(x) is adopted converting the loss function in the dual problem to equation (3.62).

$$L_D\left(w, w_0, \alpha_i\right) = \sum_{i=1}^{N} \alpha_i - \frac{1}{2} \sum_{i=1}^{N} \sum_{j=1}^{N} \alpha_i \alpha_j y_i y_j \Phi(x_i)^T \Phi(x_j) \qquad \textbf{(3.62)}$$

The dot product of $\Phi(x_i)^T(x_j)$ is the kernel function (equation 3.63).

$$k(x_i, x_j) = \Phi(x_i)^T \Phi(x_j) \qquad \textbf{(3.63)}$$

In order to approach linearity, transformation functions “add dimensions” to the variables, while kernel functions reduce (sometimes significantly) the computation complexity.

Vapnik (1995) introduced regression to SVM. SVR uses the ε-sensitive loss function of observed values y_i and data inputs x_i (equation 3.64).

$$L = \begin{cases} 0 & \text{if } \left|y_i - f(x_i, w)\right| \le \varepsilon \\ \left|y_i - f(x_i, w)\right| - \varepsilon & \text{otherwise} \end{cases} \qquad \textbf{(3.64)}$$

In line with SVM, SVR employs slack variables ξ_i and ξ_i^* for measuring the deviation of the training samples outside the ε-sensitive zone and kernel functions for nonlinear regression. ξ_i and ξ_i^* are the positive differences between the observed value and ε regardless of whether the observed point is above or below the tube, created by the ε-sensitive loss function, respectively.

In particular SVR aim is to minimize $\frac{1}{2}\|w\|^2 + C\sum_{i=1}^{N}(\xi_i + \xi_i^*)$

subject to

$$y_i - f(x_i, w) \le \varepsilon + \xi_i^* \tag{3.65}$$

$$f(x_i, w) - y_i \le \varepsilon + \xi_i \tag{3.66}$$

$$\xi_i, \xi_i^* \ge 0 \tag{3.67}$$

In line to the Lagrange method the optimization problem is transformed to

$$L_P(w, w_0, \alpha_i, \alpha_i^*, \xi_i, \xi_i^*) = \frac{1}{2}\|w\|^2 + C(\sum_{i=1}^{N}\xi_i + \sum_{i=1}^{N}\xi_i^*) - \sum_{i=1}^{N}\alpha_i\left[(w^T x_i) + w_0 - y_i + \varepsilon + \xi_i\right] - \sum_{i=1}^{N}\alpha_i^*\left[(w^T x_i) + w_0 - y_i + \varepsilon + \xi_i^*\right] - \sum_{i=1}^{N}(\mu_i\xi_i + \mu_i^*\xi_i^*) \tag{3.68}$$

and the dual problem to

$$L_D = -\varepsilon\sum_{i=1}^{N}(\alpha_i + \alpha_i^*) + \sum_{i=1}^{N}(\alpha_i^* - \alpha_i) - \frac{1}{2}\sum_{i=1}^{N}\sum_{j=1}^{N}(\alpha_i^* - \alpha_i)(\alpha_j^* - \alpha_j)(x_i^T x_j) \tag{3.69}$$

subject to

$$\sum_{i=1}^{N}\alpha_i = \sum_{i=1}^{N}\alpha_i^* \tag{3.70}$$

$$0 \le \alpha_i \le C \tag{3.71}$$

$$0 \le \alpha_i^* \le C \tag{3.72}$$

while adopting a kernel function to

$$L_D = -\varepsilon\sum_{i=1}^{N}(\alpha_i + \alpha_i^*) + \sum_{i=1}^{N}(\alpha_i^* - \alpha_i) - \frac{1}{2}\sum_{i=1}^{N}\sum_{j=1}^{N}(\alpha_i^* - \alpha_i)(\alpha_j^* - \alpha_j)K(x_i^T x_j) \tag{3.73}$$

Pérez-Cruz et al. (2000) presented an Iterative Re-Weighted Least Square (IRWLS) algorithm application in training SVR. Compared to Quadratic programming IRWLS improves the speed of the SVR train process and reduces the computational complexity. First, they rearranged equation (3.68) [including

nonlinear transformation function Φ(x)] based on equations (3.74) and (3.75) leading to (3.76)

$$C - \alpha_i - \xi_i = 0 \quad \textbf{(3.74)}$$

$$C - \alpha_i^* - \xi_i^* = 0 \quad \textbf{(3.75)}$$

$$L_P = \frac{1}{2}\|w\|^2 - \frac{1}{2}\sum_{i=1}^{N}\left[a_i e_i^2 + a_i^*(e_i^*)^2\right] \quad \textbf{(3.76)}$$

where

$$e_i = \varepsilon - y_i + \Phi^T(x_i)w + w_0$$

$$e_i^* = \varepsilon + y_i - \Phi^T(x_i)w - w_0$$

$$a_i = \frac{2\alpha_i}{\varepsilon - y_i + \Phi^T(x_i)w + w_0}$$

$$a_i^* = \frac{2\alpha_i^*}{\varepsilon + y_i - \Phi^T(x_i)w - w_0}$$

Consequently, they applied the IRWLS algorithm that runs in three steps:

1. Fix a_i and a_i^* that minimize equation (3.76)
2. Recalculate a_i and a_i^* from the solution in step 1
3. Repeat until convergence

Similar to GP and in contrast to ANN a multi-output framework was not available in the initial SVR model setup, and SVR resulted to a single output. An alternative method could be to train the model for every output separately. In this case, however, a possible correlation between the outputs will be lost.

Still, specific methodologies have been proposed to deal with this problem. It is noted that the initial setup for SVM was for classification between two classes. Except for outputs correlation in terms of SVR the ε-sensitive zone around the estimation will not treat equally the samples over each output dimension.

In order to deal with this problem, Pérez-Cruz et al. (2002) introduced w^j weights in equation (3.68) for every output, while Sánchez-Fernández et al. (2004) added, besides the weights, a CT sum of constant terms presenting a multioutput SVR (MSVR) model setup. Both studies mentioned that quadratic programming is not feasible in the MSVR, and employed IRWLS algorithm application in training SVR. Equation (3.77) illustrates the quadratic approximation of MSVR.

$$L_P = \frac{1}{2}\sum_{j=1}^{Q}\left\|w^j\right\|^2 + \frac{1}{2}\sum_{i=1}^{N} a_i u_i^2 + CT \qquad \textbf{(3.77)}$$

where

$$a_i = \begin{cases} 0, & u_i^k < \varepsilon \\ \dfrac{2C(u_i^k - \varepsilon)}{u_i^k}, & u_i^k \geq \varepsilon \end{cases}$$

$$u_i^k = \sqrt{\left(e_i^k\right)^T e_i^k}$$

$$\left(e_i^k\right)^T = y_i^T - \Phi^T\left(x_i\right) w^k - \left(w_0^k\right)^T$$

The way that MSVR has been used for predicting pedestrian's velocity in this research is presented in section 5 (see section 5.2.3).

3.5.5. Locally weighted regression

Locally weighted regression (Loess, Cleveland 1979) is employed as the fourth data-driven technique. It is a widely applied data-driven method used for predicting and regression analysis that fits data points, based on a smoothing technique and weighted least squares. Particularly, relying on k-NN clustering algorithm, Loess utilizes local regression functions (equation 3.78).

$$y_i = g(x_i) + e_i \qquad \textbf{(3.78)}$$

where y_i is the dependent variable, x_i the predictors (independent variables), $g(x_i)$ the local regression function and e_i an error term. Local fitting is the principle of

Loess (Cleveland and Devlin, 1988). Initially, the number of the selected data points around predictor x_i (span) that will be used is specified. Namely, span is the ratio of the selected data points (x_i) to the total data points of the specific predictor. If all the given data points will be used, span equals to 1 (100%) and a total smoothed curve will be produced, while for a span value of 0 the curve will fit exactly the data points. Subsequently, the used data points around predictor x_i are weighted to their distance from x_i according to a tricube weighted function (equation 3.79). Hence, significantly high weighting is given to the closest data points. A scaled distance z_j is employed relating the data point x_j, the predictor x_i and the span.

$$w(z_j) = \begin{cases} (1-|z_j|^3)^3, \text{for } |z_j| < 1 \\ 0, \text{for } |z_j| \geq 1 \end{cases} \quad \textbf{(3.79)}$$

An n-degree polynomial regression function $g(x_i)$ then fits the data points around the predictor. The objective function minimizes the weighted sum of square errors:

$$\min \sum w * e^2$$

Among others, Loess has been employed for modeling ozone concentration based on solar radiation, wind speed and temperature (Loess predictors) in missing data (Cleveland and Devlin, 1988) and on criminal and civil justice expense relying on crime rate and taxable wealth (Cleveland et al., 1988). Additionally Loess has been applied in space galaxy velocity smoothing (noise reduction) with remarkable results (Cleveland and Devlin, 1988).

Nonetheless Loess suffers of the so called “curse of dimensionality”. In practice, the method performs efficiently in one predictor modeling while its performance is reduced as the number of predictors increases. The cause of this drawback rises from the fact that the smoothing process becomes more complicated with the extra dimensions, while the span remains fixed (Cleveland and Devlin, 1988 and Cleveland et al., 1988).

Loess application in traffic simulation was examined by Antoniou et al. (2013), and Papathanasopoulou and Antoniou (2015). Antoniou et al. (2013) employed

data-driven methods for predicting traffic states. Initially the data were clustered (in specific traffic states). Subsequently rules were set up for predicting the next traffic state (based on the sequence of the previous states). Loess was the crucial tool, along with goodness-of-fit statistics, that provided the relationships between the fundamental traffic quantities (speed, density, volume) for each cluster. Loess contributed a lot in speed prediction. Goodness-of-fit statistics, e.g. root mean square error and Theil's coefficients, measured model's validity and preciseness.

Papathanasopoulou and Antoniou (2015) highlighted that data-driven models' added value in traffic simulation, incorporating it into microscopic traffic models. They estimated span and polynomial degree using the RMSN (normalized root mean square error) indicator. The contribution of Loess in traffic simulation has been outlined alongside to its advantages that comprise in:

- Managing data (generally for machine learning methods)
- Non-Requirement for model function (non-parametric)
- Useful in many traffic situations
- Convenient incorporation of additional parameters
- Proper outliers' management

Loess compared to simple regression analysis outweighs on the one hand in the fact that it weighs each input and on the other hand it constitutes a non-parametric method. The lack of mathematical function could be considered as a drawback for Loess when parameter relationships should clearly be demonstrated. Moreover large datasets are computationally expensive and extreme outliers could mislead significantly the researcher.

An extensive Loess application in terms of pedestrian modelling is presented in section 5 (see section 5.2.3).

Table 3.2 presents the pros and cons of the aforementioned data-driven methods.

Table 3.2: Data-driven methods pros and cons

Method	Strength	Weakness
ANN	Initial setup for multi-dimensional outputs	High number of hyperparameters (number of nodes, activation function etc.) – model complexity
GP	Provides confidence intervals	Lacks in high dimensional spaces – regression with many features
		Single output initial setup
SVR	Low model complexity	Sensitive to support vectors
		Single output initial setup
Loess	Simple mathematical equations (in comparison to the other data-driven methods)	Limited number of variables
		"Curse of dimensionality"

The complexity of each type of model is related to its structure. In particular, ANN complexity [O((n+p)*q)] involves the number of neurons in the input layer (n), in the output layer (p) and in the hidden layer (q), while SVR (RBF kernel) complexity [$O(n_{sv}d)$] is affected by the number of inputs (d) and the number of the support vectors (n_{sv}). Also, as mentioned above, GP high complexity [$O(n^3)$] encumbers model training process with large datasets, while Loess complexity depends on the number of data points that are used [O(n)].

3.6. Model's Comparison

In a fair model comparison, the main principle, when examining different types of models, is to set them in a way to be comparable to each other, while respecting the models characteristics and dynamics. Thus, the results that each model will provide can be compared with the results of the other models and their performance can be evaluated. Data-driven models do not include any pedestrian movement modeling. Hence, this should be set by the researcher. Apart from the absence of the pedestrian movement model, the main principle of the models' comparison (i.e. the fact that the models must be comparable) should be also considered. Due to the fact that the social force model incorporates a clear simulation framework, the same framework is set in the data-driven models. In other words, the same parameters that social force model includes are also employed by the data-driven models. Furthermore, there might be cases where the social force model parameters cannot be incorporated in the same manner in the data-driven models. Hence, appropriate transformation for these parameters is conducted (an extensive description of these parameters is provided in section 5.1 / parameters of distance).

Another issue that should be considered during the comparison process is the method that will be employed. Due to the fact that data-driven models suffer from overfitting a cross-validation procedure was employed in the current research. In cross-validation, the total dataset is separated into k parts (folds). In each run, one of the k folds is used as the testing set while all the others as the training set. The model is applied in the training set by calibrating its parameters and selecting the parameter values combination that minimizes the total error (GoF measure). Subsequently the model with the selected parameter values is applied to the testing dataset capturing its validity (the error in the testing set is computed). When all of the k folds have been used as a testing set, the cross-validation process is complete and the total error of the testing sets is computed. The model type with the lowest error value implies to be more appropriate for simulating the phenomenon.

Furthermore, issues that are related to the time and computational cost reduction are also discussed in the present study. A naïve approach could be the calibration of all the model parameters during the training process. This would

result in an extremely large computational and time cost. Thus, three different approaches are examined including the one-at-a-time (OAT) sensitivity analysis, the Global Sensitivity Analysis (GSA) and the genetic algorithms, with the latter being the most efficient one and thus utilized at the cross-validation process.

Last, a set of GoF measures was employed for capturing models' performance. The appropriate velocity type (Euclidean norm, etc.) that is used as the error in the GoF measures is described explicitly during the experimental procedure in section 5.

4. DATA COLLECTION AND PREPARATION

4.1. Overview

Data collection is one of the essential steps in the research, as it provides the appropriate data required in the model development procedure. Data comprise a crucial element, utilized in model development through the calibration and validation processes. Hence, accurate data is a prerequisite for designing a reliable simulation model. With the evolution of machine learning methods and data-driven techniques, data inherent properties have become even more significant. Data-driven models do not incorporate the physical theory between the relevant parameters and are solely constructed by the data, while including only statistical correlations.

In microscopic traffic simulation, data mostly involves vehicle, bicycle or pedestrian trajectories, while there are several tools for collecting them. Data collection tools include radars, lasers, cameras, sensors, GPS and exhibit different merits and limitations, and different accuracy levels (Antoniou et al., 2011).

In the present experiment, video cameras are employed for recording pedestrian trajectories. As they often rely on techniques that have not been perfected, errors in the tracking process should be anticipated. At the same time, their contribution to model calibration is significant, affecting the validity of the investigated model (more in data-driven methods – see section 3.4.).

Pedestrian trajectories comprise the output of the pedestrian tracking process following data collection. At the same time, and regardless of the selected tool, the collected data may contain noise levels that exceed an acceptable threshold, thus requiring a data noise reduction step. The existence of data noise may affect significantly model development and may lead to a less accurate and reliable model. Hence, measurement error reduction methods must be employed. The methods that reduce data noise have been presented in the section 3.2, while their applications in pedestrian (and traffic) movements are described in section 4.4.1. Furthermore, this research presents an algorithm for eliminating data

noise, based on the Kalman filter and moving average extensions. A state-space formulation with the use of Unscented Kalman Filter (UKF) as an initial smoothing filter and the incorporation of the symmetric Simple Moving Average (sSMA) for producing an improved algorithm is introduced. Noise elimination and trajectory smoothness processes are described below.

4.2. Pedestrian Tracking

The experimental design of this research focuses on facilities where only pedestrians are present, without the interactions of other traffic modes (e.g. vehicles, bicycles). Existing databases with pedestrian trajectories have been published, including the noted one from the University of Edinburgh (Majecka, 2009), where the agent's characteristics (e.g. agent's height) are not provided and a special knowledge is required in order to evaluate false recordings. Thus, existing databases would not be appropriate for the present research and were then not utilized. To collect the relevant data, two data collection experiments were designed. The selected data collection sites displayed pedestrian movement characteristics required for this research (see section 3.1).

Data collection took place at the platforms of Moschato metro station (Figure 4.1a) in the morning (8:30 am) in a working day (28/12/2016) and at the indoor shopping mall in Athens (Figure 4.1b) in the evening (7:40 pm) in a non-working day (08/04/2017). Agents were tracked, with a recording frequency of 30 frames per second (fps), during their entire movement in the frame, and their walk lasted between 12 seconds and 45 seconds.

(a) **(b)**

Figure 4.1: Collection data locations: (a) Metro station, (b) Shopping mall indoor

In total, 20281 trajectory data points were extracted from 111 moving pedestrians. Data size in studies that utilize trajectory data to develop and/or calibrate pedestrian simulation models can vary significantly. Examples include 36 trajectories with a total of 1675 observed positions in 3 frames/second (Antonini et al., 2006) and 150 trajectories (when referring mainly to machine learning based models) recorded at a section of a basketball stadium (Wang et al., 2019). Studies with substantially larger data size have been found, e.g. Tordeux et al. (2018a) and Torres-Ruiz et al. (2017) with 400 participants tracked in a bottleneck with a width of 2.20m and in three corridors with variable width (ranging from 1.8m to 3.0m) respectively. In the current research, an integrated approach has been conducted where the data capture a mix of pedestrian behavior including agents that walk in a relaxed mode and others displaying a rush mode, while the data was collected in two areas. It should be mentioned that the utilized data collection method ensured agents' unawareness of being captured, achieving unbiased pedestrian behavior, which in turn enhances model applicability.

In the metro station platform pedestrians/agents were walking from/to the exit of the platforms (top of Figure 4.1a) towards/from the exit of the station (bottom of Figure 4.1b), while in the mall areas pedestrians did not follow a specific route, but walked in all possible directions (e.g. store entrances). Both single pedestrians and pedestrians walking in small groups (2 persons) were tracked in both sites. Considering the size of the recorded walking areas captured in the data, this was about 5m wide and 6.5m long for the metro platform data and about 8m wide and 13m long for the mall data.

Video recordings were conducted using two digital cameras that were placed at both locations at an upper level point. This is in line with similar experiments. For example, Ma and Song (2013) and Giannis and Vlahogianni (2018) who also collected data for extracting pedestrian trajectories utilizing video-recordings placed the cameras on the top of the recorded area. The first camera was focused on the terrain where pedestrians walk and the second captured their characteristics (height, gender etc.). Camera steadiness is crucial during the whole recording process for avoiding extra and significant noise in pedestrian trajectories. In cases where the recordings are not steady the appropriate software must be utilized to correct the recorded data (i.e. export a steady video recording). In the present experiment, in order to avoid additional and significant noise, the cameras were placed on tripods to achieve high levels of steadiness.

Subsequently video recordings were imported in a tracking software named "Tracker – Video Analysis and Modeling Tool" (version 4.90), which has already been used in vehicle tracking (Barmpounakis et al., 2016a; Barmpounakis et al., 2016b). The software employs a semi-automatic detection and tracking process. In particular, object detection, whether this involves pedestrians, vehicles or bicycles, is made by the user and object tracking by the software. First, the user detects the first point of the object trajectory and places it in the frame so as to identify the object, while automatic tracking conducted by the software follows. The possibility of manual corrections considering the object's trajectory (noisy points) is also available. Prior to this, a perspective filter is applied in order to remove lens distortion and compute the appropriate trajectory's coordinates. Alternatively, photogrammetric tools can be utilized in order to convert image points to actual coordinates. This method is described in section 4.3, while an extension of this procedure leads to the calculation of the height of the recorded agents (see section 5.3). Agent's height is required as it is used as an additional variable in the data-driven methods (section 5.3).

The employed software surpasses other tracking algorithms and software, based on computer vision, as it does not extract false trajectories from non-existent objects (that may occur due to luminousness errors) and allows for manual corrections. On the other hand, manual detection adds requisite time to the user, proportionate to the estimated trajectories that fully automatic tracking algorithms do not require.

In this experiment a fully manual procedure is utilized in order to extract agents' positions with high precision. As already mentioned, data accuracy is crucial for model calibration and validation, and even more vital for the development of data-driven models.

Pedestrian trajectories are thus exported. However, they include noise from measurements that needs to be eliminated. Noise elimination and trajectory smoothness processes are described further below (section 4.4).

4.3. Image points to real world coordinates

Photogrammetric tools are useful for converting image points to real world coordinates. In particular, the application of photogrammetric processes allows for the extraction of an agent's position in actual coordinates from video recordings.

Initially camera lens distortion needs to be removed. Focal length is the parameter that defines distortion, which is produced by the camera lens, and is measured in pixel units. If the camera is not used in auto-focus mode, the estimation of focal length is carried out once. Checkerboard pattern is a common method for removing lens distortion. Images (optimally 10 to 20) are captured in different angles and sites illustrating a checkerboard. Through computer vision techniques square edges are detected. Square edges color contrast (black and white colors) is optimum for their exact detection that consequently leads to the specification of checkerboard orientation and site. Applying the Camera Calibration Toolbox for Matlab (Heikkila and Silven, 1997), the camera's focal length and image coordinates of the principal point (x_o, y_o) are computed. Image principal point is the projection of the center of projection in the image plane and it differs from the image plane center (Figure 4.2).

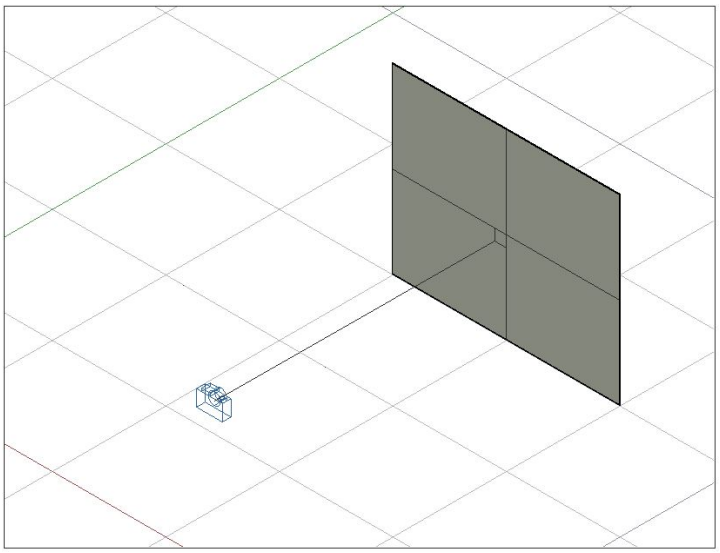

Figure 4.2: Image's principal point

An alternative method has also been employed for computing camera intrinsics (i.e. focal length and principal point's image coordinates) providing similar results to the Matlab algorithm (Table 4.1). With the aid of Fauccal (Fully Automated Camera Calibration), an open source software that is implemented in Matlab (Douskos et al., 2009), camera calibration can be accomplished. Likewise the software relies on the chess–board pattern. The algorithm extracts feature points on the image and uses the medians of their x, y coordinates for calculating camera parameters. A bundle adjustment is needed for parameters final estimation (Douskos et al., 2007).

Table 4.1: Camera calibration results

	Matlab		**Fauccal**	
Intrinsics				
	X - axis	Y - axis	X - axis	Y - axis
Focal length (pixels)	233.85 ± 0.21	231.60 ± 0.21	235.68 ± 0.55	233.29 ± 0.54
Principal point (pixels)	151.19 ± 0.22	114.68 ± 0.17	151.17 ± 0.57	113.81 ± 0.43
Radial distortion	4.03*10^(-7) ± 8.49*10^(-8)	-5.08*10^(-11) ± 1.04*10^(-11)	3.49*10^(-7) ± 9.17*10^(-8)	-3.51*10^(-11) ± 4.07*10^(-12)

Subsequently to intrinsics estimation, extrinsics, i.e. camera's site and angles during video recording, need to be identified. It is very important that the camera remains steady during the entire video recording. Otherwise camera exterior orientation will be changed and must be recomputed after every alteration. One video frame should be extracted in order to assign at least four points with known coordinate values. For advanced extrinsics evaluation the assigned points should cover the main part of the recorded area. Extra points can also improve camera calibration. Collinearity equations are utilized for estimating camera site (X_o, Y_o, Z_o coordinates) and angles (omega – turn in X–axis, phi – in Y–axis and kappa – in Z–axis). Matlab Photogrammetric Toolbox (MPT) is an open source software specified in extrinsics estimation (Kalisperakis et al. 2006). Camera constant (*c*), principal point's coordinates and radial distortion coefficients, i.e. camera's interior orientation parameters, are considered as inputs, while MPT software outputs the camera's exterior orientation. In case of approximate prior knowledge of the camera's site and orientation, initial values can be used to improve software's efficacy. It is worth mentioning that as focus distance (*S*) tends to approach infinity values, focal length (*f*) equals to camera constant (equation 4.1).

$$\frac{1}{f} = \frac{1}{S} + \frac{1}{c} \qquad \textbf{(4.1)}$$

Following the estimation of the camera's interior and exterior orientation, the pedestrian's location in actual coordinates can be easily defined with the aid of orientation coefficients. First, one of the video frames illustrating the pedestrian is extracted. Second, camera's orientation coefficients are computed as:

$$\begin{aligned}
r_{11} &= \cos(\text{phi})\cos(\text{kappa}) \\
r_{12} &= \cos(\text{omega})\sin(\text{kappa}) + \sin(\text{omega})\sin(\text{phi})\cos(\text{kappa}) \\
r_{13} &= \sin(\text{omega})\sin(\text{kappa}) - \cos(\text{omega})\sin(\text{phi})\cos(\text{kappa}) \\
r_{21} &= -\cos(\text{phi})\sin(\text{kappa}) \\
r_{22} &= \cos(\text{omega})\cos(\text{kappa}) - \sin(\text{omega})\sin(\text{phi})\sin(\text{kappa}) \\
r_{23} &= \sin(\text{omega})\cos(\text{kappa}) + \cos(\text{omega})\sin(\text{phi})\sin(\text{kappa}) \\
r_{31} &= \sin(\text{phi}) \\
r_{32} &= -\sin(\text{omega})\cos(\text{phi}) \\
r_{33} &= \cos(\text{omega})\cos(\text{phi})
\end{aligned} \qquad \textbf{(4.2)}$$

where omega, phi and kappa stand for the camera angles across X, Y and Z axis respectively.

Pixel coordinates of pedestrian's lowest point (x_1,y_1) are computed by removing principal point's coordinates $[x_1' = x_1 - x_0,\ y_1' = -(y_1 - y_0)]$. It is reminded that pixel values are descending in the Y – axis (from the bottom to the top of the frame). Pedestrian world coordinates (X, Y) are computed as:

$$X = ((Z - Z_0)(\frac{x_1' r_{11} + y_1' r_{21} - cr_{31}}{x_1' r_{13} + y_1' r_{23} - cr_{33}})) + X_0$$
$$Y = ((Z - Z_0)(\frac{x_1' r_{12} + y_1' r_{22} - cr_{32}}{x_1' r_{13} + y_1' r_{23} - cr_{33}})) + Y_0 \quad \textbf{(4.3)}$$

where Z can take an initial value (e.g. 0). The method is outlined below.

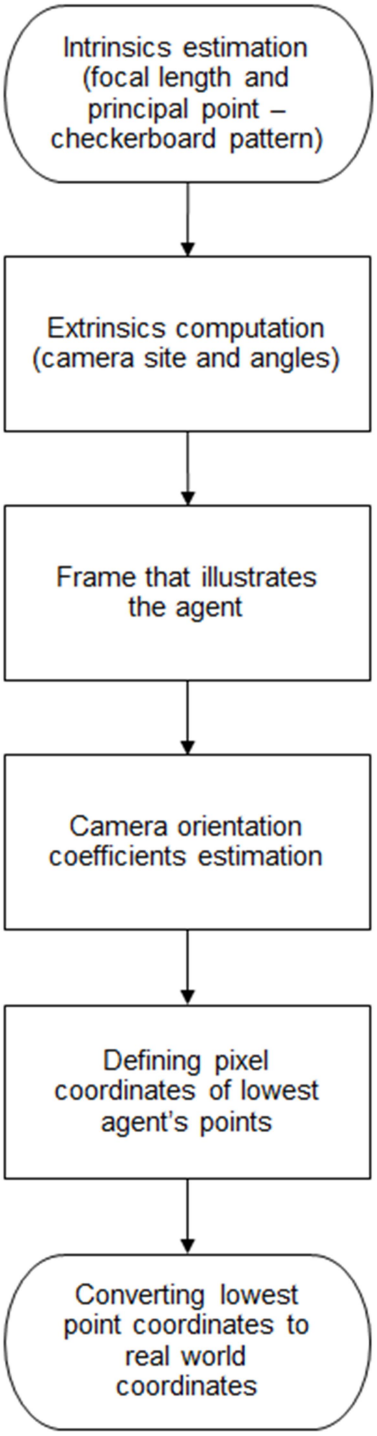

Figure 4.3: Converting pixel to real world coordinates

4.4. Trajectory smoothing

4.4.1. Smoothing filters applications

Kalman filter approximations have been applied in studies for pedestrian tracking (e.g. Bertozzi et al., 2004; Heikkila and Silven, 2004; Foxlin, 2005; Zampella, et al., 2012; Particke et al., 2017) in order to eliminate measurement noise. Bertozzi et al. (2004) employed Kalman filter for preventing pedestrian overlapping during detection phase. Foxlin (2005) presented pedestrian detection and tracking application with sensors that were placed into the agent's shoelaces. Through a process that includes EKF algorithm, he specified pedestrian's position with high accuracy. Heikkila and Silven (2004), in their study for automatical pedestrian and cyclist classification, assumed white Gaussian noises' distribution in the tracking process (both prediction and measurement noise). Zampella et al. (2012) employed Kalman filter extensions. Particularly they proposed the use of UKF due to the higher order approximation instead of EKF (EKF relies on first order). Particke et al. (2017) compared the basic Kalman filter algorithm accuracy with and without the employment of a pedestrian simulation model. The simulation model, titled Generalized Potential Field Approach (GPFA), is based on the social force model principles. Wang et al. (2007) relied on the particle filter algorithm. Its principle is similar to Kalman filter (estimates the probability based on the past observations). Rather than noises, particle filter algorithm calculates weights for each subsequent sample point (particle).

Splines have been also applied in pedestrian tracking (Philomin et al., 2000, Siebel and Maybank, 2001). Nonetheless, the aim of these studies was the smoothness of pedestrian shapes.

In terms of moving average, Dodge et al. (2009) employed the filter in order to smooth moving point objects' (i.e. vehicles, motorcycles, bicycles and pedestrians) trajectories and further to classify them in distinct object type categories. Nevertheless, moving average application on trajectories tend to reduce velocity peaks duration, i.e. the duration of the period when a pedestrian stands motionless (Hen et al., 2004). Symmetric moving average provides an improved version, as data points in the following time steps (t+1) are also included in the prediction of time step t. Thiemann et al. (2008) employed

symmetric exponential moving average for smoothing NGSIM data (a well know group of datasets for traffic data – vehicle trajectories).

Attempts have been made for specifying moving average parameters (i.e. the number of data points used for smoothing and the smoothing factor for EMA). Gudmundsson et al. (2012) used the symmetric simple moving average of nine points for preprocessing data in order to cluster movements in team sports and weather phenomena (e.g. hurricanes). Ossen and Hoogendoorn (2008) employed a simple moving average smoothing method for vehicle trajectories, with a nine observations time span (referred to 0.9s) that provided trajectory smoothness and moving dynamics at the same time. They mentioned that the number of smoothing data points are of high importance as in extremely high time span the gain of smoothness will be supplanted by the loss of kinematics. Thiemann et al. (2008), in a more holistic approach, utilized different smoothing widths for vehicle acceleration, velocity and position relying on their variances.

4.4.2. Methodology

This study employs a combination of Kalman filter [Unscented Kalman Filter (UKF)] and moving average (symmetric simple moving average) to filter pedestrian data. Noise reduction is conducted in three steps (Figure 4.4). The first step includes video recording segmentation, in the second UKF extension is adopted and in the third step the moving average filter is incorporated to UKF.

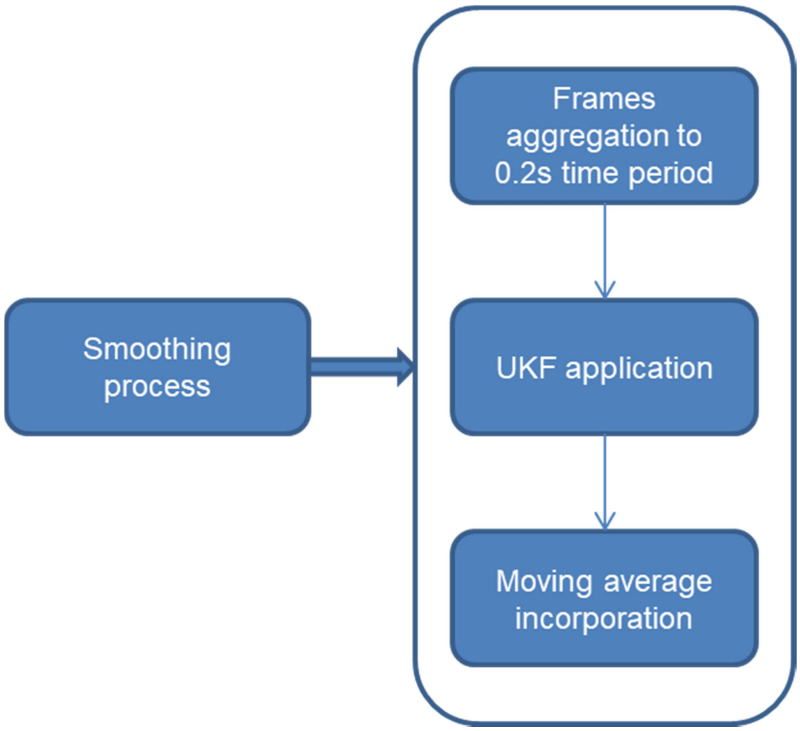

Figure 4.4: Smoothing process

Due to the high recording frequency (30fps) pedestrian steps are tracked in a 0.03s time period and thus pedestrian velocity is exposed to high false recording (slight differences in the agent's cite lead to high velocity variations). A first step for reducing noise is to aggregate frames. By altering the time period of the tracking process to 0.2s (i.e. tracking pedestrian's next step after 6 frames) the noise that is caused from the aforementioned short period time of tracking is significantly reduced. The selected time step is in agreement with Guo et al. (2010), Zanlungo et al. (2011) and Ridel et al. (2019), while other studies employ smaller time steps (0.04s) (e.g. Daamen and Hoogendoorn, 2012) or larger ones (0.5s) (e.g. Teknomo, 2006; Zanlungo et al., 2014b; Zeng et al., 2014). None of the aforementioned papers employed further smoothing algorithms.

In the second step, the Kalman filtering framework is used. In order to relax the basic Kalman filter's hypotheses, UKF is applied. State vector X is defined as in equation (3.5), while the covariance matrix P is assumed to be diagonal (equation 3.6) as state variables are assumed to be independent. Five sigma points are selected, as the state dimension equals 2 (the number of sigma points is defined as 2n+1, where n is the state dimension). Sigma points are extracted as:

$$
\begin{aligned}
&X_0(t \mid t) = \hat{x}(t \mid t) \\
&W_0^m = \frac{k}{n+k} \\
&W_0^c = \frac{k}{n+k} + 1 - a^2 + b \\
&X_i(t \mid t) = \hat{x}(t \mid t) + (\sqrt{(n+k)P(t \mid t)})_i \\
&X_{i+n}(t \mid t) = \hat{x}(t \mid t) - (\sqrt{(n+k)P(t \mid t)})_i \\
&W_i = W_{i+n} = \frac{k}{2(n+k)}
\end{aligned}
\qquad \textbf{(4.4)}
$$

where $X_i(t|t)$ stands for the sigma points at frame t, W_i for their weights, k is a scaling parameter, n the dimensions of the state, a is a factor that assigns the scale of each sigma point from the mean [Wan and van der Merwe, (2000), define α equals to 10^{-3}] and b a prior knowledge factor which has an optimal value equal to 2 for Gaussian distributions (Antoniou, 2004). Julier et al. (2000) mentioned that by setting n+k=3 the optimal Gaussian approximation is achieved (as they propose a heuristic method). $\sqrt{(n+k)P(t \mid t)}_i$ is the i^{th} row or column element of the root matrix that resulted from the Cholesky decomposition method (Julier et al., 2000). In the present study $A=LL^T$ is selected as the form of the square root; therefore the i^{th} column element is chosen. UKF equations are presented below:

$$
\begin{aligned}
&X_i(t+1 \mid t) = AX_i(t \mid t) \\
&x(t+1 \mid t) = W_0^m X_0(t+1 \mid t) + \sum_i^{2n} W_i X_i \\
&P(t+1 \mid t) = W_0^c (X_0(t+1 \mid t) - x(t+1 \mid t)) * (X_0(t+1 \mid t) - x(t+1 \mid t))^T + \\
&+ \sum_i^{2n} W_i (X_i(t+1 \mid t) - x(t+1 \mid t)) * (X_i(t+1 \mid t) - x(t+1 \mid t))^T + Q
\end{aligned}
\qquad \textbf{(4.5)}
$$

Equations (4.5) illustrate the predicted state where A is the transition matrix which equals to

$$
A = \begin{bmatrix} 1 & 0 & \Delta t & 0 \\ 0 & 1 & 0 & \Delta t \\ 0 & 0 & 1 & 0 \\ 0 & 0 & 0 & 1 \end{bmatrix}
\qquad \textbf{(4.6)}
$$

Kalman filter requires a simulation model in the prediction state (in order to predict velocity at t+1 time step). However, the objective of Kalman filter's application in the current study is to smooth velocity without any knowledge of the moving dynamics. Velocity alterations result from the moving average algorithm (see below) and the prediction state noise part.

$$
\begin{aligned}
&Y_i(t+1|t) = HX_i(t+1|t) \\
&y(t+1|t) = W_0^m Y_0(t+1|t) + \sum_i^{2n} W_i Y_i \\
&P_y(t+1) = W_0^c (Y_0(t+1|t) - y(t+1|t)) * (Y_0(t+1|t) - y(t+1|t))^T + \\
&+ \sum_i^{2n} W_i (Y_i(t+1|t) - y(t+1|t)) * (Y_i(t+1|t) - y(t+1|t))^T + R
\end{aligned}
\tag{4.7}
$$

Equations (4.7) provide the measurement state, where H is the transition matrix which equals to

$$
H = \begin{bmatrix} 1 & 0 & 0 & 0 \\ 0 & 1 & 0 & 0 \\ 0 & 0 & 1 & 0 \\ 0 & 0 & 0 & 1 \end{bmatrix} \tag{4.8}
$$

$$
\begin{aligned}
&P_{xy}(t+1) = W_0^c (X_0(t+1|t) - x(t+1|t)) * (Y_0(t+1|t) - y(t+1|t))^T + \\
&+ \sum_i^{2n} W_i (X_i(t+1|t) - x(t+1|t)) * (Y_i(t+1|t) - y(t+1|t))^T
\end{aligned}
\tag{4.9}
$$

$$
K = P_{xy}(t+1) P_y(t+1)^{-1} \tag{4.10}
$$

Kalman gain (K) is the product (equation 4.10) of the predicted and measured states covariance matrix (P_{xy}) and the inverse of the measurement covariance matrix (P_y). The output of the UKF is the state estimation in t+1 time step as presented below:

$$
\begin{aligned}
&x(t+1) = x(t+1|t) - K(y(t+1) - y(t+1|t)) \\
&P(t+1) = P(t+1|t) - KP_y(t+1)K^T
\end{aligned}
\tag{4.11}
$$

An improvement has been accomplished in the presented UKF by introducing the moving average component. Velocity is crucial for predicting pedestrian's next

time step in UKF prediction equation. Moving average is applied for estimating the velocity (among to X and Y axis) during the UKF process, as it reduces agent's velocity noise and, as a consequence, enhances UKF efficiency. Additionally, the symmetric moving average (moving average extension that is implemented in the present study) reflects the tendency of the agent's movement as it incorporates previous and following time steps (smoothing width) in the estimation and relaxes the model absence at UKF prediction state.

As mentioned in section 3.2.3, three moving average types exist, the simple moving average (SMA), the weighted (WMA) and the exponential (EMA). The difference the between simple versus the weighted and exponential moving average relies on the fact that SMA treat equally the regarded data points, while WMA and EMA set weights on them. Notably, EMA weighting is decreased exponentially to the previous data points, while in WMA the weights are assigned optionally. As a consequence, a considerably higher importance is given in the most recent data points and the existence of outliers will lead in false estimation at the current time step. Hence, a simple moving average is employed in this study. Further, for reducing smoothing in peak points, the symmetric type is utilized (symmetric simple moving average – sSMA), as presented in equation (4.12).

$$\left(\frac{u_x}{u_y}\right)(t) = \frac{1}{2D+1}\sum_{t=t-D}^{t+D}\left(\frac{u_x}{u_y}\right)(t) \qquad \textbf{(4.12)}$$

where u_x and u_y stand for the speeds across X and Y axis respectively and D for the smoothing width.

To sum up, UKF is applied for eliminating data noise, after aggregating frames to 0.2s time step, while the symmetric simple moving average reduces velocity false variance and improve UKF's efficiency. UKF requires noises' covariances determination while sSMA smoothing width specification.

The Kalman filter algorithm relies on prediction and measurement errors. In case of no primary knowledge or sense for the error values (as in the current case), most of the studies insert a priori error values. In this study a consideration has been made based on the Q/R ratio that affects Kalman gain.

Initially, velocity variance for the first three time steps is computed. Three time steps stand for a 0.6 seconds time period in the specific example. For this duration, pedestrian velocity should stay almost unchanged. Hence, velocity variance indicates noises in measurement process.

For the following frames, velocity constancy should be relaxed by assuming vector state variance, including prediction noise, as acceptable. Due to the absence of a simulation model in the prediction state, measurement noise should not exceed prediction noise (Q/R >1).

An investigation has been conducted for examining the effect of noises ratio (Q/R) in trajectory estimation. It was experimentally observed, that Q/R ratio affects edge trajectory points' locations and thus their divergence is considered as the critical indicator. It is highlighted that, by changing the number of the initial "accepted" trajectory points (in the current study this is 3), the divergence must differ. Hence, this is kept constant in the experiment.

On the other hand, smoothing width affects velocity variance (velocity variance is reduced inversely to the number of data points). Adopting an extremely high number of data points, velocity variance approaches zero even in cases where the agent alters its velocity (oversmoothing). In this case movement dynamics will be diminished. Thereafter, velocity variance elimination by preserving pedestrian kinematics is required.

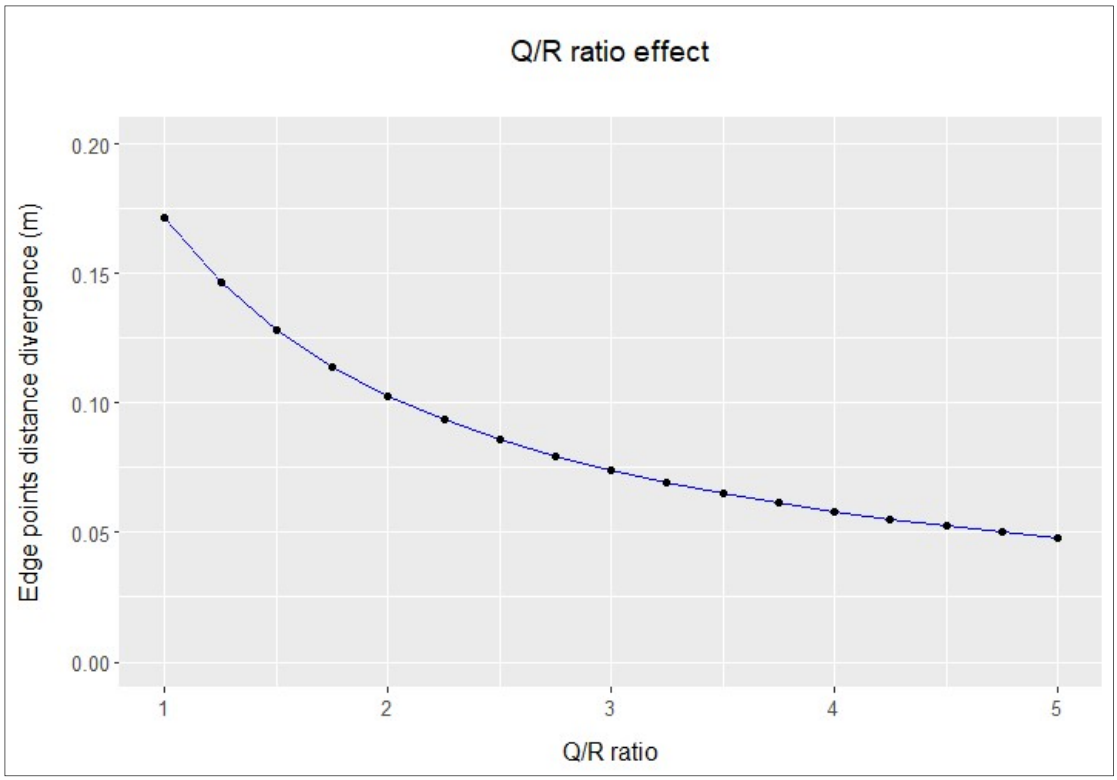

Figure 4.5: Q/R ratio effect

First, smoothing width (D) remains constant at the value of 2 and Q/R ratio varies. Figure 4.5 illustrates that edge points' distance divergence decreases logarithmically as Q/R ratio increases. In order to avoid overfitting (estimated trajectory points are close to measured) and high velocity alterations, high ratio values are rejected. As shown in Figure 4.5, insignificant differences in distance divergence are noted in ratio values higher than 2.5. Hence, a Q/R ratio equal to 2.5 seems to be reasonable, for avoiding overfitting and accepting low velocity alterations, and is therefore selected.

Alternatively, a threshold value on the gradient of the curve of Figure 4.5 could be adopted. Low threshold values indicate that an extra increase of the Q/R ratio does not significantly alter distance deviation. Namely, a threshold value of 0.03 suggests that an increase of 1 of the Q/R ratio decreases distance divergence per 0.03 m, which seems to be an acceptable value. The aforementioned threshold value appears at around 2.5 Q/R ratio value (Table 4.2).

Table 4.2: Q/R ratio curve gradient

Q/R ratio	Edge points distance divergence (m)	Curve gradient
1.00	0.172	
1.25	0.146	0.101
1.50	0.128	0.074
1.75	0.114	0.056
2.00	0.103	0.045
2.25	0.094	0.036
2.50	0.086	0.030
2.75	0.080	0.026
3.00	0.074	0.022
3.25	0.069	0.019
3.50	0.065	0.017
3.75	0.061	0.015
4.00	0.058	0.013
4.25	0.055	0.012
4.50	0.053	0.011
4.75	0.050	0.010
5.00	0.048	0.009

Further, Q/R ratio is kept fixed at 2.5 and smoothing width is being modified. In this case velocity variance is the critical index. Five specific trajectories exhibiting almost constant velocity, as indicated from the video recordings, were selected randomly. The aim is to accomplish, for the specific trajectories, zero velocity variances (or almost 100% reduction) while preserving movement dynamics. Velocity variance decreases inversely to the number of data points, as illustrated in Table 4.3. The first data row of the table presents velocity variance of each pedestrian ID, while the other rows exhibit the reduction in the velocity variance with the increasing smoothing width.

Table 4.3: Velocity variance reduction

Smoothing width / Ped id	Ped001	Ped013	Ped017	Ped029	Ped035	Average
0	0.145	0.118	0.159	0.101	0.104	
1	91%	80%	80%	79%	74%	**81%**
2	96%	89%	87%	87%	88%	**89%**
3	98%	93%	91%	91%	91%	**93%**
4	99%	95%	93%	96%	95%	**96%**
5	99%	97%	96%	98%	97%	**97%**

A significant reduction is accomplished by adding only two data points symmetrically to the current time step (D=1). When smoothing width exceeds the value of 2, an additional increase does not significantly reduce velocity variance. Thus, the value of 2 is adopted for the smoothing width as kinematics should be maintained. Hence, the number of total data points that are considered in the symmetric moving average is 5 (2D+1). 5 data points correspond to 1s duration time, which approaches Moussaïd et al. (2009), Moussaïd et al. (2011) and Ossen and Hoogendoorn (2008) smoothing widths (0.83s), though the latter study referred to vehicle trajectories rather than pedestrian ones. In cases of not enough trajectory data points (<25, prior to frames aggregation) smoothing width is adjusted according to them.

In the current stage, all but the initial “accepted” trajectory steps have been estimated. The process is executed backwards for estimating them. In order to avoid high acceleration alterations that exist despite noise elimination, pedestrian acceleration is computed in 1 second time step. Additionally, acceleration in the first step (as it cannot be extracted from velocity alteration) is specified as equal to the second step. Alternatively, an approach that employs UKF and sSMA in separate stages (first UKF and after sSMA) has been examined providing higher velocity and acceleration variances, that cannot be deduced from the specific pedestrian movements. UKF application combined to sSMA indicates trajectory smoothness and data noise reduction. Figure 4.6 displays the results of this process, i.e. a comparison between the two phases (before and after filters’ application) for 3 pedestrian trajectories.

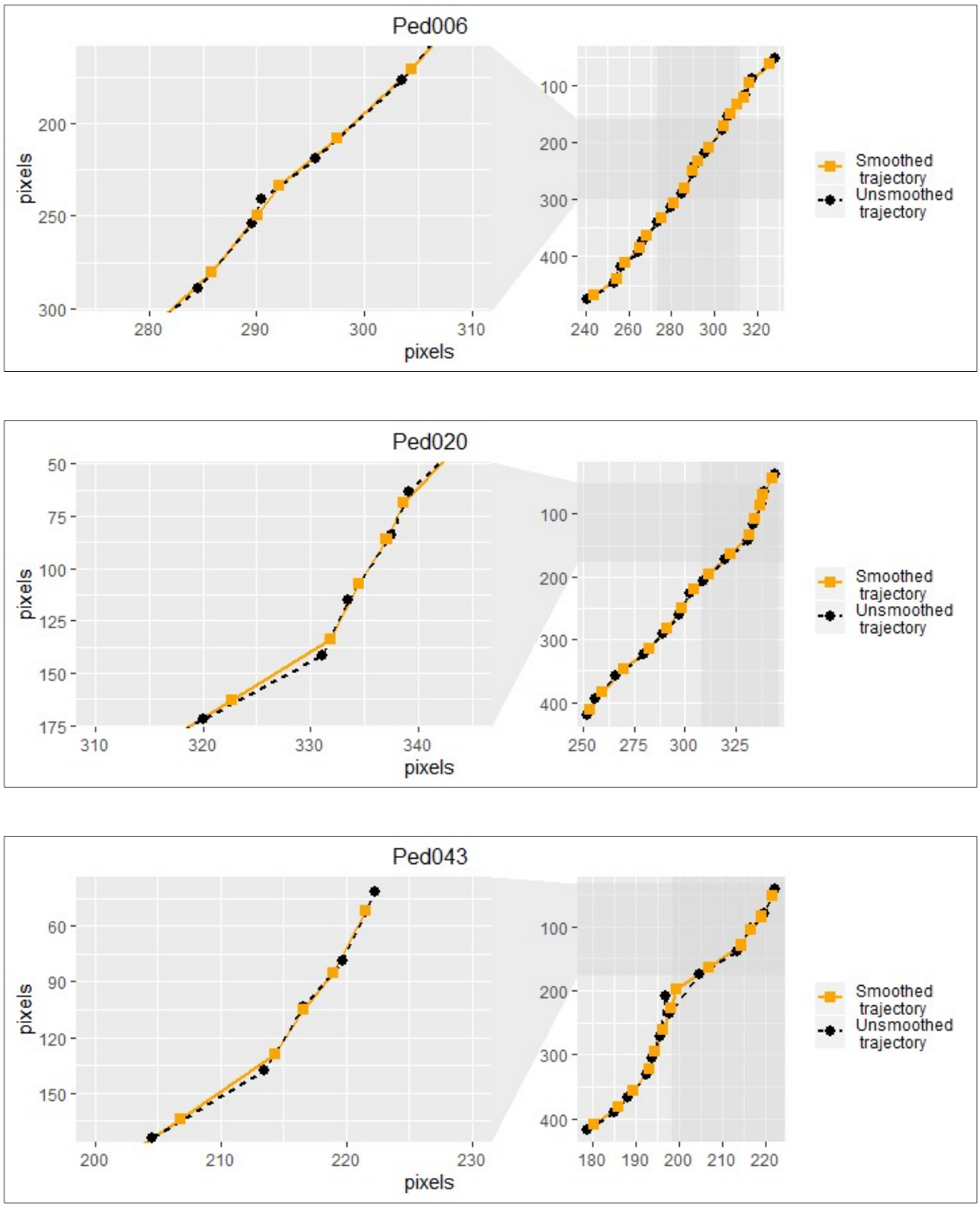

Figure 4.6: Pedestrian's trajectories smoothing

5. CASE STUDIES

5.1. Case Studies Setup / Experimental Setup

In this research, we consider two modeling approaches: (i) a theory-derived social force model, and (ii) four data-driven techniques. A visual overview of their modeling assumptions is provided in Figure 5.1.

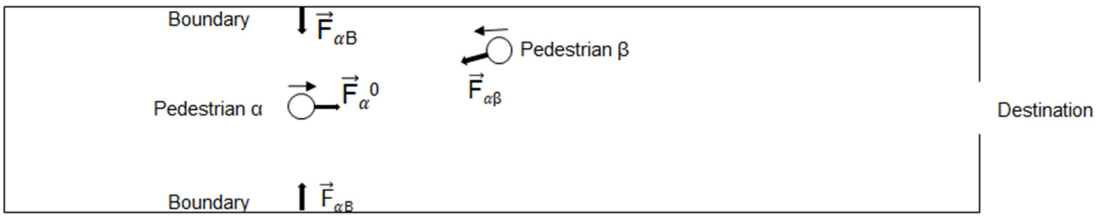

(a) Social force description

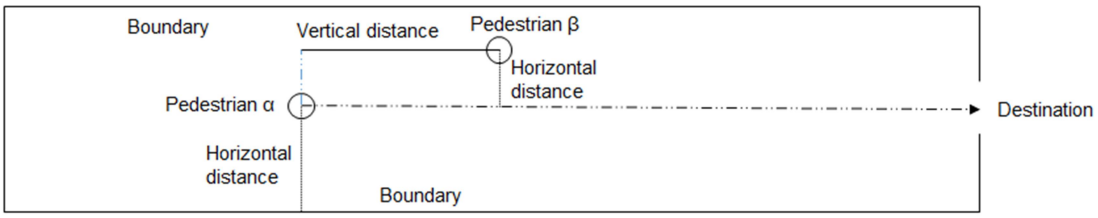

(b) Data-driven model setup

Figure 5.1: Distance separation

As mentioned in section 3, Helbing and Molnár (1995) presented the social force model to simulate pedestrian kinematics. The model set the principles for specifying the rules of pedestrian movement and has been employed in widely applied simulation software, such as VisWalk (PTV, 2015) and SimWalk (Zainuddin et al., 2009). Social force model simulates pedestrian's velocity in the next time step (the same is simulated with the data-driven models in the current experiment). It represents the following dynamics: as an agent walks they receive forces from their surroundings that coerce them to amend their velocity, similarly to the forces in fluid molecules. Social forces are distinguished in attractive and

repulsive, and the total force that the agent receives from their surroundings is condensed as:

$$\vec{F_\alpha} = \frac{1}{\tau_\alpha}(u_\alpha^0 \vec{e_\alpha} - \vec{u_\alpha}) + (Ae^{-b/B} \frac{\left\|\vec{r_{\alpha\beta}}\right\| + \left\|\vec{r_{\alpha\beta}} - (\vec{u_\beta} - \vec{u_\alpha})\Delta t\right\|}{2b}$$
$$\frac{1}{2}\left(\frac{\vec{r_{\alpha\beta}}}{\left\|\vec{r_{\alpha\beta}}\right\|} + \frac{\vec{r_{\alpha\beta}} - (\vec{u_\beta} - \vec{u_\alpha})\Delta t}{\left\|\vec{r_{\alpha\beta}} - (\vec{u_\beta} - \vec{u_\alpha})\Delta t\right\|}\right))(\lambda_\alpha + (1-\lambda_\alpha)\frac{1+\cos(\varphi_{\alpha\beta})}{2}) + \quad (5.1)$$
$$(-\nabla_{\vec{r}_{\alpha B}} U_{\alpha B}(\left\|\vec{r_{\alpha B}}\right\|)) + ((-\nabla_{\vec{r}_{\alpha i}} W_{\alpha i}(\left\|\vec{r_{\alpha i}}\right\|, t)(\lambda_\alpha + (1-\lambda_\alpha)\frac{1+\cos(\varphi_{\alpha i})}{2}))$$

Equation (5.1), which is adopted in the present research, corresponds to the improved version of the social force model presented by Helbing and Johansson (2010), and Helbing (2012) and described in section 3.3.2. The equation denotes that pedestrian motion relies on five variables. One can add pedestrian velocity in the current time step (t) as a sixth variable for predicting pedestrian velocity in the next time step (t+1). In other words (and based on equation (5.1)), pedestrian velocity can be computed as:

$$\vec{u_\alpha}(t+1) = f(\vec{u_\alpha}(t), \vec{r_{\alpha\beta}}, \vec{r_{\alpha B}}, \vec{r_\alpha^k}, \vec{r_{\alpha i}}, \vec{u_\beta}) \quad (5.2)$$

where $\vec{u_\alpha}(t)$ stands for the pedestrian velocity in the current time step, $\vec{r_{\alpha\beta}}$ the distance between the examined agent and the pedestrians triggering repulsive effects and $\vec{u_\beta}$ their velocity, $\vec{r_{\alpha B}}$ the distance between the examined agent and space boundaries, $\vec{r_{\alpha i}}$ the distance between the examined agent and the pedestrians triggering attractive effects, and $\vec{r_\alpha^k}$ the distance to the next destination point, implied in equation (3.10) by the desired direction factor ($\vec{e_\alpha}$).

To assess the effectiveness of the developed data-driven models a fair comparison between the social force model and the data-driven ones was designed. Therefore the data-driven pedestrian simulation models are developed with agents updating their velocity according to social force model parameters. Thus, pedestrian velocity (in the data-driven models) in the next time step [$\vec{u_\alpha}(t+1)$] is estimated based on the:

- agent's velocity $\overrightarrow{u_\alpha}(t)$ in the current time step;
- distance $\overrightarrow{r_{\alpha\beta}}$ between the examined agent and the pedestrians triggering repulsive effects;
- distance $\overrightarrow{r_{\alpha B}}$ between the examined agent and space boundaries;
- distance $\overrightarrow{r_{\alpha i}}$ between the examined agent and the pedestrians triggering attractive effects;
- distance $\overrightarrow{r_\alpha^k}$ to the next destination point; and
- pedestrians triggering repulsive effects velocity $\overrightarrow{u_\beta}$.

However, as -due to implementation details- and only in terms of Loess technique its variables are limited to three, i.e. the following variables are considered i) pedestrian velocity in the current time step ($\overrightarrow{u_\alpha}(t)$, ii) distance between the examined agent and the pedestrians triggering repulsive effects ($\overrightarrow{r_{\alpha\beta}}$) and iii) distance between the examined agent and space boundaries ($\overrightarrow{r_{\alpha B}}$).

In all models, distances $\overrightarrow{r_{\alpha\beta}}$, $\overrightarrow{r_{\alpha B}}$, $\overrightarrow{r_{\alpha i}}$ and $\overrightarrow{r_\alpha^k}$ are separated into two axes representing the horizontal and the vertical projections of the adjacent pedestrian/obstacle [Figure 5.1(b)]. In cases of more than one "repulsive" or "attractive" agents or/and obstacles, a selection criterion needs to be specified for determining the agent and the obstacle that has the highest impact on the examined pedestrian. Contrary to the social force model, data-driven models consider one value for every predictor and thus the appropriate one must be adopted. In an initial approach the closest obstacle/pedestrian could be selected. Helbing and Johansson (2010) and Helbing (2012) pointed out in their updated version of the social force model, an angular dependence factor (based on agent's view) is a crucial measure in forces effects. Pedestrians who walk outside of the agent's sight view (i.e. behind them) or close to its contour (i.e. vertically to agent) affect the simulated pedestrian's movement much less than those who are in front of them and close to their trajectory. Further investigation considering the

determination of the “influence” area has been conducted from Giannis and Vlahogianni (2018), though their study referred to overtaking situations (two elliptical axis in front and behind the agent) considering both unidirectional and bidirectional flows. They suggested that the asymmetry of this area is related to the kinematics and the general characteristics of the examined pedestrians (those who overtake and those who are overtaken). In the present research, in accordance to Helbing and Johansson (2010) and Helbing (2012), the sight view factor is adopted as the selection criterion in the present model. The same factor is employed in “attractive” pedestrians. In terms of “repulsive” pedestrians the density measure could be considered as an extra predictor in a future model in order to take into account not only one pedestrian but also the rest that affect the simulated one.

Furthermore, pedestrian velocity is a two (or three) dimensional quantity. As agents are tracked in a steady coordinated system, an appropriate transformation is required for computing vertical and horizontal velocity in each time step. Trajectory slope is considered as crucial in a 1 second time step (the current frame, two prior and two posterior frames are taken into account). The coordinated system is thus rotated to the slope axis, and agent velocity $\begin{bmatrix} u_x \\ u_y \end{bmatrix}$ is transformed according to equation (5.3).

$$\begin{bmatrix} u_x' \\ u_y' \end{bmatrix} = \begin{bmatrix} \cos\theta & \sin\theta \\ -\sin\theta & \cos\theta \end{bmatrix} \begin{bmatrix} u_x \\ u_y \end{bmatrix} \tag{5.3}$$

where $\begin{bmatrix} u_x' \\ u_y' \end{bmatrix}$ stands for the velocity in the rotated coordinated system and θ for the angle rotation. As also noticed in 4.3 section pixel values are descending in the Y – axis. For a clear description see Fig. 5.2.

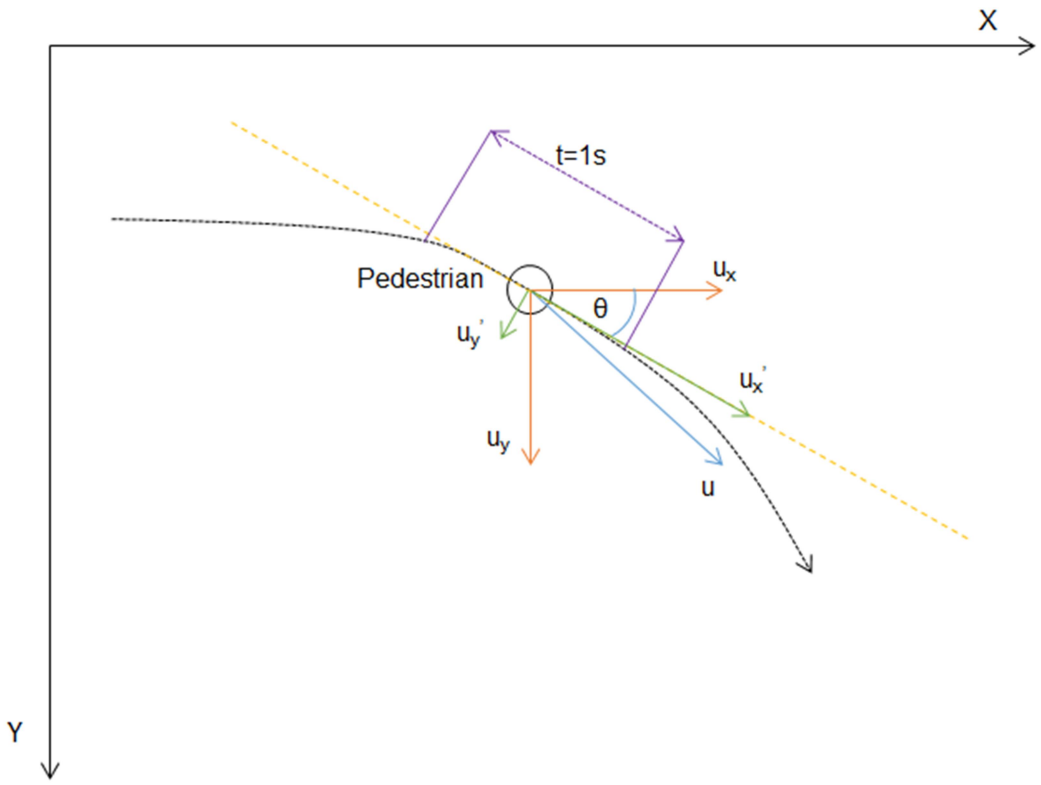

Figure 5.2: Velocity rotation

In cases where specific variables cannot be computed, suitable large or low values are selected, depending on the impact of the variable on the output value (i.e. agent's velocity in the next time step), in the following manner. Namely, when an agent walks with no attractive or/and repulsive pedestrians for a certain period of time, and thus the distances between the agent and the pedestrians (horizontal and vertical) are not determinable, large values are allocated to distances while pedestrian velocities are set to zero. In other words, a pseudo-agent is assumed with their position being set far away (outside the recording area) from the examined agents, while they are assumed to be stationary (their velocity set to zero). The reason for this is that agents' and obstacles' distance is inversely proportional to pedestrians' velocity. Hence, setting a high value to this parameter, results to the impact of this predictor in the specific data input to be substantially small.

In terms of the destination points, while the recorded area covers a part of the agent's trajectory, the social force model refers to the next destination point (i.e. an intermediate destination point) for the pedestrians that in the current

experiment can be easily defined for both the employed collection data locations. These are the ticket gates (entrance / exit) for the metro platforms and points following pedestrian's trajectory outside the recorded area (e.g. next corner) for the shopping mall, according to its geometry (for pedestrians that do not stop inside the recorded area).

5.2. Comparison of social force model with data-driven models (with same number of variables)

Following data collection, trajectory extraction and noise reduction, the employed models were designed and calibrated. Sensitivity analysis is performed to estimate the impact of the social force model parameters in the derived outputs in order to detect possible non-influencing parameters (or parameters that affect at a rather low degree) and set them as constants during the calibration process, to achieve a reduction in computational time.

Two different methods for sensitivity analysis are described next, the simple one-at-a-time and the global sensitivity, while an approach based on genetic algorithm, for calibrating social force model parameters, has also been taken into consideration. The genetic algorithm does not require the a priori knowledge of the most affective parameters (provided by the sensitivity analysis). Hence, it is employed for training the social force model, while sensitivity analysis methods are only presented indicatively.

5.2.1. One-at-a-time (OAT) sensitivity analysis

A one-at-a-time (OAT) sensitivity analysis has been performed on the parameters of the social force model. Every parameter was been examined separately, within a predetermined range, while all the other parameters are given a reasonable value. The values of the fixed parameters and their ranges are presented in Table 5.1. Mean squared error (MSE), as described in equation 5.7 and also employed in the next sections, is used as the metric to capture the sensitivity analysis performance. Following Zanlungo et al. (2011), the agent's desired

speed is regarded to differ between pedestrians (its values are drawn randomly from its distribution). Both mean desired speed and its standard deviation are considered to follow a Gaussian distribution (Helbing and Molnár, 1995 and Zeng et al., 2014).

Table 5.1: Parameters fixed values and ranges

Parameter	Range	Fixed value	Units
Relaxation time	0.1-4.5	0.5	seconds
Desired speed (mean)	0.5-5.0	1.34	m/s
Desired speed (std)	0.05-1.00	0.26	m/s
Maximal acceptable speed	1.47-5.09	1.74	m/s
Strength of interactions from behind	0.02-0.19	0.1	
Repulsive force from obstacle function constant	0.5-20.0	10	m^2/s^2
Repulsive force from obstacle exponential parameter	0.1-2.0	0.2	m
Repulsive force from pedestrian - interaction strength	0.03-8.21	4.3	m/s^2
Repulsive force from pedestrian - interaction range	0.001-3.89	1.07	m

The sensitivity analysis suggests that most of the parameters affect simulation results with the critical determining parameters being the maximum acceptable

speed, and the mean and standard deviation of the desired speed, as anticipated. Results indicated that desired speed standard deviation parameter values higher than 0.5m/s might increase the simulation error substantially. Low values for relaxation time (<0.2s) and attractive force exponential parameter (<0.3m) lead to false model estimations. Additionally, the values of the repulsive force from pedestrian interaction range, the attractive force function constant and the repulsive force from obstacle force function constant should not exceed 0.8, 0.5 and 3.0 respectively. On the other hand, the strength of interactions from the behind parameter does not seem to affect significantly simulation results. At this point it should be stated that most of the aforementioned parameters are correlated (e.g. function constant and exponential parameters) and OAT sensitivity analysis might not be the appropriate method for examining their impact, and is only presented as an initial approach. Further investigation on the sensitivity analysis is conducted adopting global sensitivity analysis, as described in the next section.

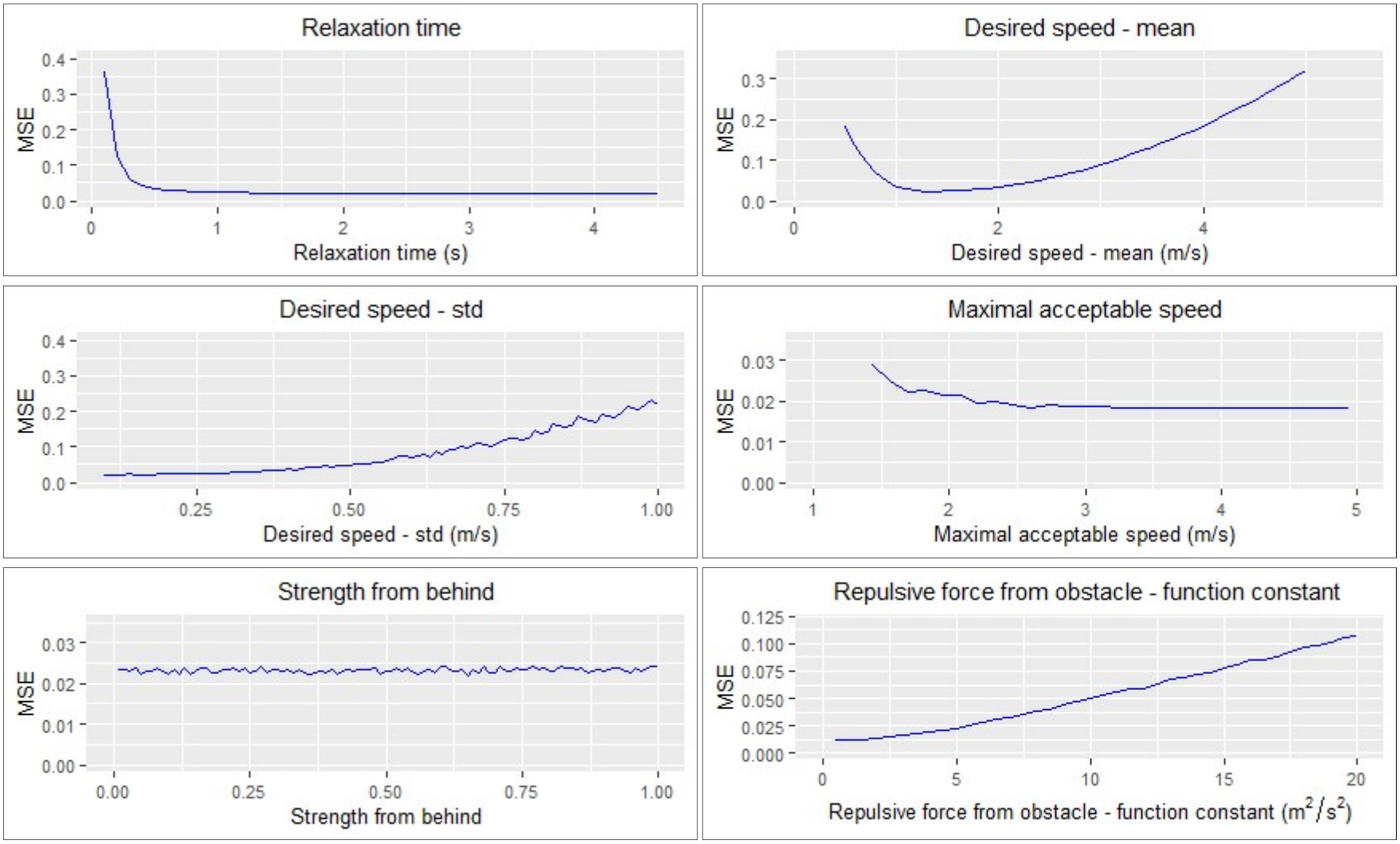
Relaxation time
MSE
0.4
0.3
0.2
0.1
0.0
0
1
2
3
4
Relaxation time (s)
Desired speed - mean
MSE
0.3
0.2
0.1
0.0
0
2
4
Desired speed - mean (m/s)
Desired speed - std
MSE
0.4
0.3
0.2
0.1
0.0
0.25
0.50
0.75
1.00
Desired speed - std (m/s)
Maximal acceptable speed
MSE
0.03
0.02
0.01
0.00
1
2
3
4
5
Maximal acceptable speed (m/s)
Strength from behind
MSE
0.03
0.02
0.01
0.00
0.00
0.25
0.50
0.75
1.00
Strength from behind
Repulsive force from obstacle - function constant
MSE
0.125
0.100
0.075
0.050
0.025
0.000
0
5
10
15
20
Repulsive force from obstacle - function constant (m²/s²)

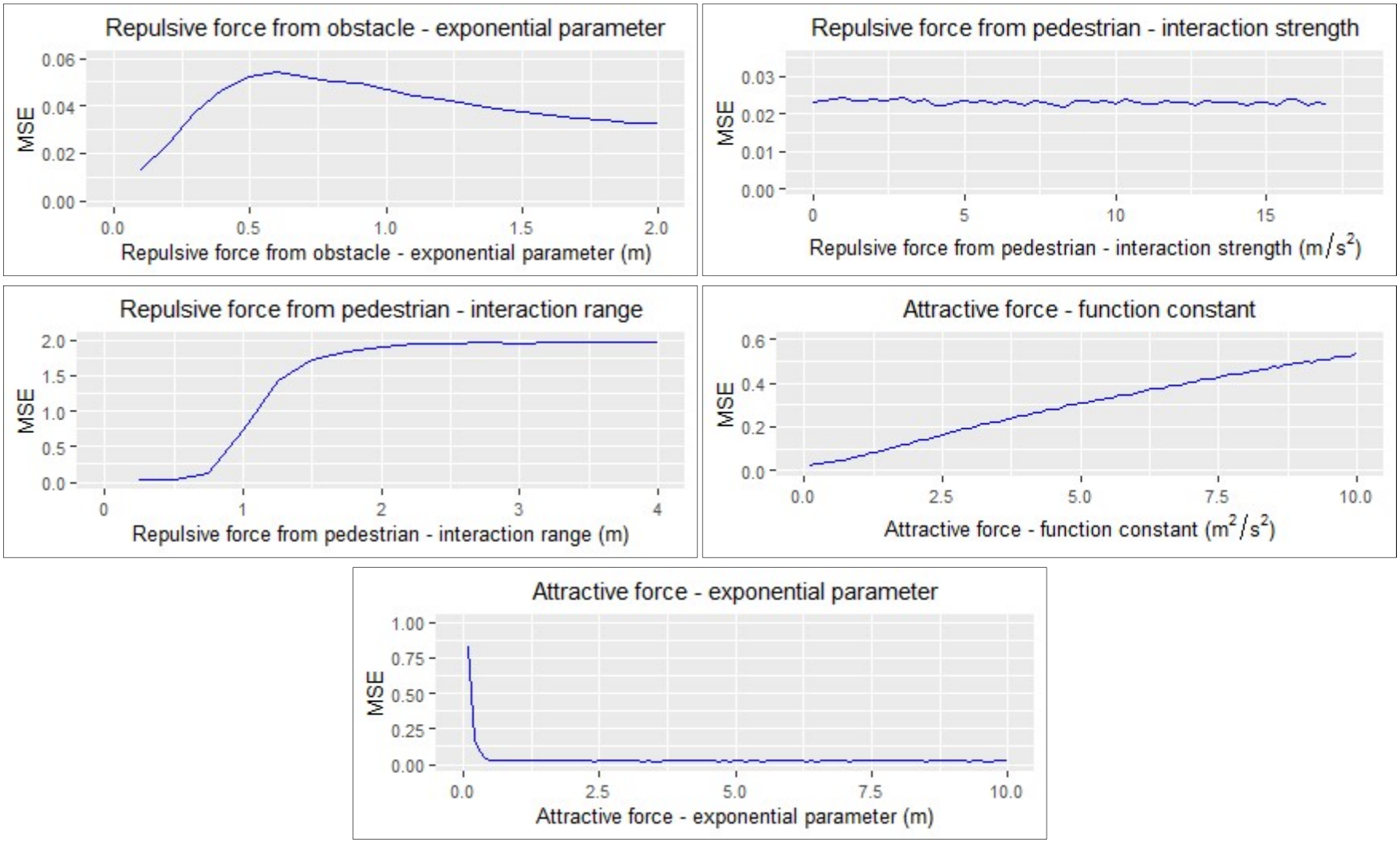

Figure 5.3: Social Force Model parameters impact

5.2.2. Global sensitivity analysis (GSA)

In order to obviate parameters correlation the global sensitivity analysis (GSA) was employed. GSA method is described in Saltelli et al. (2008). It is a variance based approach conducted in terms of a Monte Carlo experiment. The Monte Carlo experiment size (N) is required to be large for precise coefficients estimation (small experiment size leads to high confidence intervals). GSA computes sensitivity indices S_i of parameter i. First-order index is a sensitivity measure that presents the impact of parameter i over the model output (Y) without considering parameters' interaction while higher-order sensitivity indices (total effects) capture parameters correlation. The principle of GSA arises on the fact that sensitivity indices are computed not on a single parameter value (as the selection of the value impacts sensitivity analysis output), but on the average of all the possible values. High values of sensitivity indices (i.e. approach value of 1) indicate important parameters.

A brute-force estimation of sensitivity indices requires a N^2 procedure. Saltelli et al. (2008) proposed a method where sensitivity indices estimation cost is reduced to N(k+2) (k is the number of model parameters). The principle of this method arises on the fact that two different matrices (A, B) are set as standard. Subsequently a group of matrices C_i are generated where all of the matrix columns are extracted from B except from the i-th column that is extracted from A matrix. Thus, the number of C_i matrices is equal to k. All of the aforementioned matrices are used as model inputs. Model outputs are then computed as follows (equations 5.4, 5.5, 5.6) and are utilized in the sensitivity indices estimation.

$$y_a = f(A) \tag{5.4}$$

$$y_b = f(B) \tag{5.5}$$

$$y_{c_i} = f(C_i) \tag{5.6}$$

A N(2k+2) (24.000 simulations) experiment was performed in order to estimate second order (Saltelli, 2002) indices (experiment size N = 1000). Second order sensitivity indices include the interactions between two parameters. To avoid second order effects computation a 13.000 simulations experiment will be

required. In contrast, a brute-force estimation experiment will end after 10^6 simulations. Thus, the reduction in computational time is significant.

In every simulation the error between the predicted (according to the social force model) and the actual (subsequently to the smoothing application) velocities was computed. MSE (equation 5.7) is used as the metric to capture the sensitivity analysis performance, in line to OAT. Following Zanlungo et al. (2011), similarly to the application in the OAT sensitivity analysis, the agent's desired speed differs between pedestrians (its values are drawn randomly from its distribution). Both mean desired speed and its standard deviation follow the Gaussian distribution (Helbing and Molnár, 1995 and Zeng et al., 2014).

Table 5.2: Global sensitivity analysis

Parameter	STi	confidence interval	Si	confidence interval
Relaxation time	0,540	0,1060	0,253	0,0908
Desired speed - mean	0,594	0,0918	0,282	0,0877
Desired speed - std	0,142	0,0373	0,042	0,0376
Maximal acceptable speed	0,007	0,0029	0,000	0,0049
Strength of interactions from behind	0,001	0,0004	0,000	0,0022
Repulsive force from obstacle - function constant	0,061	0,0095	0,052	0,0213
Repulsive force from obstacle - exponential parameter	0,015	0,0033	0,004	0,0093
Repulsive force from pedestrian - interaction strength	0,001	0,0004	0,000	0,0029
Repulsive force from pedestrian - interaction range	0,003	0,0006	0,000	0,0036
Attractive force - function constant	0,001	0,0002	0,000	0,0017
Attractive force - exponential parameter	0,001	0,0003	0,000	0,0023

Table 5.2 presents the total effects and the first-order sensitivity indices for the social force model as applied in the collected data. The sensitivity analysis suggests that desired speed and relaxation time are the critical determining parameters, as also extracted from OAT sensitivity analysis. A false estimation in them will cause significant errors in applying the social force model. The other parameters do not seem to affect substantially simulation results.

In addition, the sum of the first order indices (0.633) indicates the non-additivity of the social force model. Parameter ranges were determined according to section

3.3.3, while the attractive forces parameters' ranges were selected randomly as no particular reference considering their values was found.

5.2.3. Comparative analysis

As mentioned in previous sections, a fair comparison is attempted in this research by employing the same social force model parameters as data-driven models' predictors. In terms of the ANN method, a 50 nodes network is utilized with one hidden layer (around 4 times the nodes in the input layer), Rectified Linear Unit (ReLU) activation function among all nodes and the Adam optimization algorithm (Kingma and Ba, 2015) with 0.001 learning rate. Glorot et al. (2011) pointed out the superiority of rectifier neural networks (ANN employing ReLU activation function) compared to those using previously widely applied activations such as logistic sigmoid and tangent hyperbolic ones. They also mentioned that rectifier units are closer to biological neurons. The number of nodes has been selected during a trial-and-error process in order to avoid overfitting. ReLU function is a recently applied activation function in the field of ANN that restricts the limitations (e.g. vanishing gradient problem) of the previously used activated functions (sigmoid, hyperbolic tangent, linear etc) that is further enhanced with employment of the Adam algorithm with a small learning rate. The output consists of two nodes (u_x, u_y) following the pedestrian velocity dimension. An initial approach, where the cost function is referred to the errors between the velocities in the Euclidean norm (u) reveals that low error values do not necessarily lead to low errors in each velocity dimension (u_x, u_y) separately, but rather to substantially high ones. Thus, a cost function, where the errors are related in each dimension separately is employed (Equation 5.7). ANN were modeled in the python programming language, with the aid of the Tensorflow library and the Keras API. Tensorflow can use system GPU (Graphics Processing Unit) sources in order to speed up model training (and testing) procedures (Abadi et al., 2016).

$$MSE = \frac{1}{N}\sum_{n=1}^{N}\frac{(u_{x_n}^{sim} - u_{x_n}^{obs})^2 + (u_{y_n}^{sim} - u_{y_n}^{obs})^2}{2} \tag{5.7}$$

where u^{sim} and u^{obs} stands for predicted and observed agent's velocity.

The number of epochs during the training of an ANN plays a very important role in the overfitting phenomenon (explained below). As the number of epochs is increasing the train error (the error on the training dataset) decreases (as this is the aim of the training procedure), but on the other hand the test error (the error on the test dataset) might increase. Figure 5.4 presents overfitting for the ANN model. From a number of epochs the test error stops to decrease and starts to increase while the gap between the type of errors (train and test) commences to increase substantially. In this experiment, this happens at around 500 epochs. Thus, an ANN model with 500 epochs in the training procedure is employed.

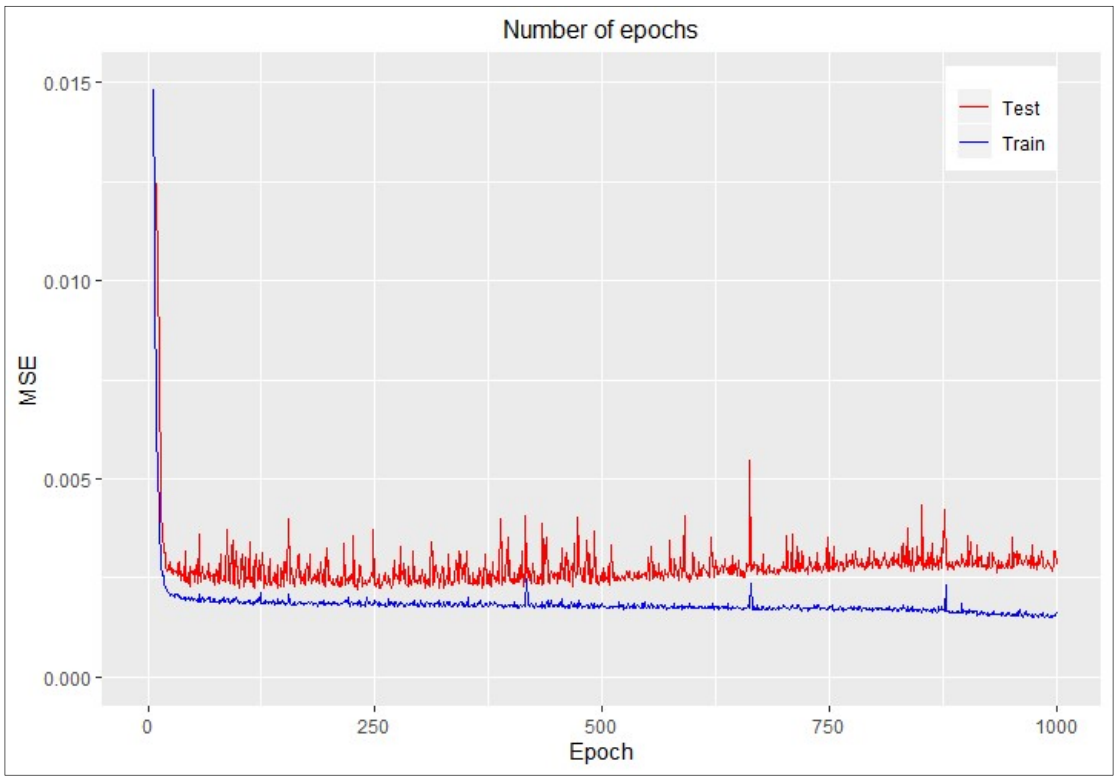

Figure 5.4: Number of epochs

As a multi-output regression has to be performed in this experiment (we distinguish pedestrian velocity in two axes and consider their correlation) MSVR and multi-output GP (in particular LMC type) are employed. MSVR was modelled in the Matlab programming language utilizing the Alvarez et al. (2018) code, with RBF kernel of 4.5 lengthscale, 5.0 penalty parameter C, 0.02 error of the ε-sensitive zone and the IRWLS optimization algorithm. An RBF kernel is also used in the GP model, whose hyperparameters are estimated during the training process, modelled in the python programming language. In terms of the Loess

method a model of 0.5 span and second polynomial degree is employed. Span ranges from 0 to 1 and represents the smoothness of the curve that fits data. Lower span values evince less smooth curves and vice versa. Polynomial degree ranges in 0, 1 or 2, while 0 is generally avoidable. Cohen (1999) employed bias corrected Akaike information criterion (AIC) for span estimation. It is stated that in contrast to the other data-driven methods Loess does not have the ability of examining possible correlations of the outputs in cases of multi-output experiments such the current one. The model has been implemented and estimated in R statistical computing environment through Rstudio IDE.

As also stated in terms of specifying the number of epochs for the ANN model, generally data-driven methods tend to perform well (or very well) in the training datasets, though their performance in test sets is under consideration. A model with low error values in the training sets and high in the test sets is a typical situation of overfitting, where the model can replicate only the given datasets and lacks generalization to other sets. On the other hand, theoretical simulation models, due to the fact that they rely on their own modeling principles and are not built on data solely, may not suffer from overfitting.

Thus, specific attention was given when comparing theoretical and data-driven models towards the overfitting problem. Hence, cross-validation is employed for the comparison and in particular a 5-fold one, as it overcomes overfitting problems.

In the specific experiment all of the selected pedestrian trajectories (both in the metro station and the shopping mall sites) are used for the application and comparison of the social force and data-driven models, in a full cross-validation pattern (5-fold cross-validation). The distinct recorded datasets are not of the same size, however the folds used in the cross-validation process require to be of equal size. Thus, the two datasets are merged together. Subsequently, the data in the dataset are shuffled and then divided in to five (5-fold cross-validation) equally sized datasets. Each time, four of the datasets are used for training, and the remaining one for testing. The training part involves the estimation of all model parameters, i.e. synaptic weights for ANN, weights for SVR, kernel parameters for GP, weights for Loess and the appropriate parameters for the social force model, by minimizing the cost function (Equation 5.7), which is the

same in all models. Then the trained model is applied to the test dataset, providing predicted values for the datapoints in the test set, in order to capture model generalization capability. When all of the datasets are utilized once as test sets the cross-validation process is completed. The result of the cross-validation leads to predicted values for all the datapoints (as are included in the test sets). Thus, with the employment of the appropriate GoF measures, comparing predicted and observed values, the generalization capability of each model can be estimated.

Considering the social force model training, the objective is to estimate the value of 11 model parameters that minimize Equation 5.7 in every cross-validation run (training process). As described in sections 5.2.1 and 5.2.2 [while also by Kouskoulis et al. (2019)] a two-step approach could be an option for training the social force model. At the first step (prior to cross-validation runs), the global sensitivity analysis (as a more holistic method as opposed to the OAT sensitivity analysis) is performed in the social force model in order to specify model parameters with high impact. In the second step (during the cross-validation process), the training revolves around the determination of these parameters.

This study attempts to train the social force model in terms of metaheuristics optimization. Especially, as the scope is to estimate 11 parameters that minimize a certain cost function, a genetic algorithm is employed. Genetic algorithms have proven their robustness in the field of optimization. They overcome the need of examining the most affecting parameters and then train the model only around them, as they inspect all the model parameters in an effective procedure.

A population of 30 chromosomes, with 0.8 and 0.2 crossover and mutation probabilities, respectively, and the best 2 fitness individuals to survive at each generation (elitism), was used to train the social force model (the hyperparameters of the genetic algorithm were set after a trial and error process) with the aid of R statistical software (Scrucca, 2013). Parameter bounds are specified according to Section 3.3.3.

A set of GoF measures, apart from the MSE, have been employed in order to evaluate the performance of each model and to compare them as each of them denotes different types of errors. Root mean square percentage error (RMSPE) penalizes large errors, mean percentage error (MPE) and Theil's bias proportion

(U_M) indicate the existence of systematic bias, Theil's covariance proportion (U_C) the existence of unsystematic error, Theil's inequality coefficient (U) and Theil's variance proportion (U_S) high values (close to 1) indicate high model inequality and difference in the distributions of predicted and observed data respectively. U_M, U_S and U_C sum to 1 considering MSE decomposition and thus population standard deviations for predicted (σ^{sim}) and observed agent's velocities (σ^{obs}) are used. It is noted that r stands for the correlation coefficient among predicted and observed values.

The errors of the predicted (relying on the social force model) and the measured pedestrian's velocity comprise the crucial indicator for evaluating model's efficacy. Particularly, pedestrian's actual speed is taken into account. Both in the social force and data-driven model simulations zero velocities (when pedestrian stands still) are disregarded as they do not show tendency for moving.

The GoF measures are presented in Equations 5.8 – 5.13 and utilize agent's velocity Euclidean norm (u) in order to capture model's performance. By computing agent's velocity according to MSE (as described above), i.e. the errors are related in each dimension separately, will lead to extremely high values for the GoF measures (particularly RMSPE) and will not reflect the exact performance of each model. As the aim in this part is not to estimate model weights, agent's velocity Euclidean norm (u) is utilized. This also has been applied in the same metrics for the social force model.

$$RMSPE = \sqrt{\frac{1}{N}\sum_{n=1}^{N}\left(\frac{u_n^{sim} - u_n^{obs}}{u_n^{obs}}\right)^2} \tag{5.8}$$

$$MPE = \frac{1}{N}\sum_{n=1}^{N}\left(\frac{u_n^{sim} - u_n^{obs}}{u_n^{obs}}\right) \tag{5.9}$$

$$U = \frac{\sqrt{\frac{1}{N}\sum_{n=1}^{N}\left(u_n^{sim} - u_n^{obs}\right)^2}}{\sqrt{\frac{1}{N}\sum_{n=1}^{N}\left(u_n^{sim}\right)^2} + \sqrt{\frac{1}{N}\sum_{n=1}^{N}\left(u_n^{obs}\right)^2}} \tag{5.10}$$

$$U_M = \frac{\left(\bar{u}_n^{sim} - \bar{u}_n^{obs}\right)^2}{\frac{1}{N}\sum_{n=1}^{N}\left(u_n^{sim} - u_n^{obs}\right)^2} \quad (5.11)$$

$$U_S = \frac{\left(\sigma^{sim} - \sigma^{obs}\right)^2}{\frac{1}{N}\sum_{n=1}^{N}\left(u_n^{sim} - u_n^{obs}\right)^2} \quad (5.12)$$

$$U_C = \frac{2(1-r)\sigma^{sim}\sigma^{obs}}{\frac{1}{N}\sum_{n=1}^{N}\left(u_n^{sim} - u_n^{obs}\right)^2} \quad (5.13)$$

Table 5.3 presents the performance of each model. The computed GoF measures indicate that data-driven methods have higher capability of simulating pedestrian movements, as they perform better according to all of GoF measures. This implies the outperformance of data-driven techniques in the specific simulations. The theoretical simulation model (social force) includes further large errors compared to the data-driven models, while the Loess method displayed the highest performance. The social force model performs sufficiently well in terms of model inequality [social force model Theil index (U) is not significantly higher than those of the data-driven techniques]. On the other hand, the social force model includes both systematic (MPE and U_M) and unsystematic (U_C) biases that almost do not exist in the data-driven models. Furthermore, the data-driven methods accomplish the presented cross-validation process significantly faster that the social force model, that is 129 seconds for the ANN, 16.5 minutes for the GP, 53 seconds for the SVR and 18 seconds for the Loess, while around 70 hours were required for the social force model employing the aforementioned genetic algorithm in the training process. All simulations were performed in an Intel i7 CPU @ 1.80GHz laptop with 8GB of RAM and 64-bit Windows 10.

In addition, a comparison among the four data-driven methods (ANN, GP, SVR and Loess) reveals that Loess performs better according to almost every index, ANN and GP present similar performance levels, while SVR provides inferior predictions. It should also be mentioned that Loess technique performs better even though it employs less predictors than the other data-driven methods, while accomplishing the cross-validation procedure in significantly less time.

In contrast, it is clear that there are limitations, related with the opacity and the (lack of) interpretability of the data-driven models. Yet, they seem a promising avenue for model development, when model fit is the primary concern. On the other hand, the social force model provides an integrated simulation framework where every parameter is directly related to the model output. It explains in a clear manner the way that pedestrians interact and walk (high level of interpretability), while data-driven methods are treated, at some level, as black boxes.

Table 5.3: Models performance comparison

Model / GoF	MSE	RMSPE	MPE	U	U_M	U_S	U_C
Social force model	0,005341	19,32%	8,06%	0,0382	0,3760	0,1996	0,4244
ANN	0,002174	11,57%	0,70%	0,0245	0,0002	0,0045	0,9953
GP	0,002171	10,76%	0,50%	0,0241	0,0003	0,0058	0,9940
SVR	0,003109	15,42%	1,29%	0,0304	0,0011	0,0709	0,9280
Loess	0,002349	8,76%	0,50%	0,0226	0,0002	0,0047	0,9952

Complementary to the above, a comparison of the GoF measures in every run of the cross-validation procedure (both train and test measures) is presented in Figures 5.5 and 5.6 for every model. The x-axis illustrates the datasets that were used in the training and test procedures during the cross-validation process. In accordance to the previous analysis the Figures indicate better capability of data-driven methods for simulating pedestrian movements as they perform better for almost all of them with the only one exception being the GP in the test set of the first run (RMSPE).

This implies that data-driven models can simulate more effectively pedestrian movements. On the other hand, data-driven methods tend to overfit as they learn/develop from the data (as mentioned above), indicated by the gap of the measures between the training and the test datasets.

To sum up data-driven methods strengths comprise:

- Higher simulation performance
- No need for mathematical equations
- Substantially lower computational time

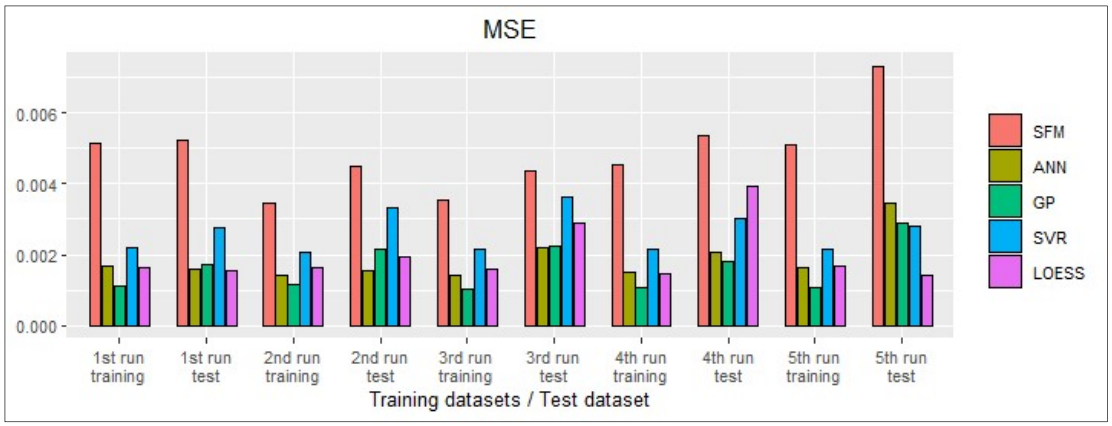

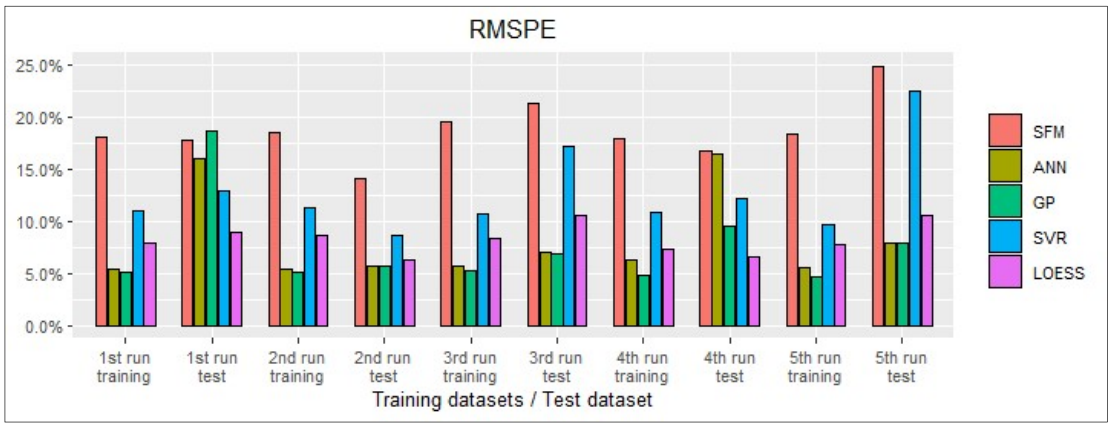

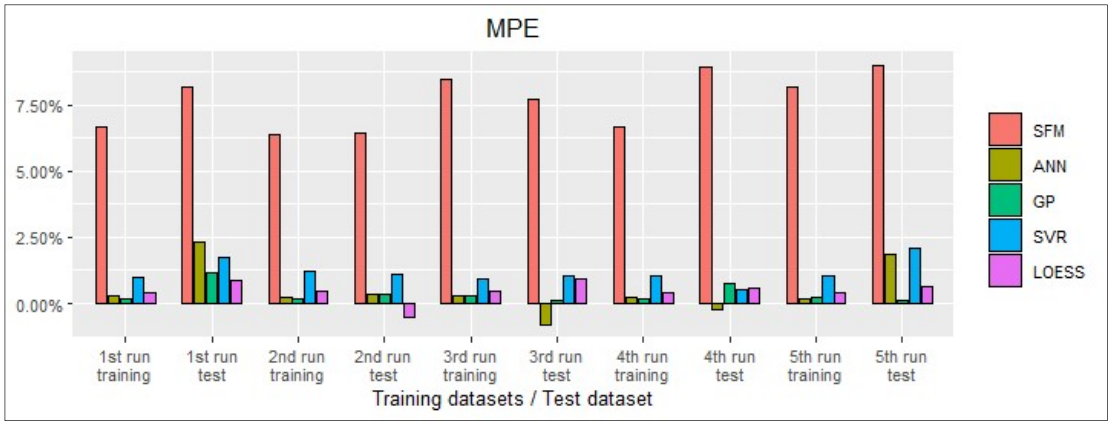

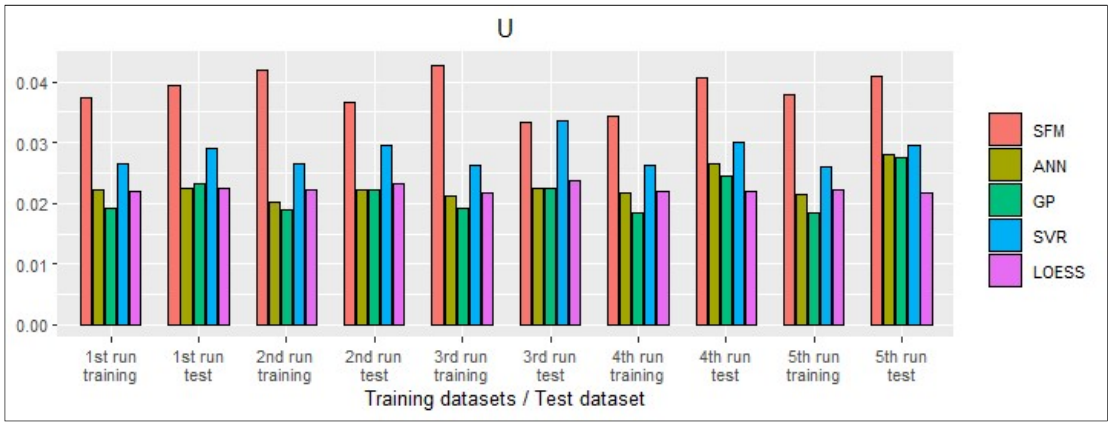

Figure 5.5: GoFs in every CV run – MSE, RMSPE, MPE, Theil coefficient

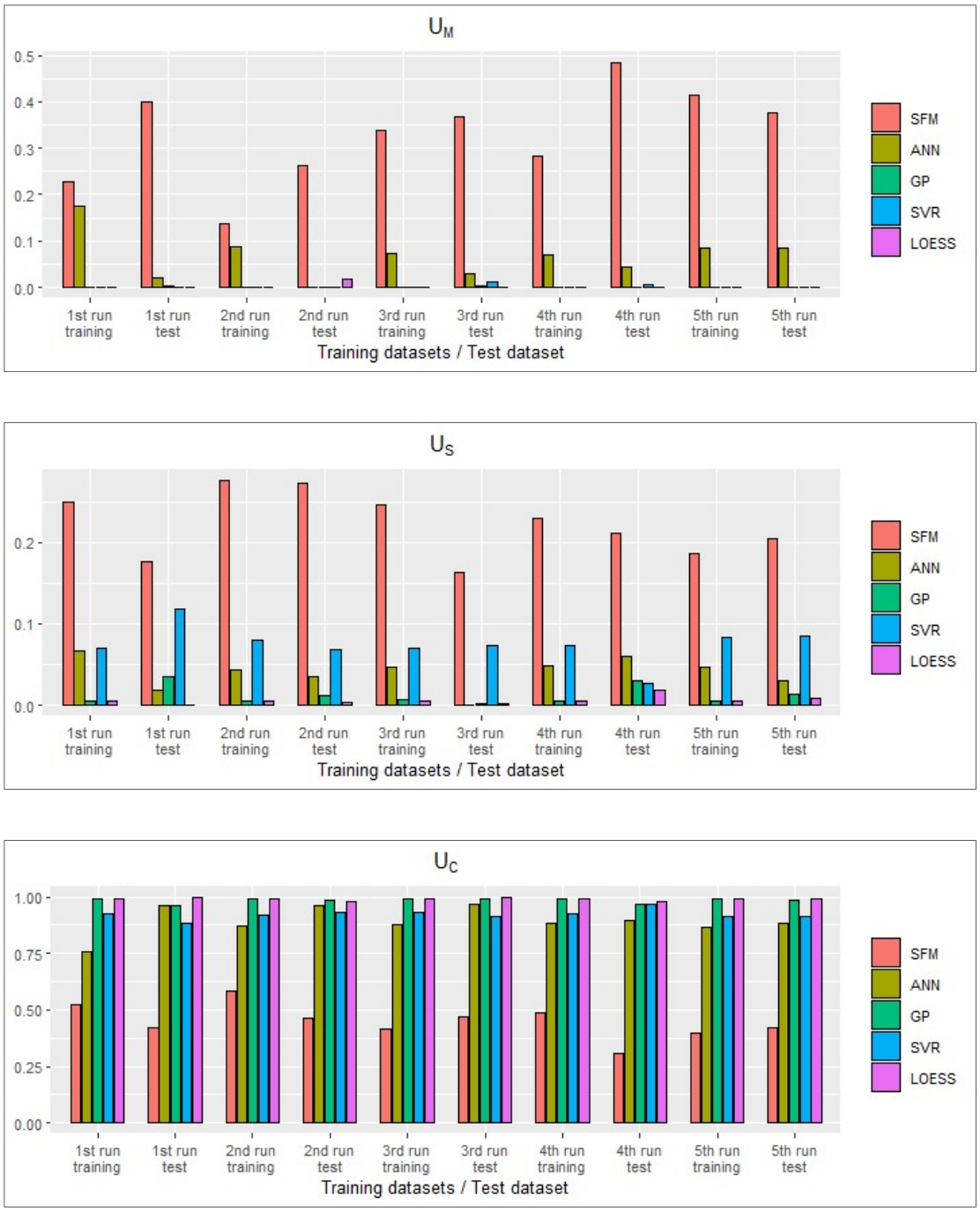

Figure 5.6: GoFs in every CV run – Theil bias, Theil variance, Theil covariance

5.3. Introduction of Additional Variables in Data-Driven Models

Following the assessment of the performance of data-driven models in pedestrian simulation considering only variables from existed and widely applied pedestrian simulation models, further analysis is conducted in order to specify if additional variables can improve data-driven models efficacy. The additional variables have been selected from section 2 (where the literature review in pedestrian modelling is presented).

Initially the height and the gender of the agents are used for exploring data-driven modelling improvement. While agents' gender is obvious (as the datasets have been extracted from video recordings), their height needs to be estimated. The aid of photogrammetric tools was substantial.

Apart from transforming image points to real world ones, photogrammetric methods are also useful for calculating the dimensions of every item, and thereby agent's height, from a video recording.

The process is the same with the methodology employed for the conversion of an image point to real world coordinates, regarding the steps of a) removing lens distortion, b) cameras site and angles estimation In addition to the pedestrian's lowest point pixel coordinates (x_1,y_1), those of the highest point (x_2, y_2) are also computed by removing principal point's coordinates $[x_1' = x_1 - x_0,\ y_1' = -(y_1 - y_0),\ x_2' = x_2 - x_0,\ y_2' = -(y_2 - y_0)]$.

Subsequently, pedestrian world coordinates (X, Y) are computed according to equation (4.3), where Z can take an initial value (e.g. 0). Knowing pedestrian world coordinates (X, Y) we insert them in equation (4.3), replace (in equation 4.3) pedestrian's lowest point (x_1,y_1) to pedestrian's highest point (x_2, y_2) and compute the new Z value. Agent's height comprises the difference between the initial value of Z and the new one. Figure 5.7 presents the method.

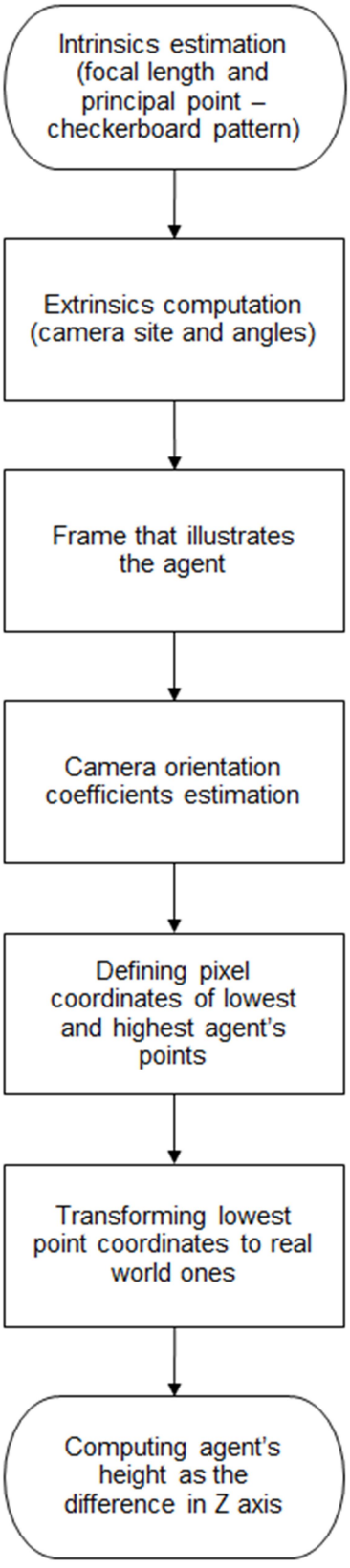

Figure 5.7: Agent's height estimation

The agent's gender has been transformed to a numeric (dummy) variable with the appropriate encoding in order to be incorporated in the data-driven models.

Due to implementation details (mentioned in section 5.1) the Loess technique cannot be applied in this analysis as it cannot employ further variables. In all of the other three data-driven techniques (i.e. ANN, SVR and GP) the same model setup, presented in section 5.1, and the same hyperparameters (for the models that are needed to specified a priori) have been used.

Figures 5.8 and 5.9 present the results of this analysis. Following the inclusion of agents' characteristics (height and gender), the updated data-driven pedestrian simulation models performed better than the initial ones considering almost every GoF measure (described in section 5.1). An exception of this is indicated by the Theil's bias proportion measure in the ANN model (the difference in the SVR model is negligible). This index, which implies the existence of systematic bias, performed worse in this technique. The existence of a higher systematic bias was not verified by the MPE measure. At this point it should be mentioned that Theil's bias proportion measure value was already extremely low before the adoption of the agent's height and gender, and although it increased in the updated model, it still remains very low. Other differences in the values of the GoF measure (that can imply a lower performance in the updated data-driven model) are not considerable (e.g. RMSPE index in the GP model, Theil's variance proportion in the GP and SVR models). In order to illustrate this fact (i.e. the size of the difference in the GoF measures) a comparison with social force model GoF measures is provided in Figures 5.10 and 5.11.

In addition, the incorporation of the additional variables in the pedestrian simulation model improved fairly the performance of the ANN technique, while not as much the performance of GP and SVR techniques where the differences in the GoF measures are low (or very low) before and after the incorporation. On the other hand, the ANN model, with the aforementioned exception of the Theil's bias proportion index, performed significantly better in all of the other GoF measures.

Finally, the parameter of time is also tested for its impact in the data-driven pedestrian simulation model (i.e. whether the incorporation of time can further enhance the improvement of the model). As GP and SVR techniques are not

time-series models, in contrast to ANN where with its class of Recurrent Neural Network (RNN) or the Long short-term memory (LSTM), an architecture of RNN, can incorporate the parameter of time, an extra previous time-step of the agent's trajectory is included in the data-driven models. The aim of this research was to examine if the parameter of time can upgrade the performance of the data-driven models after the incorporation of agent's height and gender.

The results of this process (Figures 5.8 and 5.9) resemble a lot with the results of the data-driven model with the additional variables of the agent's characteristics. In particular the models after the incorporation of time parameter seem to perform better, but not for all the of the GoF measures. Theil's bias proportion index is increased in all of the data-driven models (including GP), but still this lower performance is not verified from the MPE index. It should be mentioned that even Theil's bias proportion index increased it remained extremely low for all of the data-driven techniques (see also Figure 5.11). ANN model performs better (with the exception of Theil's bias proportion) after the incorporation of time parameter, while the differences of GP and SVR models are slightly better.

Interestingly the adoption of the additional variables cannot enhance the performance of some of the employed data-driven models in order to surpass Loess model performance (even Loess model employs only three pedestrian simulation variables). In particular, SVR model performs worse than Loess even if the former employs agent's characteristics (i.e. height and gender) and time variables. GP model performs worse than Loess if only employing pedestrians' characteristics variables (it requires also time variable for outperforming Loess model). On the other hand ANN model performs better in the majority of the GoF measures than Loess even when employing only pedestrians' characteristics variables.

In general, the adoption of the additional variables seems to improve mainly the performance of the ANN model implying that this technique can "handle" more efficiently the incorporation of these variables.

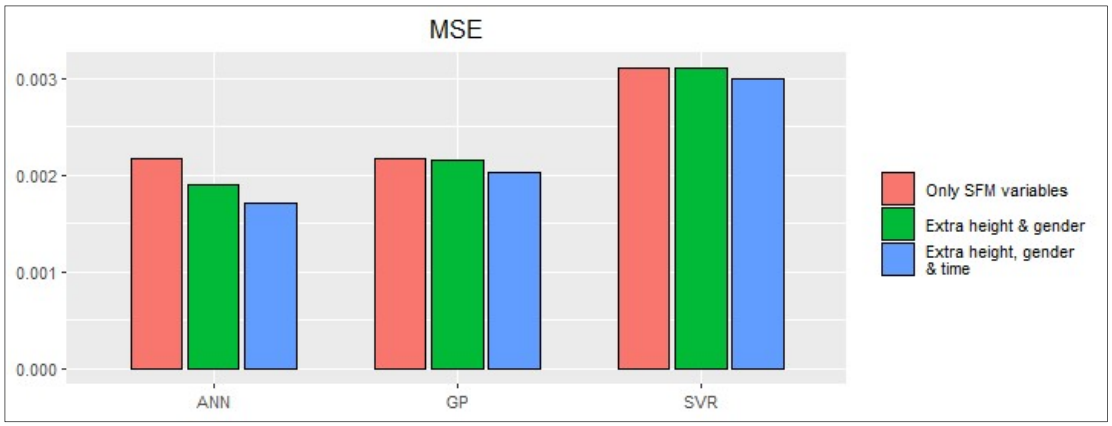

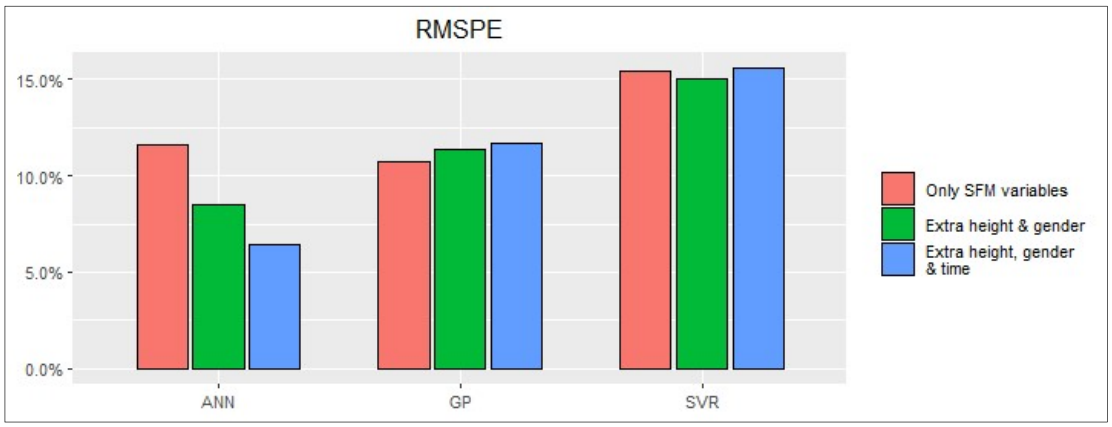

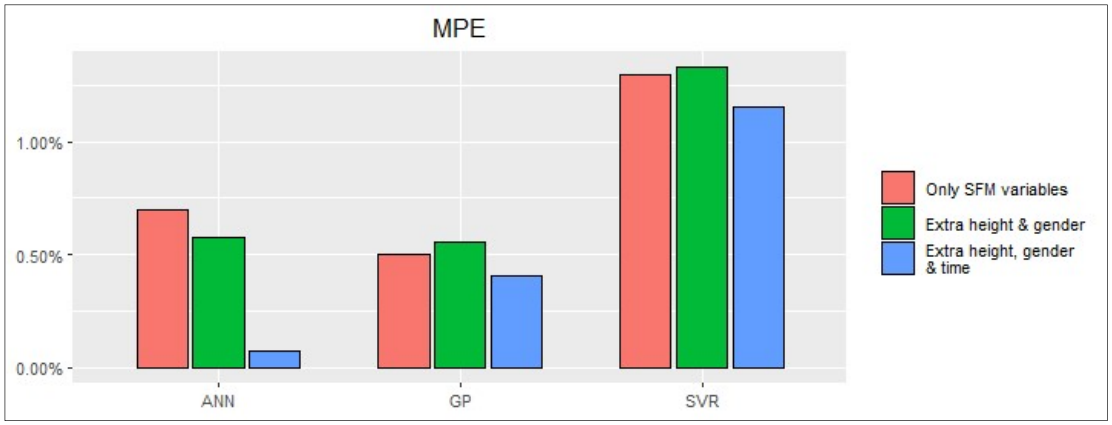

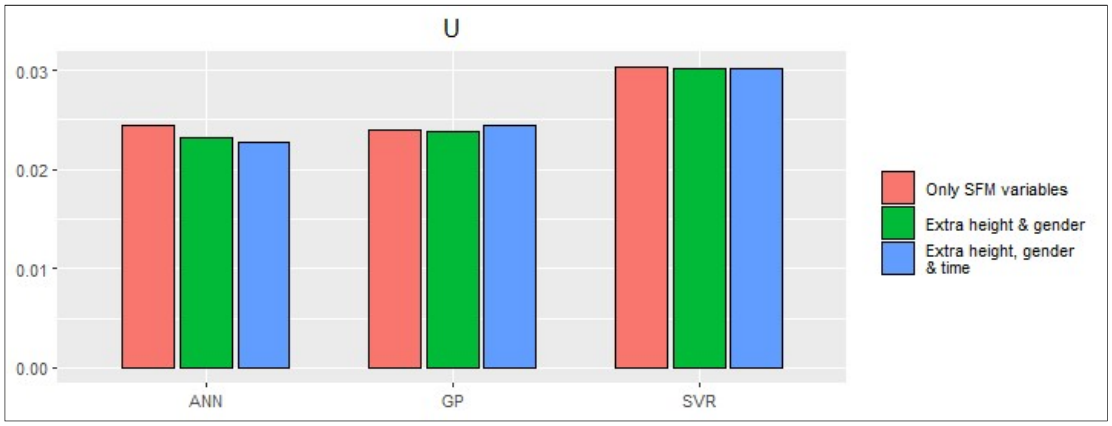

Figure 5.8: GoFs with extra variables – MSE, RMSPE, MPE, Theil coefficient

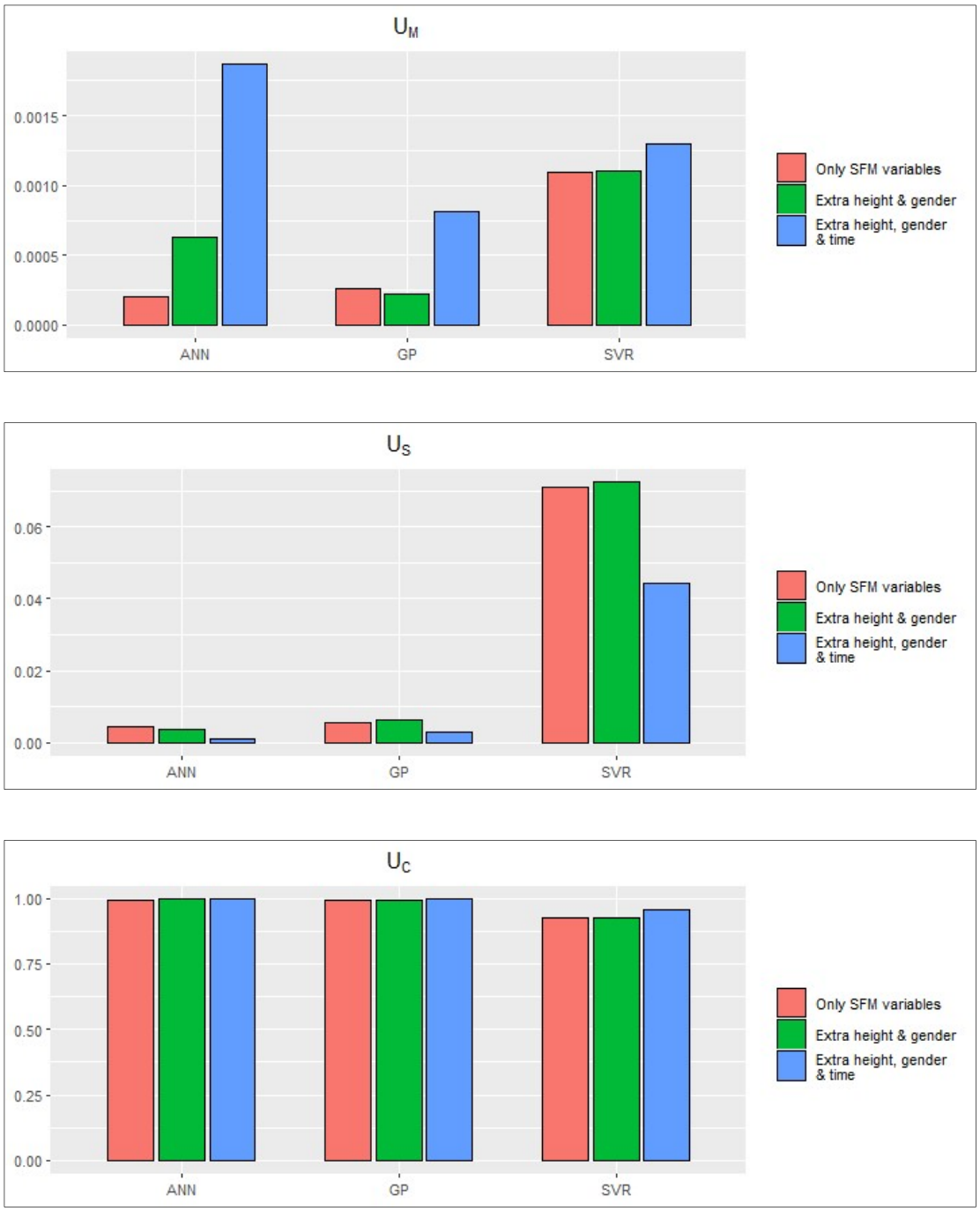

Figure 5.9: GoFs with extra variables – Theil bias, Theil variance, Theil covariance

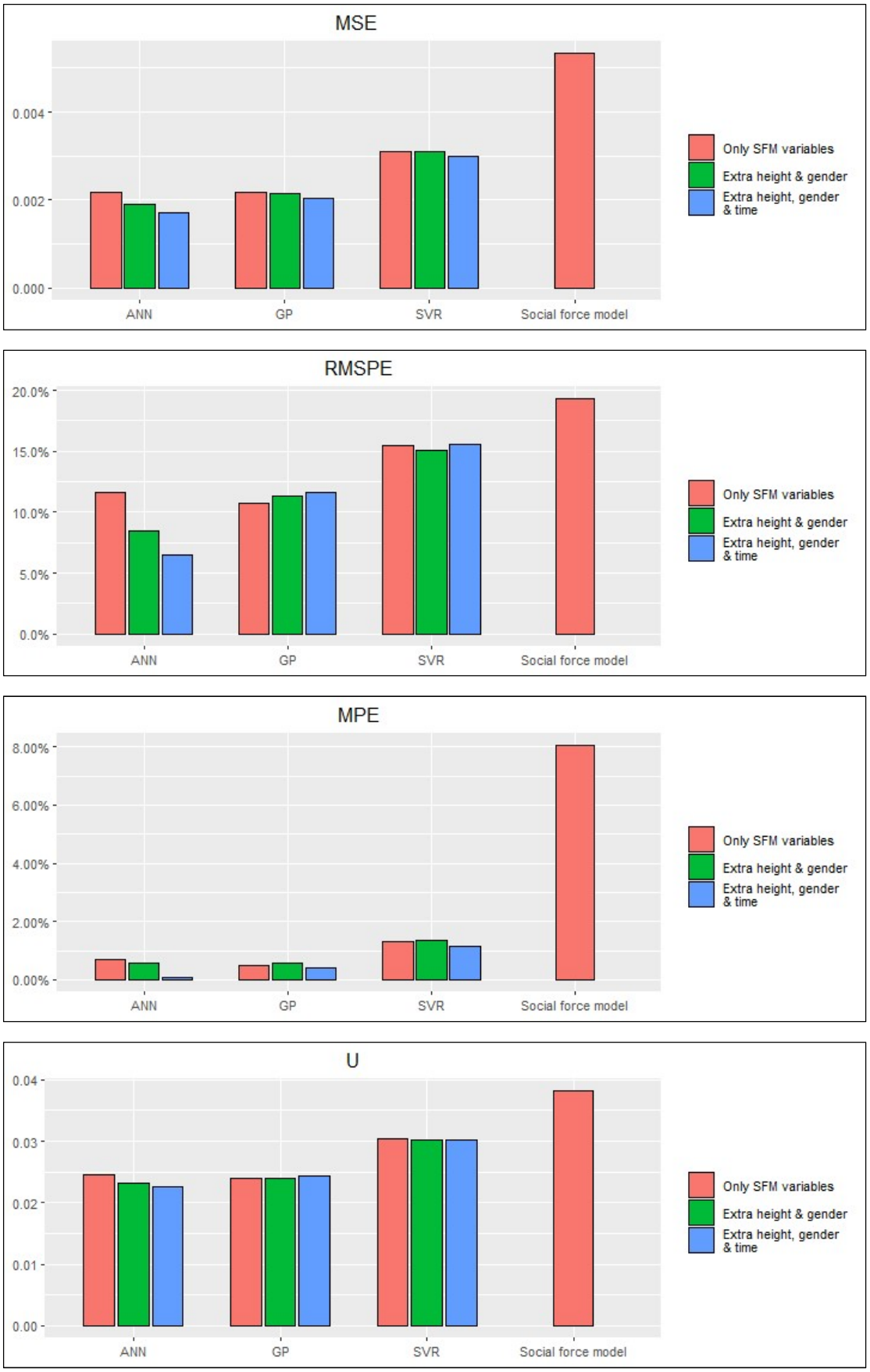

Figure 5.10: GoFs with extra variables including social force model – MSE, RMSPE, MPE, Theil coefficient

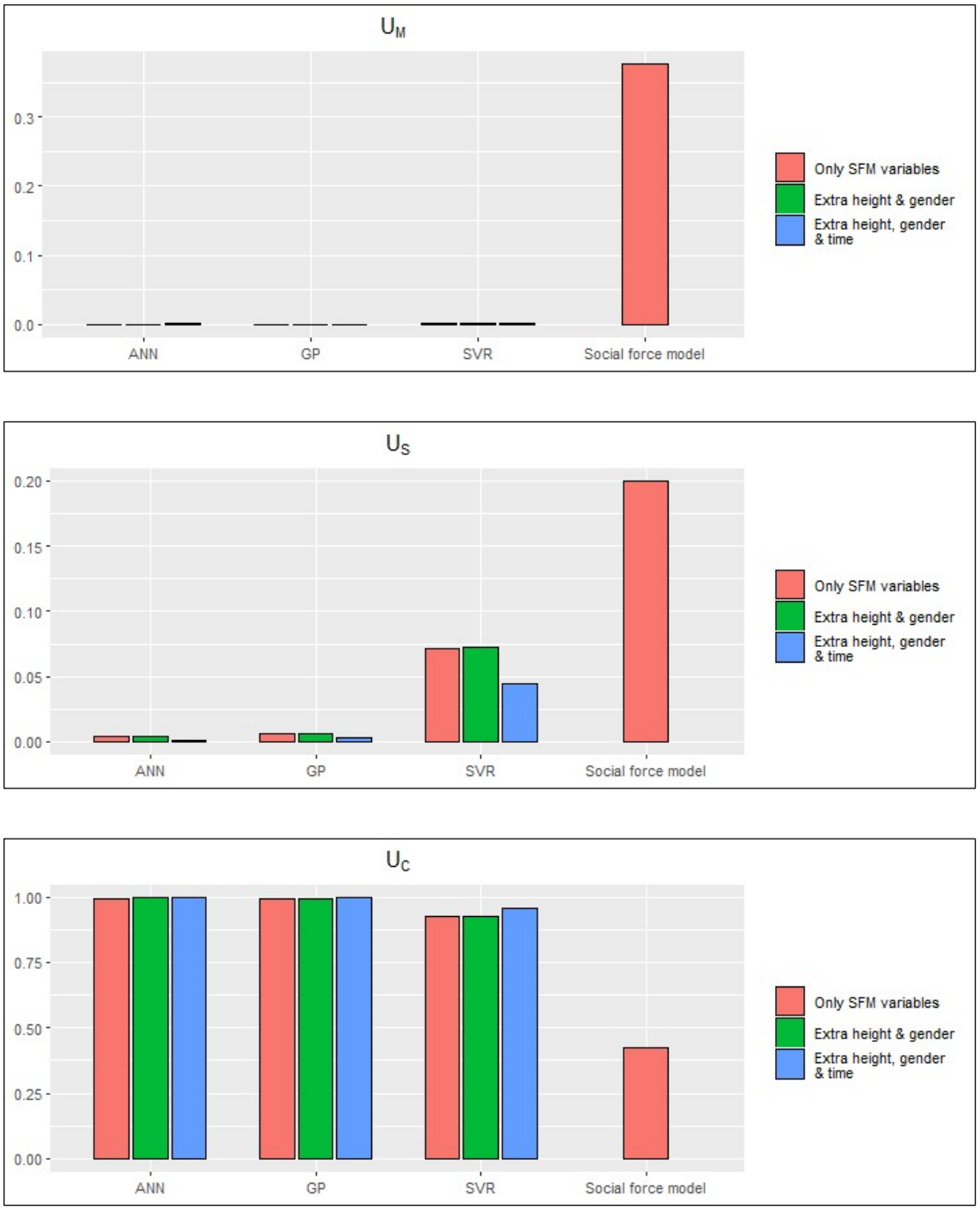

Figure 5.11: GoFs with extra variables including social force model – Theil bias, Theil variance, Theil covariance

6. DISCUSSION/CONCLUSION

6.1. Overview

This thesis explores the capabilities of data-driven methods in the field of pedestrian simulation and provides an assessment of the model's validity through a comparative analysis of the models' performance against a traditional theoretical model. Four of the most widely used methods - namely, ANN, SVR, GP and Loess - were compared with a theoretical pedestrian simulation model, the social force model. The model set the principles/rules of pedestrian movement and has been employed in widely applied simulation software, such as VisWalk (PTV, 2015) and SimWalk (Zainuddin et al., 2009). According to the social force model, as an agent walks they receive forces from their surroundings that coerce them to amend their velocity, similarly to the forces in fluid molecules. Social forces are distinguished in attractive and repulsive, and the total force that the agent receives from their surroundings. The model estimates agent's velocity in the next time step [$\overrightarrow{u_\alpha}(t+1)$] relying on: a) the agent's velocity $\overrightarrow{u_\alpha}(t)$ in the current time step, b) the distance $\overrightarrow{r_{\alpha\beta}}$ between the examined agent and the pedestrians triggering repulsive effects, c) the distance $\overrightarrow{r_{\alpha B}}$ between the examined agent and space boundaries, d) the distance $\overrightarrow{r_{\alpha i}}$ between the examined agent and the pedestrians triggering attractive effects, e) the distance $\overrightarrow{r_\alpha^k}$ to the next destination point and f) the pedestrians triggering repulsive effects velocity $\overrightarrow{u_\beta}$.

To design the models, a data collection experiment was designed. The data was collected via video recordings at two different sites where pedestrians were anticipated to adopt different walking patterns. Data collection was performed at a metro station during peak hours, where most of the agents were on their way to work/study, and a shopping mall during afternoon hours, where pedestrians enjoyed their walk, stared at shop displays and shopped. Video recordings were performed utilizing two digital cameras that were placed at both locations at an upper level point. The first camera was focused on the terrain, where pedestrians

walk, and the second captured their characteristics (height, gender etc.). Subsequently, a tracking software was employed for extracting pedestrian trajectories. An appropriate transformation based on photogrammetric tools allowed the conversion of image points to real world coordinates.

The extracted data included noise that needs to be eliminated. A data noise reduction algorithm, that combines existing methods, was presented in this research. In particular, an extension of the Kalman filter algorithm was applied in the problem of pedestrian trajectory noise reduction with promising results. While most of the studies in pedestrian tracking employ standard Kalman filter and consequently adopt its assumptions, the present research utilized UKF in order to relax them. As noise matrices (predicted and measurement states) were unknown, a procedure for estimating the noise covariance ratio was also presented. Experiments were conducted for selecting the appropriate ratio value.

Moreover sSMA was incorporated in the UKF. Kalman filter prediction for the next time step relies on the velocity of the moving object. In cases of velocity noisy values Kalman filter finds it difficult to provide an accurate estimation for the next time step pedestrian cite. Hence, the incorporation of sSMA in the velocity part of UKF reduces velocity noise and thus leads to a higher filter performance. On the other hand, exorbitant smoothing was avoided by maintaining pedestrian kinematics. The results of the filter in pedestrian trajectory data indicated significant noise reduction, with velocity variance of trajectories that approach steady movement (zero velocity variance) being substantially reduced.

Due to the fact that data-driven techniques are not inherently a pedestrian simulation model, an appropriate model setup has been developed. In order to provide a fair comparison between the social force model and the data-driven methods the same parameters that the social force model employs (as mentioned before) were also used in the data-driven pedestrian models for estimating pedestrian’s velocity in the next time step. Considering the Loess model, and due to technique limitations, the model variables were limited to three (agent’s velocity in the current time step, distance between the examined agent and the pedestrians triggering repulsive effect and distance between the examined agent and space boundaries).

The comparative analysis of the social force model and the data-driven models was conducted adopting the cross-validation procedure. Data-driven methods learn from the data and simulate pedestrian movements fairly. On the other hand, data-driven techniques fail in generalizing their results on unseen data (overfitting). Hence the cross-validation process was utilized in order to cater for this limitation. Though the aim of this research is not to provide a pedestrian simulation model based on the aforementioned techniques, data-driven models hyperparameters were set in order to restrict overfitting issues.

In terms of the social force model calibration a genetic algorithm (in terms of metaheuristics) has been employed. An OAT sensitivity analysis and a more holistic method (GSA) were applied and captured model parameters' impact indicating that the desired and acceptable speed and the relaxation time comprise the critical parameters. GSA surpasses OAT sensitivity analysis drawbacks and specifies parameters correlation.

A set of GoF measures have been employed to evaluate the performance of each model. Results indicate the outperformance of the data-driven methods in terms of pedestrian simulation in almost every cross-validation run and every GoF measure, although no prior knowledge of pedestrian dynamics has been incorporated into them. This indicates the suitability of data-driven methods for pedestrian simulation. Still, the tendency of data-driven techniques to overfit should be taken into serious consideration, when a researcher aims to develop a data-driven model for pedestrian simulation.

Following the comparison of the performance between the social force model and the data-driven models, with the latter including the same variables with the former additional variables were included in the data-driven models. These variables are the agents' characteristics' (height and gender) and the time parameter. Further analysis has been conducted in order to investigate if the additional parameters can enhance the performance of the data-driven models. Loess model was excluded from this procedure due to the limitations of this technique.

6.2. Research Contributions

This research provides a contribution towards exploring data-driven techniques' efficacy on pedestrian modeling. Pedestrian trajectories have been extracted from video recordings on the field and a filter that combines UKF and sSMA has been applied for eliminating data noise. Exorbitant smoothing has been avoided by maintaining pedestrian kinematics. Subsequently, the smoothened pedestrian trajectories were used for an application utilizing a representative pedestrian theoretical model and four data-driven techniques. Following model training and testing, simulation results indicated, through the RMSPE index, substantially higher (better) performance for the data-driven methods. The results of this study demonstrate that data-driven theories comprise a very promising approach for pedestrian simulation, as they can provide increased performance. Data-driven techniques offer higher simulation performance, less computational time requirements and "mathematical" simplicity making them overall a more suitable approach for pedestrian simulation.

Explicitly the contributions of the research are outlined in the following:

- Provide a framework for data (pedestrian trajectories) noise elimination
    - Enhance UKF performance with the incorporation of sSMA
    - Estimate UKF noise covariances when unknown
- Pedestrian model setup for data-driven simulations
- Apply a time efficient social force model calibration
- Display data-driven modelling efficiency in the field of pedestrian simulation (in contrast to existing theoretical models)
- Improve performance of data-driven models incorporating additional meaningful pedestrian simulation variables

Moving average enhanced UKF performance as it reduces velocity noise and further improves the estimation of pedestrian's next time step. Also due to the fact that the symmetric extension of the moving average filter was employed the tendency of the agent's movement was reflected. In addition, a framework that estimates UKF noise covariances was provided. In this framework initially the noise covariance at measurement state was estimated. Subsequently, the relationship (ratio) between the noise covariance at measurement state and the

one at the prediction state was examined attempting to avoid extremely smoothing and preserve pedestrian kinematics on the one hand, and to avoid overfitting (estimated trajectory points are close to measured), on the other hand.

A fair comparison between the social model and the data-driven techniques was performed in this thesis. Hence, the same parameters that social force utilizes in order to simulate pedestrian movements were employed in the data-driven models. The parameters of distances were set at an appropriate format (horizontal and vertical projections) so that the data-driven techniques are able to incorporate them. A suitable criterion was specified (based on the “closest” distance) for setting distance parameters as a one value variable. Towards this, agents’ coordinates were transformed according to their route (angle rotation).

A time efficient procedure was also proposed for calibrating the social force model parameters. A genetic algorithm was employed for minimizing the cost function of the social force parameters during its training process. Prior to this, a two-step approach that is related to the sensitivity analysis (OAT and GSA where the latter obviates model parameters correlation) of the social force model parameters was presented. However, as the genetic algorithm is robust and efficient, and it does not require the a priori knowledge of the most affective parameters, it was used in the present experiment.

The main contribution of this research is that data-driven techniques seem to perform better than the theoretical simulation models in the field of pedestrian simulation, and thus data-driven analytics comprise a promising theory. All of the employed data-driven methods performed better, with little and negligible exceptions, than the social force model although they do not rely on any a priori set of pedestrian movement principles. Furthermore, data-driven models proved their computation and time efficiency. Slight differences were noticed among the performance of the different data-driven methods, with SVR being the least powerful of them. On the other hand, the limitations of the data-driven methods that concern to the opacity, the (lack of) interpretability and the tendency for overfitting should be seriously considered.

Finally, with the incorporation of additional pedestrian simulation variables, the data-driven models performed better, although this improvement was not substantially, mainly, due to the fact that their performance had already reached

a high level. An increased improvement in the performance of ANN model (compared to SVR and GP) was noticed. In this experiment the agent's height and gender, and the parameter of time were considered as the additional variables.

The main contribution of the present research, as mentioned above, is the display that data-driven techniques can enhance the performance of pedestrian modeling. Improved pedestrian simulation models can be employed by many sectors in the transportation field. A typical example is this of autonomous vehicles. Self-driving cars recognize their surroundings, including the moving objects (e.g. pedestrians), and adjust their movement considering also the agent movement in their surroundings. An improved pedestrian simulation model can lead to more reliable prediction of agents' movement in the vehicles' surroundings, and thus lead to improved performance of autonomous vehicles considering pedestrian collision avoidance.

An overall outcome of the research is the outperformance of the data-driven techniques in the field of pedestrian simulation (as mentioned above). The writer of this thesis recommends the employment of these techniques for developing pedestrian simulation models, relying on their high level efficiency. Among the four data-driven techniques ANN seem to provide a more holistic modeling framework (though more complex) that can capture movement dynamics and can be enhanced with the incorporation of additional variables that improve their performance.

6.3. Study's Limitations and Future Research

Though an extended comparative analysis was conducted in the current research further issues are outlined as well. These issues could be considered as next steps for the research in the field of data-driven pedestrian simulation.

A limitation of the research was the employment of certain variables in the data-driven models, mainly, in order to provide a fair comparison between them and the social force model, while certain additional variables were also considered (based on the literature review). In future research an amplification of the data-

driven models can be accomplished with the incorporation of other relevant variables. An example of this could be the employment of a density measure. In the current thesis the distance parameters of the data-driven model included only one “repulsive” and/or “attractive” agent according to the selection criterion that was mentioned. The incorporation in the models of a density measure could capture not only one pedestrian, but also the other pedestrians affecting the simulated one.

In this experiment specific data (i.e. pedestrian trajectories) were used for examining the performance of both data-driven and social force models and comparing them. Additional data can be considered for an improved evaluation of the models, either from existing datasets or from other new data collection experiments under different conditions.

The scope of this thesis is not to provide a data-driven pedestrian simulation model. Though, due to the fact that the results of the present research demonstrate that data-driven models are able to capture pedestrian dynamics at a satisfactory level, a data-driven pedestrian simulation model could be developed in the future.

Also, in this thesis only pedestrian movements were considered. An interesting research objective is the investigation of pedestrian movement while interacting with vehicles in more complex scenarios and situations. The application of data-driven models in these scenarios should be examined. This notation is crucial as it can enhance the way that autonomous vehicles behave and perform. In particular, in future cities where autonomous vehicles move, interacting with other vehicles/bicycles/pedestrians, an advanced data-driven model that simulates pedestrian movement in these types of complex environments can improve the performance of autonomous vehicles, as pedestrian behavior will be also incorporated more efficiently. Data-driven theory can be employed as it has proven its efficiency in the present research.

In addition, in this research the parameter of time in data-driven pedestrian simulation models was also tested. RNN architecture of ANN can also be tested for its applicability in terms of pedestrian simulation. RNN or LSTM models incorporate in their structure the parameter of time. It should be mentioned that this requires data with extended pedestrian trajectories as RNN and LSTM

models make their predictions in a time series manner requiring a large amount of previous time steps of a pedestrian trajectory for predicting the next one.

Finally, a comparison in pedestrian movements between normal and emergency situations should be further explored to identify the differences in pedestrian behavior under emergencies. This will contribute to the design of pedestrian simulation models which offer a more holistic approach catering for different types of situations.

List of publications

- Kouskoulis, G., C. Antoniou, and I. Spyropoulou (2019). A Method for the Treatment of Pedestrian Trajectory Data Noise. Transportation Research Procedia, Vol. 41, pp. 782–798.

- Kouskoulis, G., I. Spyropoulou, and C. Antoniou (2019). Comparing the Performance of Artificial Neural Networks and Social Force Model on Pedestrian Simulation. In Proceedings of the 9th International Congress on Transportation Research – ICTR, Athens, Greece.

- Kouskoulis, G., C. Antoniou, and I. Spyropoulou (2018). Comparing Theoretical Pedestrian Simulation Models with Data Driven Techniques. In Proceedings of the 7th Symposium of the European Association for Research in Transportation conference – hEART 2018, Athens, Greece.

- Kouskoulis, G., I. Spyropoulou, and C. Antoniou (2018). Pedestrian Simulation: Theoretical Models vs. Data Driven Techniques. International Journal of Transportation Science and Technology, Vol. 7, No. 4, pp. 241–253.

- Kouskoulis, G., C. Antoniou, and I. Spyropoulou (2017). Data Driven – a Significant Tool in Pedestrian Simulation. In Proceedings of the 8th International Congress on Transportation Research – ICTR, Thessaloniki, Greece.

- Kouskoulis, G., and C. Antoniou (2017). A Systematic Review of Pedestrian Simulation Models with a Focus on Emergency Situations. Presented at 96th Annual Meeting of the Transportation Research Board (January 2017) and published in Transportation Research Record: Journal of the Transportation Research Board, Vol. 2604, No. 14, pp. 111–119.

- Kouskoulis, G., and C. Antoniou (2015). Influencing Factors of Pedestrian Velocity under Constraints. In Proceedings of the 7th International Congress on Transportation Research – ICTR, Athens, Greece.

- Kouskoulis, G., and C. Antoniou (2015). Determination of Parameters Affecting Safe Pedestrian Movement via Microscopic Simulation. In

Proceedings of the 6th Pan-hellenic Road Safety Conference, Athens, Greece.

REFERENCES

1. Abadi, M., P. Barham, J. Chen, Z. Chen, A. Davis, J. Dean, M. Devin, S. Ghemawat, G. Irving, M. Isard, M. Kudlur, J. Levenberg, R. Monga, S. Moore, D. Murray, B. Steiner, P. Tucker, V. Vasudevan, P. Warden, M. Wicke, Y. Yu, and X. Zheng (2016). Tensorflow: A System for Large-Scale Machine Learning. In Proceedings of USENIX Symposium on Operating Systems Design and Implementation (OSDI '16), Savannah, GA, USA.

2. Akin, D., and V. Sisiopiku (2007). Modeling Interactions between Pedestrians and Turning Vehicles at Signalized Crosswalks Operating Under Combined Pedestrian–Vehicle Interval. In Proceedings of the 86th Annual Meeting of the Transportation Research Board, Washington, D.C..

3. Alahi, A., K. Goel, V. Ramanathan, A. Robicquet, L. Fei-Fei, and S. Savarese (2016). Social LSTM: Human Trajectory Prediction in Crowded Spaces. In Proceedings of IEEE Conference on Computer Vision and Pattern Recognition (CVPR), Las Vegas, Nevada, 26 June – 1 July 2016.

4. Aleksandrov, M., R. Lovreglio, A. Rajabifard, M. Kalantari, and V. Gonzalez (2018). People Choice Modelling for Evacuation of Tall Buildings. Fire Technology, Vol. 54, No. 5, pp. 1171–1193. doi: 10.1007/s10694-018-0731-1

5. Alvarez, M., L. Rosasco, and N. Lawrence (2012). Kernels for Vector-Valued Functions: a Review. Foundations and Trends® in Machine Learning, Vol. 4, No. 3, pp. 195–266. doi: 10.1561/2200000036

6. Alvarez, J., M. Ramon, J. Mari, and G. Valls (2018). Digital Signal Processing with Kernel Methods. John Wiley & Sons, Ltd., West Sussex, UK.

7. Antonini, G., M. Bierlaire, and M. Weber (2006). Discrete choice models of pedestrian walking behavior. Transportation Research Part B: Methodological, Vol. 40, No. 8, pp. 168–177.

8. Antoniou, C. (2004). On–line Calibration for Dynamic Traffic Assignment. PhD Dissertation, Department of Civil and Environmental Engineering,

Massachusetts Institute of Technology.

9. Antoniou, C., M. Ben-Akiva, and H.N. Koutsopoulos (2007). Non–linear Kalman filtering algorithms for on–line calibration of dynamic traffic assignment models. In Proceedings of IEEE Transactions on Intelligent Transportation Systems, Vol. 8, No. 4, pp. 661–670.

10. Antoniou, C., R. Balakrishna, and H.N. Koutsopoulos (2011). A synthesis of emerging data collection technologies and their impact on traffic management applications. European Transport Research Review, Vol. 3, pp. 139–148.

11. Antoniou, C., H. Koutsopoulos, and G. Yannis (2013). Dynamic data-driven local traffic state estimation and prediction. Transportation Research Part C: Emerging Technologies, Vol. 34, pp. 89–107.

12. Barmpounakis, E., E. Vlahogianni, and J. Golias (2016). Extracting Kinematic Characteristics from Unmanned Aerial Vehicles. In Proceedings of the 95th Transportation Research Board Annual Meeting, Washington, D.C..

13. Barmpounakis, E., E. Vlahogianni, and J. Golias (2016). Vision-based multivariate statistical modeling for powered two-wheelers maneuverability during overtaking in urban arterials. Transportation Letters, Vol. 8, No. 3, pp. 167–176.

14. Bavdekar, V., A. Deshpande, and S. Patwardhan (2001). Identification of process and measurement noise covariance for state and parameter estimation using extended Kalman filter. Journal of Process Control, Vol. 21, No. 4, pp. 585–601.

15. Bertozzi, M., A. Broggi, A. Fascioli, A. Tibaldi, R. Chapuis, and F. Chausse (2004). Pedestrian Localization and Tracking System with Kalman Filtering. In Proceedings of IEEE Intelligent Vehicles Symposium, Parma, Italy, pp. 584–589.

16. Blue, V., and J. Adler (2001). Cellular automata microsimulation for modeling bi-directional pedestrian walkways. Transportation Research

Part B: Methodological, Vol. 35, No. 3, pp. 293–312.

17. Broyden, C. G. (1970). The Convergence of a Class of Double Rank Minimization Algorithms: 2. The new algorithm. Journal of Applied Mathematics, Vol. 6, No. 3, pp. 222–231.

18. Brščic, D., T. Kanda, T. Ikeda, and T. Miyashita (2013). Person tracking in large public spaces using 3D range sensors. IEEE Transactions on Human-Machine Systems, Vol. 43, No. 6, pp. 522–534.

19. Brščic, D., F. Zalungo, and T. Kanda (2014). Density and velocity patterns during one year of pedestrian tracking. Transportation Research Procedia, Vol. 2, pp. 77–86.

20. Burstedde, C., K. Klauck, A. Schadschneider, and J. Zittartz (2001). Simulation of pedestrian dynamics using a two-dimensional cellular automaton. Physica A: Statistical Mechanics and its Applications, Vol. 295, No. 3–4, pp. 507–525.

21. Byrd, R., P. Lu, J. Nocedal, and C. Zhu (1995). A limited memory algorithm for bound constrained optimization. SIAM Journal on Scientific Computing, Vol. 16, pp. 1190–1208. doi: 10.1137/0916069.

22. Cao, S., L. Fu, P. Wang, G. Zeng, and W. Song (2018). Experimental and modeling study on evacuation under good and limited visibility in a supermarket. Fire Safety Journal, Vol. 102, 2018, pp. 27–36. doi: 10.1016/j.firesaf.2018.10.003.

23. Chang, C.C., and C.J. Lin (2011). LIBSVM: A Library for Support Vector Machines. ACM Transactions on Intelligent Systems and Technology, Vol. 2, No. 3, Article No. 27. doi: 10.1145/1961189.1961199

24. Chen, C., B. Shih, and S. Yu (2012). Disaster prevention and reduction for exploring teachers' technology acceptance using a virtual reality system and partial least squares techniques. Natural Hazards, Vol. 40, No. 3, pp. 1217–1231.

25. Chraibi, M., A. Seyfried, and A. Schadschneider (2010). Generalized Centrifugal Force Model for Pedestrian Dynamics. Physical Review E,

Vol. 82, No. 4, 046111.

26. Cleveland, W.S. (1979). Robust locally weighted regression and smoothing scatterplots. Journal of the American Statistical Association, Vol. 74, No. 368, pp. 829–836.

27. Cleveland, W.S., and S.J. Devlin (1988). Locally Weighted Regression: An Approach to Regression Analysis by Local Fitting. Journal of the American Statistical Association, Vol. 83, No. 403, pp. 596–610.

28. Cleveland, W.S., S.J. Devlin, and E. Grosse (1988). Regression by Local Fitting: Methods, Properties, and Computational Algorithms. Journal of Econometrics, Vol. 37, pp. 87–114.

29. Cohen, R.A. (1999). An Introduction to PROC LOESS for Local Regression. In Proceedings of the 24th SAS users group international conference, Paper 273.

30. Craven, P., and G. Wahba (1979). Smoothing noisy data with spline functions. Numerische Mathematik, Vol. 31, pp. 377–403.

31. Daamen, W., P. Bovy, and S. Hoogendoorn (2002). Modelling Pedestrians in Transfer Stations. Pedestrian and Evacuation Dynamics, Springer, Berlin, pp. 59–73.

32. Daamen, W., and S. Hoogendoorn (2012). Calibration of pedestrian simulation model for emergency doors by pedestrian type. Transportation Research Record: Journal of the Transportation Research Board, Vol. 2316, No. 1, pp. 69–75.

33. Daamen, W., V. Knoop, and S. Hoogendoorn (2015). Generalized Macroscopic Fundamental Diagram for Pedestrian Flows. Traffic and Granular Flow ’13, Springer, Switzerland, pp. 41–46.

34. Das, P., M. Parida, and V. Katiyar (2014). Review of Simulation Techniques for Microscopic Mobility of Pedestrian Movement. Trends in Transport Engineering and Applications, Vol. 1, No. 1, pp. 26–45.

35. Dodge, S., R. Weibel, and E. Forootan (2009). Revealing the physics of

movement: Comparing the similarity of movement characteristics of different types of moving objects. Computers, Environment and Urban Systems, Vol. 33, No. 6, pp 419–434.

36. Douskos V., I. Kalisperakis, and G. Karras (2007). Automatic calibration of digital cameras using planar chess-board patterns. Optical 3-D Measurement Techniques VIII, Wichman, Vol. 1, pp.132–140.

37. Douskos, V., L. Grammatikopoulos, I. Kalisperakis, G. Karras, and E. Petsa (2009). FAUCCAL: an open source toolbox for fully automatic camera calibration. In Proceedings of the XXII CIPA Symposium on Digital Documentation, Interpretation & Presentation of Cultural Heritage, Kyoto, Japan.

38. Duives, D., W. Daamen, and S. Hoogendoorn (2013). State-of-the-art crowd motion simulation models. Transportation Research Part C: Emerging Technologies, Vol. 37, pp. 193–209.

39. Duives, D., G. Wang, and J. Kim (2019). Forecasting Pedestrian Movements Using Recurrent Neural Networks: An Application of Crowd Monitoring Data. Sensors (Basel), Vol. 19, No. 2, pp.1–19, doi: 10.3390/s19020382.

40. Federici, M., A. Gorrini, L. Manenti, and G. Vizzari (2014). An innovative scenario for pedestrian data collection: the observation of an admission test at the University of Milano-Bicocca. Pedestrian and Evacuation Dynamics, Springer, Switzerland, pp. 143–150.

41. Fletcher, R. (1970). A New Approach to Variable Metrics Algorithms. The Computer Journal, Vol. 13, No. 2, pp. 317–322.

42. Flötteröd, G., and G. Lämmel (2015). Bidirectional pedestrian fundamental diagram. Transportation Research Part B: Methodological, Vol. 71, pp. 194–212.

43. Foxlin, E. (2005). Pedestrian tracking with shoe-mounted inertial sensors. IEEE Computer Graphics and Applications, Vol. 25, No. 6, pp. 38–46.

44. Gelb, A. (1974). Applied Optimal Estimation, M.I.T. Press.

45. Giannis, F., and E. Vlahogianni (2018). Asymmetry of pedestrian influence area in unidirectional and bidirectional crowd flows: Empirical evidence and statistical modeling. Advances in Transportation Studies, Vol. 44, pp. 5–20. doi: 10.4399/97888255143461

46. Gipps, P., and B. Marksjo (1985). A micro-simulation model for pedestrian flows. Mathematics and Computers in Simulation, Vol. 27, No. 2–3, pp. 95–105.

47. Gloor, C., P. Stucki, and K. Nagel (2004). Hybrid Techniques for Pedestrian Simulations. Cellular Automata, Springer, Berlin, pp. 581–590.

48. Glorot, G., A. Bordes, and Y. Bengio (2011). Deep Sparse Rectifier Neural Networks. In Proceedings of the 14th International Conference on Artificial Intelligence and Statistics, pp. 315–323.

49. Goldfarb, D. (1970). A Family of Variable-Metric Methods Derived by Variational Means. Mathematics of Computation, Vol. 24, No. 109, pp. 23–26.

50. Gong, J., W. Li, Y. Li., and M. Huang (2009). Networked Collaborative Virtual Geographic Environments: Design and Implementation. In Virtual Geographic Environments, Science Press, Beijing, pp. 245–254.

51. Gudmundsson, J., A. Thom, and J. Vahrenhold (2012). Of motifs and goals: mining trajectory data. In Proceedings of the 20th International Conference on Advances in Geographic Information Systems. ACM, pp. 129–138.

52. Guo, R., S. Wong, H. Huang, P. Zhang, and W. Lam (2010). A microscopic pedestrian-simulation model and its application to intersecting flows. Physica A: Statistical Mechanics and its Applications, Vol. 389, No. 3, pp. 515–526.

53. Guo, R., H. Huang, and S. Wong (2012). Route choice in pedestrian evacuation under conditions of good and zero visibility: Experimental and simulation results. Transportation Research Part B, Vol. 46, pp. 669–686.

54. Hamed, M. (2001). Analysis of pedestrians' behavior at pedestrian

crossings. Safety Science, Vol. 38, No. 1, pp. 63–82.

55. Heikkila, J., and O. Silven (1997). A Four-step Camera Calibration Procedure with Implicit Image Correction. In Proceedings of IEEE Computer Society Conference on Computer Vision and Pattern Recognition, San Juan, Puerto Rico, USA.

56. Heikkila, J., and O. Silven (2004). A real-time system for monitoring of cyclists and pedestrians. Image and Vision Computing, Vol. 22, No. 7, pp 563–570.

57. Helbing, D. (1992). A Fluid-Dynamic Model for the Movement of Pedestrians. Complex Systems, Vol. 6, pp. 391–415.

58. Helbing, D., and P. Molnár (1995). Social force model for pedestrian dynamics. Physical Review E, Vol. 51, pp. 4282–4286.

59. Helbing, D., I. Farkas, and T. Vicsek (2000). Simulating dynamical features of escape panic. Nature, Vol. 407, pp. 487–490.

60. Helbing, D., M. Isobe, T. Nagatani, and K. Takimoto (2003). Lattice gas simulation of experimentally studied evacuation dynamics. Physical Review E, Vol. 67, No. 6, 067101.

61. Helbing, D., R. Jiang, and M. Treiber (2005). Analytical Investigation of Oscillations in Intersecting flows of Pedestrian and Vehicle Traffic. Physical Review E, Vol. 72, No. 4, 046130.

62. Helbing, D., A. Johansson, and H. Al-Abideen (2007). The Dynamics of Crowd Disasters: An Empirical Study. Physical Review E, Vol. 75, No. 4, 046109.

63. Helbing, D., and A. Johansson (2010). Pedestrian, Crowd and Evacuation Dynamics. Encyclopedia of Complexity and Systems Science, Vol. 16, pp. 6476–6495, Print ISBN 978-0-387-75888-6, Online ISBN 978-0-387-30440-3, Publisher Springer New York

64. Helbing, D. (2012). Social Self-Organization, Agent-Based Simulations and Experiments to Study Emergent Social Behavior, Understanding

Complex Systems, ISBN 978-3-642-24003-4, DOI 10.1007/978-3-642-24004-1, Springer-Verlag Berlin Heidelberg.

65. Hen, I., A. Sakov, N. Kafkafi, I. Golani, and Y. Benjamini (2004). The dynamics of spatial behavior: how can robust smoothing techniques help?. Journal of Neuroscience Methods, Vol. 133, No. 1-2, pp. 161–172.

66. Hoogendoorn, S., and P. Bovy (2003), Simulation of pedestrian flows by optimal control and differential games, Optimal Control Applications and Methods, Vol. 24, No. 3, pp. 153–172.

67. Hoogendoorn, S., W. Daamen, and P. Bovy (2003). Extracting Microscopic Pedestrian Characteristics from Video Data. In Proceedings of the 82nd Annual Meeting of the Transportation Research Board, Washington, D.C.

68. Hoogendoorn, S., and P. Bovy (2004). Pedestrian route-choice and activity scheduling theory and models. Transportation Research Part B: Methodological, Vol. 38, No. 2, pp. 169–190.

69. Hoogendoorn, S., and W. Daamen (2007). Microscopic calibration and validation of pedestrian models: cross-comparison of models using experimental data. Traffic and Granular Flow ’05, Springer, Berlin, pp. 329–340.

70. Huang, B., and X. Pan (2007). GIS coupled with traffic simulation and optimization for incident response. Computers, Environment and Urban Systems, Vol. 31, No. 2, pp. 116–132.

71. Hughes, R.L. (2000). The flow of large crowds of pedestrians. Mathematics and Computers in Simulation, Vol. 53, No. 4–6, pp. 367–370.

72. Isobe, M., T. Adachi, and T. Nagatani (2004). Experiment and simulation of pedestrian counter flow. Physica A: Statistical Mechanics and its Applications, Vol. 336, No. 3–4, 2004, pp. 638–350.

73. Johansson, A., D. Helbing, and P. Shukla (2007). Specification of a microscopic pedestrian model by evolutionary adjustment to video

tracking data. Advances in Complex Systems, Vol. 10, No. 2, pp. 271–288.

74. Joo, J., N. Kim, R. Wysk, L. Rothrock, Y. Son, Y. Oh, and S. Lee (2013). Agent-based simulation of affordance-based human behaviors in emergency evacuation. Simulation Modelling Practice and Theory, Vol. 32, pp. 99–115.

75. Julier S., J. Ulhmann and H. Durrant-Whyte, (2000). A new method for nonlinear transformation of means and covariances in filters and estimators. IEEE Transactions on Automatic Control, Vol. 45, No. 3, pp. 472–482.

76. Kalisperakis I., L. Grammatikopoulos, E. Petsa and G. Karras, (2006). An open-source educational software for basic photogrammetric tasks. In Proceedings of the FIG-ISPRS-ICA International Symposium on Modern Technologies, Education & Professional Practice in Geodesy & Related Fields, Sofia, Bulgaria, pp. 581–586.

77. Kalman, R. E., (1960). A New Approach to Linear Filtering and Prediction Problems. Journal of Basic Engineering, Vol. 82, No. 1, pp. 35–45.

78. Karlaftis, M., and E. Vlahogianni (2011). Statistical methods versus neural networks in transportation research: Differences, similarities and some insights. Transportation Research Part C: Emerging Technologies, Vol. 19, No. 3, pp. 387–399.

79. Kerridge, J., S. Keller, T. Chamberlain, and N. Sumpter (2007). Collecting Pedestrian Trajectory Data In Real-time. Pedestrian and Evacuation Dynamics 2005, Springer, Berlin, pp. 27–39.

80. Kingma, D., and J. Ba (2015). ADAM: A method for stochastic optimization. In Proceedings of the 3rd International Conference for Learning Representations, San Diego, CA, USA.

81. Klingsch, W.W.F., C. Rogsch, A. Schadschneider, and M., Schreckenberg, (2010). Pedestrian and Evacuation Dynamics, Springer, Wuppertal, Köln, Duisburg.

82. Kneidl, A., and A. Borrmann (2011). How Do Pedestrians find their Way? Results of an experimental study with students compared to simulation results. Emergency Evacuation of people from Buildings, Warsaw, Poland, pp. 163–172.

83. Koo, J., Y. Kim, B. Kim, and K. Christensen (2013). A comparative study of evacuation strategies for people with disabilities in high-rise building evacuation. Expert Systems with Applications, Vol. 62, No. 2, pp. 408–417.

84. Kourogi, M., N. Sakata, T. Okuma, and T. Kurata (2006). Indoor/Outdoor Pedestrian Navigation with an Embedded GPS/RFID/Self-contained Sensor System. In Proceedings of 16th International Conference on Artificial Reality and Telexistence (ICAT2006), Hangzhou, Chin.

85. Kouskoulis, G., and C. Antoniou (2017). A Systematic Review of Pedestrian Simulation Models with a Focus on Emergency Situations. Transportation Research Record: Journal of the Transportation Research Board, Vol. 2604, No. 1, pp. 111–119. doi:10.3141/2604-14

86. Kouskoulis, G., I. Spyropoulou, and C. Antoniou, (2018). Pedestrian simulation: Theoretical models vs. data driven techniques. International Journal of Transportation Science and Technology, 7, 241–253.

87. Kouskoulis, G., I. Spyropoulou, and C. Antoniou (2019). Comparing the Performance of Artificial Neural Networks and Social Force Model on Pedestrian Simulation. In Proceedings of the 9th International Congress on Transportation Research, Athens, Greece.

88. Kretz, T., (2011). A level of service scheme for microscopic simulation of pedestrians that integrates queuing, uni-and multi-directional flow situations. European Transport Research Review, Vol. 3, No. 4, pp. 211–220.

89. Kretz, T., A. Große, S. Hengst, L. Kautzsch, A. Pohlmann, and P. Vortisch, (2011). Quickest Paths in Simulations of Pedestrians. Advances in Complex Systems, Vol. 14, No. 5, pp. 733–759.

90. Lesani, A., E. Nateghinia and L. Miranda-Moreno (2020). Development and evaluation of a real-time pedestrian counting system for high-volume conditions based on 2D LiDAR. Transportation Research Part C: Emerging Technologies, Vol. 114, pp. 20–35.

91. Li, N, and R. Y. Guo (2020). Simulation of bi-directional pedestrian flow through a bottleneck: Cell transmission model. Physica A: Statistical Mechanics and its Applications, Vol. 555, 124542.

92. Li, Y., D. Wang, Y. Chen, C. Song, H. Jia, and Y. Lin (2019). Pedestrian choice behavior analysis and simulation of ticket gate machine in rail transit station. International Journal of Modern Physics C, Vol. 20, No. 4, 1950027, doi: 10.1142/S012918311950027X.

93. Liao, W., X. Zheng, L. Cheng, Y. Zhao, Y. Cheng, and Y. Wang (2014). Layout effects of multi-exit ticket-inspectors on pedestrian evacuation. Safety Science, Vol. 70, pp. 1–8.

94. Löhner, R., and E. Haug (2014). On Critical Densities and Velocities for Pedestrians Entering a Crowd. Transportation Research Procedia, Vol. 2, pp. 394–399.

95. Løvås, G. (1994). Modeling and simulation of pedestrian traffic flow. Transport Research Board, Vol. 28B, No. 6, pp. 429–443.

96. Lu, A., B. Ren, C. Wang, and D. Chan (2015). Application of SFCA pedestrian simulation model to the signalized crosswalk width design. Transportation Research Part A: Policy and Practice, Vol. 80, pp. 76–89.

97. Ma, J., and W. Song (2013). Automatic clustering method of abnormal crowd flow pattern detection. Procedia Engineering, Vol. 62, pp. 509–518.

98. Ma, Y., E. Lee, and R. Yuen (2016). An Artificial Intelligence-Based Approach for Simulating Pedestrian Movement, IEEE Transactions on Intelligent Transportation Systems, Vol. 17, No. 11, 2016, pp. 3159–3170.

99. Majecka, B. (2009). Statistical models of pedestrian behavior in the Forum, MSc Thesis, School of Informatics, University of Edinburgh.

100. Manley, M., and Y. Kim (2012). Modeling emergency evacuation of individuals with disabilities (exitus): An agent-based public decision support system. Expert Systems with Applications, Vol. 39, No. 9, pp. 8300–8311.

101. Martinez-Gil, F., M. Lozano, and F. Fernández (2017). Emergent behaviors and scalability for multi-agent reinforcement learning-based pedestrian models. Simulation Modelling Practice and Theory, Vol. 74, pp. 117–133.

102. Matthews, M., G. Chowdhary, and E. Kieson (2017). Intent Communication between Autonomous Vehicles and Pedestrians. arXiv preprint

103. McCullogh, W., and W. Pitts (1943). A logical calculus and the ideas immanent in the nervous activity. Bulletin of Mathematical Biophysics, Vol. 5, pp. 115–133.

104. Moussaïd, M., D. Helbing, S. Garnier, A. Johansson, M. Combe, and G. Theraulaz (2009). Experimental study of the behavioural mechanisms underlying self-organization in human crowds. In Proceedings of the Royal Society B, Vol. 276, pp. 2755–2762. doi:10.1098/rspb.2009.0405

105. Moussaïd M., N. Perozo, S. Garnier, D. Helbing, and G. Theraulaz (2010). The Walking Behaviour of Pedestrian Social Groups and Its Impact on Crowd Dynamics. PLoS ONE, Vol. 5, No. 4, e10047.

106. Moussaïd M., D. Helbing, and G. Theraulaz (2011). How simple rules determine pedestrian behavior and crowd disasters, In Proceedings of National Academy of Science, Vol. 108, No. 17, 2011, pp. 6884–6888.

107. Müller, F., and A. Schadschneider (2016). Evacuation dynamics of asymmetrically coupled pedestrian pairs. Traffic and Granular Flow'15, pp. 265–272.

108. Muramatsu, M., T. Irie, and T. Nagatani (1999). Jamming transition in pedestrian counter flow. Physica A: Statistical Mechanics and its Applications, Vol. 267, No. 3–4, pp. 487–498.

109. Muramatsu, M., and T. Nagatani (2000). Jamming transition in two-dimensional pedestrian traffic. Physica A: Statistical Mechanics and its Applications, Vol. 275, No. 1–2, pp. 281–291.

110. Nagatani, T. (2001). Dynamical transition and scaling in a mean-field model of pedestrian at a bottleneck. Physica A, Vol. 300, No. 3–4, pp. 558–566.

111. Nagatani, T. (2002). Dynamical transition in merging pedestrian flow without bottleneck, Physica A: Statistical Mechanics and its Applications, Vol. 307, No. 3–4, pp. 505–515.

112. Nagel, K., and M. Schreckenberg (1992). A cellular automaton model for freeway traffic. Journal de Physique I, 1992, Vol. 2, pp. 2221–2229.

113. Nikolić, M, B. Farooq, and M. Bierlaire, (2013). Exploratory analysis of pedestrian flow characteristics in mobility hubs using trajectory data. In Proceedings of the 13th Swiss Transport Research Conference, Ascona, Switzerland.

114. Nikolić, M., M. Bierlaire, B. Farooq, and M. de Lapparent (2016). Probabilistic speed–density relationship for pedestrian traffic. Transportation Research Part B: Methodological, Vol. 89, 2016, pp. 58–81.

115. Okazaki, S., and S. Matsushita (1993). A study of simulation model for pedestrian movement with evacuation and queuing. In proceedings of the International Conference on Engineering for Crowd Safety, London, UK, pp. 271–280.

116. Ossen, S., and S. P. Hoogendoorn (2008). Validity of Trajectory-Based Calibration Approach of Car-Following Models in the Presence of Measurement Errors, Transport Research Record: Journal of the Transportation Research Board, Vol. 2088, pp. 117–125.

117. Papadimitriou, E., G. Yannis, and J. Golias (2009). A critical assessment of pedestrian behaviour models. Transportation Research Part F: Traffic Psychology and Behaviour, Vol. 12, No. 3, pp. 242–255.

118. Papadimitriou, E., J. Auberlet, G. Yannis, and S. Lassarre (2014). Simulation of Pedestrians and Motorised Traffic: Existing Research and Future Challenges. International Journal of Interdisciplinary Telecommunications and Networking, Vol. 6, No. 1, pp. 57–73.

119. Papathanasopoulou, V., and C. Antoniou (2015). Towards data-driven car-following models. Transportation Research Part C: Emerging Technologies, Vol. 55, 2015, pp. 496–509.

120. Papathanasopoulou, V., and C. Antoniou (2017). A comparison of machine learning techniques for data-driven car-following models. In Proceedings of the International Conference on Intelligent Transport Systems in Theory and Practice, mobil.TUM, Munich, Germany, 4-5 July.

121. Parisi, D., and C. Dorso (2005). Microscopic dynamics of pedestrian evacuation. Physica A, Vol. 354, pp. 606–618.

122. Particke, F., M. Hiller, L. Patiño-Studencki, C. Sippl, C. Feist, and J. Thielecke (2017). Improvements in Pedestrian Tracking by a Generalized Potential Field Approach. In Proceedings of the International Conference on Intelligent Transport Systems in Theory and Practice, mobil.TUM. Munich, Germany.

123. Paton, D. (2003). Disaster preparedness: A social-cognitive perspective. Disaster Prevention and Management, Vol. 12, No. 3, pp. 210–216.

124. Pérez-Cruz, F., A. Navia-Vázquez, P.L. Alarcón-Diana, and A. Artés-Rodríguez (2000). An IRWLS procedure for SVR. In Proceedings of IEEE 10th European Signal Processing Conference, Tampere, Finland, 4 – 8 September.

125. Pérez-Cruz, F., G. Camps-Valls, E. Soria-Olivas, J.J. Pérez—Ruixo, R. Figueiras-Vidal, and A. Artés-Rodríguez (2002). Multi-dimensional Function Approximation And Regression Estimation. In Proceedings of the International Conference Artificial Neural Networks, Madrid, Spain, 28 – 30 August, pp.757–762. doi:10.1007/3-540-46084-5_123

126. Philomin, V., R. Duraiswami, and L. Davis (2000). Pedestrian tracking

from a moving vehicle. In Proceedings of the IEEE IV, Dearborn, MI, USA, pp. 350–355.

127. Pidd, M., F. Silva, and R. Eglese (1996). A simulation model for emergency evacuation. European Journal of Operational Research, Vol. 90, No. 3, pp. 413–419.

128. PTV VISSIM 7 User Manual. PTV AG, 2015.

129. Rasmussen, C.E., and C. Williams (2006). Gaussian Processes for Machine Learning. The MIT Press, ISBN 026218253X, Cambridge, Massachusetts.

130. Reades, J., F. Calabrese, A. Sevtsuk, and C. Ratti (2007). Cellular census: Explorations in urban data collection. In Proceedings of the IEEE Pervasive Computing, Vol. 6, No. 3, pp. 30–38.

131. Ridel, D., N. Deo, D. Wolf, and M. Trivedi (2019). Understanding Pedestrian-Vehicle Interactions with Vehicle Mounted Vision: An LSTM Model and Empirical Analysis. In Proceedings of the IEEE Intelligent Vehicles Symposium, pp. 913–918.

132. Robin, Th., G. Antonini, M. Bierlaire, and J. Cruz (2009). Specification, estimation and validation of a pedestrian walking behavior model. Transportation Research Part B: Methodological, Vol. 43, No. 1, pp. 36–56.

133. Rumelhart, D., G. Hinton, and R. Williams (1986). Learning Internal Representations by Error Propagation. Parallel distributed processing: explorations in the microstructure of cognition, Vol. 1, pp. 318–362, MIT Press Cambridge, MA, USA, ISBN:0-262-68053-X.

134. Saltelli, A. (2002). Making best use of model evaluations to compute sensitivity indices. Computer Physics Communications, Vol. 145, pp. 280–297.

135. Saltelli, A., M. Ratto, T. Andres, F. Campolongo, J. Cariboni, D. Gatelli, M. Saisana, and S. Tarantola (2008). Global Sensitivity Analysis. The Primer, ISBN 978-0-470-05997-5, Publisher Wiley New York.

136. Sánchez-Fernández, M., M. de-Prado-Cumplido, J. Arenas-García, and F. Pérez-Cruz (2004). SVM Multiregression for Nonlinear Channel Estimation in Multiple-Input Multiple-Output Systems. In Proceedings of the IEEE Transactions on Signal Processing, Vol. 52, No. 8, 2004, pp. 2298–2307, doi:10.1109/TSP.2004.831028.

137. Scrucca, L. (2013). GA: A Package for Genetic Algorithms in R. Journal of Statistical Software, Vol 53, No. 4, pp. 1–37.

138. Seyfried, A., B. Steffen, W. Klingsch, and M. Boltes (2005). The fundamental diagram of pedestrian movement revisited. Journal of Statistical Mechanics: Theory and Experiment, Vol. 10, pp. 116–132.

139. Shanno, D.F. (1970). Conditioning of Quasi-Newton Methods for Function Minimization. Mathematics of Computation, Vol. 24, pp. 647–656.

140. Siebel, N., and S. Maybank (2001). Real-time tracking of pedestrians and vehicles. In Proceedings of IEEE workshop on PETS, Kauai, HI.

141. Siques, J. (2002). The Effects of Pedestrian Treatments on Risky Behavior. In Proceedings of the 81st Transport Research Board Annual Meeting, Washington, D.C.

142. Song, W., Y. Yu, B. Wang, and W. Fan (2006). Evacuation behaviors at exit in CA model with force essentials: A comparison with social force model. Physica A, Vol. 371, pp. 658–666.

143. Song, Y., J. Gong, Y. Li, T. Cui, L. Fang, and W. Cao (2013). Crowd evacuation simulation for bioterrorism in micro-spatial environments based on virtual geographic environments. Safety Science, Vol. 53, pp. 105–113.

144. Sutheeraukul, C., N. Kronprasert, M. Kaewmoracharoen, and P. Pichayapan (2017). Application of Unmanned Aerial Vehicles to pedestrian traffic monitoring and management for shopping streets. Transportation Procedia, Vol. 25, pp. 1717–1734.

145. Tay, M.K.C., and C. Laugier (2008). Modelling Smooth Paths Using Gaussian Processes. In Proceedings of the 6th International Conference

on Field and Service Robotics, Chamonix, France.

146. Teknomo, K., Y. Takeyama, and H. Inamura (2000). Data collection method for pedestrian movement variables. Civil Engineering Dimension–Journal of Civil Engineering Science and Application, Vol. 2, No 1, pp. 43–48.

147. Teknomo, K., T. Yasushi, and I. Hajime (2001). Tracking System to Automate Data Collection of Microscopic Pedestrian Traffic Flow. In Proceedings of the 4th Eastern Asia Society For Transportation Studies, Hanoi, Vietnam, Vol. 3, No 1, pp. 11–25.

148. Teknomo, K. (2006). Application of microscopic pedestrian simulation model. Transport Research Part F, Vol. 9, No. 1, pp. 15–27.

149. Thiemann, C., M. Treiber, and A. Kesting (2008). Estimating Acceleration and Lane-Changing Dynamics Based on NGSIM Trajectory Data. Transport Research Record: Journal of the Transportation Research Board, Vol. 2088, pp. 90–101.

150. Tordeux, A., G. Lämmel, F. Hänseler, and B. Steffen (2018). A mesoscopic model for large-scale simulation of pedestrian dynamics. Transportation Research Part C, Vol. 93, pp. 128–147.

151. Tordeux, A., M. Chraibi, A. Seyfried, and A. Schadschneider, (2018). Prediction of pedestrian speed with Artificial Neural Networks. Traffic and Granular Flow'17.

152. Torres-Ruiz, M., M. Moreno-Ibarra, W. Alhalabi, R. Quintero, and G. Guzmán (2017). Towards a microscopic model for analyzing the pedestrian mobility in an urban infrastructure. Journal of Science and Technology Policy Management, Vol. 9, No. 2, pp. 170–188.

153. Vapnik, V. (1995) The Nature of Statistical Learning Theory. ISBN 978-1-4757-2442-4, Publisher Springer-Verlag New York. doi: 10.1007/978-1-4757-2440-0

154. Vermuyten, H., J. Beliën, L. De Boeck, G. Reniers, and T. Wauters, (2016). A review of optimisation models for pedestrian evacuation and

design problems. Safety Science, Vol. 87, pp. 167–178.

155. Vizzari, G., L. Manenti, and L. Crociani (2013). Adaptive pedestrian behaviour for the preservation of group cohesion, Complex Adaptive Systems Modeling, Vol. 1, pp. 1–29.

156. Voloshin, D., D. Rybokonenko, and V. Karbovskii (2015). Optimization-based calibration for micro-level agent-based simulation of pedestrian behavior in public spaces. Procedia Computer Science, Vol. 66 pp. 372–381.

157. Wan, E. A., and R. Van der Merwe, (2000). The Unscented Kalman filter for nonlinear estimation. In Proceedings of the Symposium Adaptive Systems for Signal Processing, Communications and Control, Lake Louise, AB, Canada.

158. Wang, H., H. Lenz, A. Szabo, J. Bamberger, and U. D. Hanebeck, (2007). WLAN-Based Pedestrian Tracking Using Particle Filters and Low-Cost MEMS Sensors. In Proceedings of the IEEE 4th workshop on Positioning, Navigation and Communication, Hannover, Germany.

159. Wang, K., X. Shi, A. P. X. Goh, and S. Qian (2019). A machine learning study on pedestrian movement dynamics under emergency evacuation. Fire Safety Journal, Vol. 106, pp. 163–176.

160. Weidmann, U. Transporttechnik der Fußgänger. IVT, Institut für Verkehrsplanung, Transporttechnik, Strassen – und Eisenbahnbau, Zürich, 1993.

161. Weifeng, F., Y. Lizhong, and F. Weicheng (2003). Simulation of bi-direction pedestrian movement using a cellular automata model. Physica A: Statistical Mechanics and its Applications, Vol. 321, No. 3–4, pp. 633–640.

162. Werbos, P. (1974). Beyond Regression: New Tools for Prediction and Analysis in the Behavioral Sciences, Ph. Thesis, Harvard University.

163. Wu, P. Y., R. Y. Guo, L. Ma, B. Chen, J. Wu, and Q. Zhao (2021). Simulation of pedestrian route choice with local view: A potential field

approach. Applied Mathematical Modelling, Vol. 92, pp. 687–709.

164. Xing, W., S. Zhao, S. Zhang, and Y. Cai (2017). A generic bi-layer Data-Driven Crowd Behaviors Modeling Approach. IEICE Transactions on Information and Systems, Vol. E100-D, No. 8, pp. 1827–1836.

165. Xu, D., X. Huang, J. Mango, X. Li, and Z. Li (2021). Simulating multi-exit evacuation using deep reinforcement learning. Transactions in GIS (in press).

166. Yun, J., G. Zhao, T. Fang, S. Liu, and C. Huang (2012). A swarm-based dynamic evacuation simulation model under the background of secondary disasters. Systems Engineering Procedia: Safety and Emergency Systems Engineering, Vol. 5, pp. 61–67.

167. Zainuddin, Z., K. Thinakaran, and I. Abu-Sulyman (2009). Simulating the Circumambulation of the Ka'aba using SimWalk. European Journal of Scientific Research, Vol. 38, No. 3, pp. 454–464.

168. Zampella, F., M. Khider, P. Robertson, and A. Jiménez, (2012). Unscented Kalman filter and Magnetic Angular Rate Update (MARU) for an improved Pedestrian Dead-Reckoning. In Proceedings of the 2012 IEEE/ION Position, Location and Navigation Symposium, Myrtle Beach, South Carolina, USA, pp 129–139.

169. Zanlungo, F., T. Ikeda, and T. Kanda (2011). Social force model with explicit collision prediction. Europhysics Letters, Vol. 93, pp. 1–6.

170. Zanlungo, F., D. Brščic, and T., Kanda (2014). Pedestrian group behaviour analysis under different density conditions. Transportation Research Procedia, Vol. 2, pp. 149–158.

171. Zanlungo, F., T. Ikeda, and T. Kanda (2014). Potential for the dynamics of pedestrians in a socially interacting group. Physical Review E 89, 012811, pp. 1–18.

172. Zeng, W., P. Chen, H. Nakamura, and M. Iryo-Asano (2014). Application of social force model to pedestrian behavior analysis at signalized crosswalk. Transportation Research Part C, Vol. 40, pp. 143–159.

173. Zhao, X., D. Xie, and H. Li (2012). Effect of traffic information on the stability pedestrian flow. Physics Procedia, Vol. 24, pp.1052–1059.